ELECTROMAGNETIC THEORY WITH PRACTICAL APPLICATIONS

Mary O’Neill

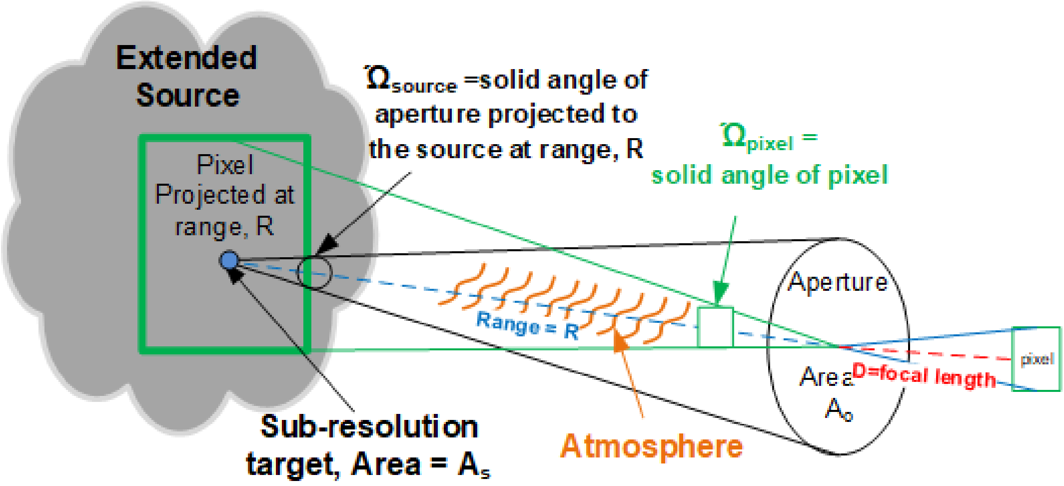

JUNE 6, 2025

PREPARED UNDER THE DIRECTION OF:

THE NEVADA NATIONAL SECURITY SITES

This work was done by Mission Support and Test Services, LLC, under Contract No. DE-NA0003624 with the U.S. Department of Energy and the National Nuclear Security Administration. DOE/NV/03624--2251.

Table of Contents

Figures

Tables

1 Introduction – Systems Engineering

As I put together this set of tools, I am reminded of my training. I am a systems engineer who started in electro-optics and analog circuits. I do not believe I can state what a systems engineer is better than Richard Hudson (Hudson, 1969):

> “ ‘Just who is this jack-of-all-trades,’ the system engineer, who oversees the entire process? Jack-of-all-trades he is, but he is usually master of at least one, the specialty he developed in depth before moving into system engineering. System engineers are rarely developed by the academic process; more often they drift into this field from the ranks of successful engineers after discovering that their interests lie in overall concepts and functional relationships rather than in a narrow area of specialization. The system engineer has shown a desire to row broad as well as deep.”

Because of the breadth of knowledge, I have gleaned in years of working on radio frequency (RF) and optical systems, this book will include a broad range of topics. For those who have the tendency towards thinking like a systems engineer, this book will include enough information to help make connections between modalities that can be useful in modeling and designing novel systems.

Excellent references for electro-optics are:

RCA Electro-Optics Handbook Paperback – January 1, 1974 – Included in provided references as Burle_electro_optics.pdf
Hudson, Richard D., *Infrared System Engineering*, John Wiley & Sons, New York, 1969
Wolfe, William L, Zissis, George J., *The Infrared Handbook*, IRIA Center, Michigan, 1985

For RF everyone should have:

M. Skolnik *Radar Handbook*, 3rd Edition, McGraw-Hill, Boston, 1990

2 Basic Radiometry

Electromagnetic energy is everywhere. In electro-optics, *everything is intensity and angles (steradian subtense).* Targets typically reflect sunlight in the visible regions and emit thermal energy in the infrared. When developing systems and algorithms, it is important to understand how the energy gets to the detector (whatever that detector might be). This requires an understanding of illumination sources, backgrounds, targets, and sensor limitations. It is obvious from the graphics of the electromagnetic spectrum in Figure 2-1 that what we see is only a small part of what can be detected.

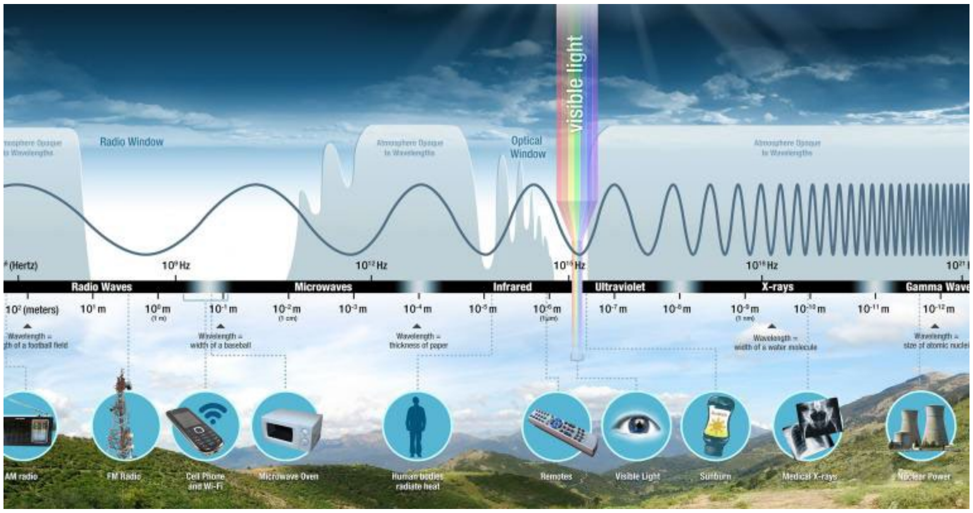

Figure 2-1. Electromagnetic spectrum (NASA, 2010). This book focusses on UV – RF.

The focus of this book is the ultraviolet (UV) through RF regions, with special considerations for the Infrared (IR). Spectral bands are typically (although this varies from group to group) identified as (Rogalski, 2004):

- 25–200 nanometer (nm) Vacuum ultraviolet VUV
- 200–400 nm Ultraviolet UV
- 400–700 nm Visible VIS
- 700–1000 nm Near infrared NIR
- 1–3 micrometer (µm) Short wavelength infrared SWIR
- 3–5 µm Medium wavelength infrared MWIR
- 5–14 µm Long wavelength infrared LWIR
- 14–30 µm Very long wavelength infrared VLWIR
- 30–100 µm Far infrared FIR
- 100–1000 µm Submillimeter SubMM

All radiometric calculations consider the target intensity, loss through the path, and the angle of the target versus the angle of the receiver – again it is all angles and intensities. The key is to follow the path from the target to the detector and then through the digitizer, as we have all been taught, keeping track of our units such as watts, meters, etc. Figure 2-2 provides a geometric diagram of an object at range, R, from a sensor with aperture, A_o, and focal length, D.

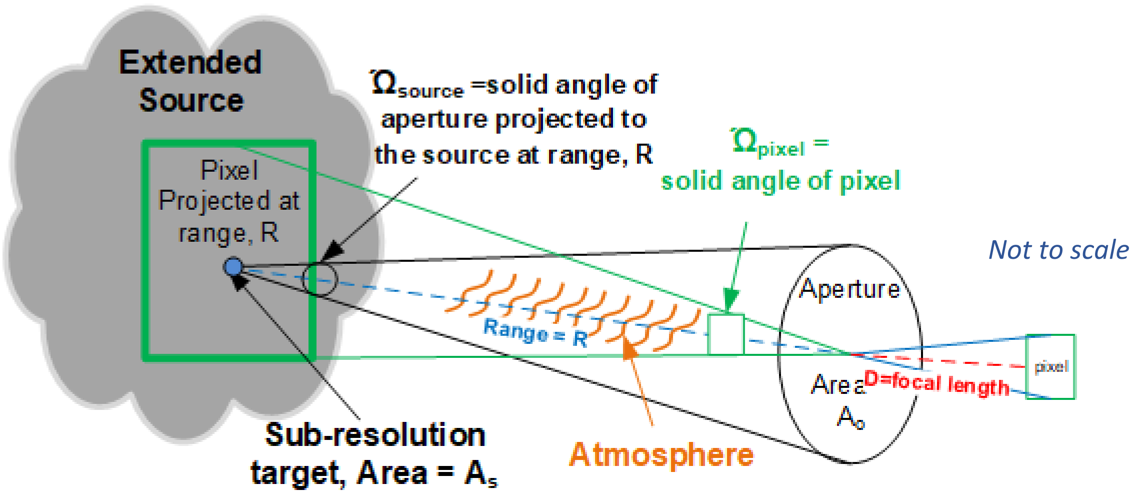

Figure 2-2. Geometric detection arrangement. The target at range, R, is seen by the optical system with aperture area, A_o, with the corresponding pixel. For a sub-resolution target, when the pixel is projected at range R, it is much larger than the object area, for an extended (resolved) source, the pixel is smaller than the object area.

The blue dotted line is called the optical axis. Photons are emitted, reflected or both off the target source. They travel through the atmosphere and are captured by the entrance aperture of the optic, which focuses the photons onto a detector. The detector converts photons to electrons. Electrons per second (current) is then converted to a voltage via a transimpedance amplifier. Voltage is typically digitized into counts denoted as a digital number (dn). All that the modeler or designer needs to do is follow the photons. The initial example in this section will consider all variables, but often, shortcuts can be taken. It is important to understand what variables are important for your system.

Table 2-1 shows basic radiometric variables and their definitions used throughout this document. Note that the variable symbols vary from book to book. For instance, one book might us M for Radiant Exitance, while another may use W. These equations will be repeated as necessary but are provided in a single place for convenience.

Table 2-1. Basic radiometric variables – passive detection (Hudson, 1969, Wolfe, 1985).

Variable (symbol)	Definition	Optical Units	Relationships
Spectral Radiance (L$_\lambda$)	Radiant flux per unit solid angle per unit area per spectral width	W/sr-cm^2-µm (aka flicks)	Planck's Law $L(\lambda,\, T) = \frac{2 \cdot 10^{16} \cdot h \cdot c^2}{\lambda^5 \left(e^{10^4 \cdot hc/\lambda kT} - 1\right)}$
Spectral Radiant photon emittance (Q)*	Radiant photon flux per unit solid angle per unit area per spectral width	Photons/sec/ sr-cm^2-µm	$Q(\lambda,\, T) = \frac{2 \cdot 10^{12} \cdot c}{\lambda^4 \left(e^{10^4 \cdot hc/\lambda kT} - 1\right)}$
Radiance (L)	Radiant flux per unit solid angle per unit area	W/cm^2-sr	$L(T) = \int_{\lambda_0}^{\lambda_1} L(\lambda,\, T) \cdot R(\lambda) \cdot d\lambda$
Radiant Exitance (W or M)	Radiant flux emitted per unit area of ***source***	W/cm^2	$W = \pi \cdot L = \frac{J \cdot \pi}{A_s}$
Radiant Intensity (J or I)	Radiant flux per unit solid angle	W/sr	$J = L \cdot A_s = \frac{W \cdot A_s}{\pi}$
Radiant energy (Q or U)	Energy Transferred by electromagnetic waves	Joule (J)	$Q = P \cdot t$
Radiant Flux (P or Φ)	Rate of transfer of Energy	Watt (W)	$P = J \cdot \phi^2$
Irradiance (H or E)	Radiant flux incident per unit area of ***aperture***	W/cm^2	$H = \frac{J}{R^2} = \frac{L \cdot A_s}{R^2}$
Reflectance (ρ)	Ratio of reflected radiant flux to incident radiant flux	unitless	W$_{\text{reflected}}$/W$_{\text{incident}}$
Emissivity (ε)	Same as absorption when target is warmer than the ambient air	unitless	W/W$_{\text{blackbody,}}$
Range (R)	Range to target	meters	
Area of source (A_s)	Source area	m^2	
Solid angle (ϕ^2)	Steradian subtense	Steradian (i.e. radians^2)	$\phi^2 = \tan\left(\frac{A_s}{R}\right)^2$

* For photon detectors it is convenient to work in photons; we thus divide the spectral Radiance, (L$_\lambda$), by the energy of a photon (using the Planck-Einstein relation), which is hc/λ.

Where:

h = Planck's constant = 6.6260693x10^{-34} W-s^2
c = speed of light = 2.99792458x10^{10} cm/s
k = Boltzmann's constant = 1.380658x10^{-23} W-s/K
λ = Wavelength in µm

Note that the units W·sr^{-1}·cm^{-2}·µm^{-1} are commonly referred to as flicks and are often used in infrared (IR) sensing. For visible, near infrared (VNIR), units are commonly W·sr^{-1}·m^{-2}·nm^{-1}, which is equal to 0.1 flick.

Also note that irradiance falls off with range (i.e. distance from the target to the entrance aperture) squared. This is because each of the two dimensions, x and y, each increase linearly with range, thus the area increases as R*R as illustrated in Figure 2-3.

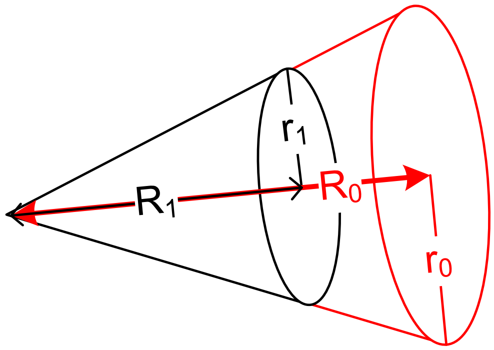

Figure 2-3. As energy from a source expands, it increases in area. The radius, r, is proportional to the distance, R, thus the area expands by R^2. Since the power (Watts) does not change, then the irradiance will reduce by R^2.

Lastly, the rule of thumb that absorption and emissivity are the same number is temperature related. If the object is cooler than the surrounding area such that it must absorb energy to reach thermal equilibrium, it will absorb based on its molecular or atomic structure. However, if it is warmer than the surrounding area such that it must release energy to reach thermal equilibrium, those same mechanisms will cause the target to emit energy in the same bands it absorbs.

In the following subsections we follow the photons from source to detector.

2.1 Targets & Backgrounds - Source Radiance

Objects either emit or reflect photons. For solids, absorptance (absorption) (α) is a measure of how much radiation is absorbed by a target, Reflectivity (ρ) is a measure of how much is reflected, and transmissivity (τ) is a measure of how much passes through the object such that:

$$\alpha(\lambda) + \rho(\lambda) + \tau(\lambda) = 1.0 \tag{2-1}$$

Notice the wavelength dependence on each of these variables. A target is reflective if the detected photons are predominantly from a source reflected off the object such as the sun reflecting off a building. Targets are emissive if the photons from the target in the sensor band are dominated by the emission from the target. Emissions are determined by temperature and absorptivity (absorption). This is because the same mechanisms that make an object absorb energy when it is colder than the surrounding area, make it emit energy when it is warmer than the surrounding area, thus, as Kirchhoff's Law indicates, absorptivity is the same as emissivity, $\varepsilon(\lambda)$ for an arbitrary body emitting radiation.

There are three types of sources, based on how the emissivity of the source varies with wavelength.

1. Selective – emissivity varies with wavelength in the spectral band of interest
2. Blackbody – emissivity is 1.0 over all wavelengths
3. Graybody – emissivity is constant, but less than 1.0 over the wavelengths of the spectral band

A selective emitter is dominated by molecular or atomic vibrations or rotations. An example is the intensity of Aluminum monoxide (AlO) from 420-580 nm as shown in Figure 2-4 (Parigger, 2023).

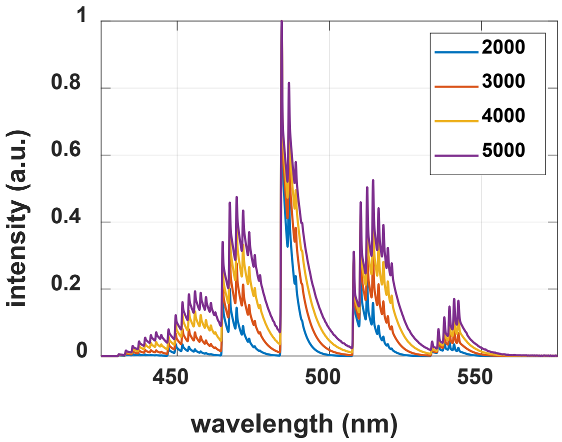

Figure 2-4. Example Aluminum Oxide (AlO) spectrum from Parriger model for four temperatures. AlO is a selective emitter or reflector

In other words, a selective emitter has an emissivity with a unique shape within the spectral region of interest. A reflective target will reflect the emissions from a source with the spectral reflectivity of the target, also dependent on the material.

One of the most important concepts described herein is blackbody radiation. In 1900, Max Planck (Planck, 1900) developed the modern theory describing radiation of a blackbody, which is fundamental to quantum theory. A blackbody is an ideal object that absorbs incident radiation while at thermal equilibrium. While a true blackbody does not exist, depending on the material, some wavelength regions (frequencies) may behave in part like a blackbody (emissivity=1). The spectral radiant exitance of a blackbody can be described based on wavelength, wavenumber or frequency as indicated in Table 2-2 (Boyd, 1983).

Table 2-2. Planck's Law for wavelength, wavenumber, and frequency in Watts.

Wavelength, λ in µm per $d\lambda$	Wavenumber, σ in cm^{-1} per $d\sigma$	Frequency, f in Hz per df
$L(\lambda,\, T) = \frac{2\cdot 10^{24}\cdot h\cdot c^2}{\lambda^5\left(e^{10^6 hc/\lambda kT} - 1\right)}$ W m^{-2}sr^{-1}µm-^{1}	$L(\sigma,\, T) = \frac{2\cdot 10^{8} h\cdot c^2\cdot \sigma^3}{\left(e^{10^2 hc\sigma/kT} - 1\right)}$ W m^{-2}sr^{-1}cm	$L(f,\, T) = \frac{2\cdot h\cdot f^3}{c^2\left(e^{hf/kT} - 1\right)}$ W m^{-2}sr^{-1}Hz-^{1}

2-2

Where:

h = Planck's constant = 6.6260693x10^{-34} W-s^{2}
c = speed of light = 2.99792458x10^{8} m/s
k = Boltzmann's constant = 1.380658x10^{-23} W-s/K

In general, a physicist might prefer wavelength, a chemist might prefer wavenumber and a radio scientist might prefer frequency, but as with all generalizations, there are exceptions. The wavelength version of equation 2-2, commonly in flicks (W·sr^{-1}·cm^{-2}·µm^{-1}) is:

$$L_{bb}(\lambda,\, T) = \frac{2\cdot 10^{16}\cdot h\cdot c^2}{\lambda^5\left(e^{10^4\cdot hc/\lambda kT} - 1\right)} \qquad 2\text{-}3$$

The integrated Planck's law over all wavelengths, into π steradians is known as Stefan-Boltzmann law and is simply:

$$L_{bb}(T) = \sigma T^4 \tag{2-4}$$

Where:

$L_{bb}(T)$ = total black body radiant emittance in W/cm^2
σ = Stefan-Boltzmann constant 5.6697±0.0029 x 10^{-12} W/cm^{2}K^4

While these units are based in Watts, often it is worth working in photons/second since most detectors convert photons to electrons. This is done by understanding the energy of a photon at a given wavelength via the Einstein-Planck relationship:

$$E = \frac{hc}{\lambda} \tag{2-5}$$

Where:

E is the energy of a photon in Joules = Watt-seconds
h is Planck's constant = 6.6260693x10^{-34} W-s^2
c is the speed of light = 2.99792458 x 10^8 m/sec
λ is the wavelength in meters

Note that 1/E has the units of photons/sec/Watt by wavelength providing this conversion factor from Watts to photons per second. Both Watts and photons/second are true radiometric units. In astronomy, the units are magnitudes which is a 2,000-year-old system based on the intensity of the star, Vega. In visible bands, units are lumens which are based on the response of the eye. Radiometric units are the most precise and are required to determine system performance.

Using the Einstein-Planck relationship, we can convert Planck's law from Watts to Photons/second such that the blackbody spectral radiant photon emittance (Q) is:

$$Q_{bb}(\lambda,\, T) = \frac{2 \cdot 10^{12} \cdot c}{\lambda^4 \left(e^{10^4 \cdot hc/\lambda kT} - 1\right)} \tag{2-6}$$

The peak wavelength is found by differentiating Planck's law and solving for the maximum. This results in Wein's displacement law:

$$\lambda_{\max}(T) = \frac{a}{T} \tag{2-7}$$

Where a= 2897.8 µm-K for Watts (equation 2-3) and a=3669.73 µm-K for photons/sec (equation 2-6). The remaining descriptions in this section are with respect to wavelength and either Watts or photons per second.

Figure 2-5 shows the Normalized and absolute Planck curves (Watts) for five temperatures with units of flicks.

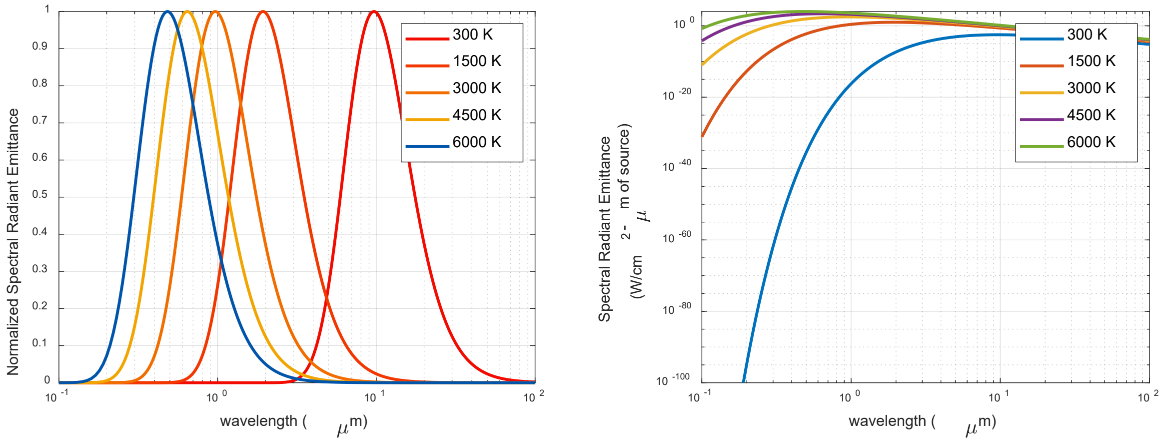

Figure 2-5. Normalized Planck curves showing the peak wavelength shift subject to Wein's law (LHS). Absolute Planck curves showing extreme variation in energy subject to Stefan-Boltzmann Law (RHS).

The normalized curves clearly show the peak wavelength subject to Wein's displacement law. The absolute curves show the temperature to the fourth dependence in Stefan-Boltzmann law.

We now must convert the ideal blackbody to a graybody or selective source which depends on spectral emissivity or reflectivity. The graybody emittance is just the blackbody times the spectral emittance such that:

$$L(\lambda,\, T) = L_{bb}(\lambda,\, T)\cdot\varepsilon(\lambda) = \frac{2\cdot 10^{16}\cdot h\cdot c^2\cdot \varepsilon(\lambda)}{\lambda^5\left(e^{10^4\cdot hc/\lambda kT}-1\right)} \tag{2-8}$$

For a reflective target, we replace $\varepsilon(\lambda)$, with the spectral reflectance, $\rho(\lambda)$, of the object reflecting the emissions from another source.

2.2 Path Effects

Path effects include propagation of the source spectral radiant emittance to the entrance aperture of the optical system along with any atmospheric effects. These include:

- Propagation of photons
- Atmospheric attenuation
- Atmospheric turbulence & scattering

We only briefly discuss each of these in this section.

2.2.1 PROPAGATION OF PHOTONS

We propagate the energy from equation 2-8 to the entrance aperture. For any target, ignoring atmospheric attenuation, spectral irradiance at the entrance aperture is:

$$H(\lambda,\, T) = \frac{L(\lambda,\, T)\cdot A_s}{R^2} = \frac{J(\lambda,\, T)}{R^2} = \frac{M(\lambda,\, T)\cdot A_s}{\pi\cdot R^2} = \frac{M(\lambda,\, T)\cdot \phi_{\text{tar}}^2}{\pi} \tag{2-9}$$

here:

H is the spectral irradiance in W/cm^2-µm of aperture area
J is radiant intensity in W/sr-µm

L is radiance in W/sr-cm^2-µm
M is radiant exitance in W/cm^2-µm of source area
A_s is area of source, in cm^2
R is range in cm
ϕ_{tar}^2 is the steradian subtense of the target at range, assuming a small angle

Note that we divide by pi and not 2-pi since most objects in imaging bands are Lambertian. A Lambertian source does not change in intensity based on view angle or distance which results in the source radiating into pi-steradians. Smith includes the pi-steradian derivation in his book (Smith, 1966, pages 184–185).

2.2.2 Atmospheric attenuation (transmission)

Equation 2-9 is often affected by the transmission through the atmosphere. The main model for estimating atmospheric transmission is MODTRAN (MODerate resolution atmospheric TRANsmission) (Berk, 2014). Originally developed as LOWTRAN as a collaboration between Spectral Sciences Inc (SSI) and the Air Force Research Laboratory (AFRL), this model computes line-of-sight (LOS) atmospheric Spectral transmittances and radiances from UV through long wave IR (LWIR). It includes the effects of molecular and particulate absorption/emission and scattering, surface reflections and emission, solar/lunar illumination, and spherical refraction. It uses the high-resolution molecular absorption (HITRAN) database (Gordon, 2022). The HITRAN database is also useful for examining narrow spectral lines and is a compilation of spectroscopic parameters used to predict and simulate the transmission and emission of light in the atmosphere.

MODTRAN was originally developed in FORTRAN and required precise 'cards' to be included in text files with exact spacing and number of lines between input parameters. The new version 6 now includes a GUI which is easier to use but is no longer free. MODTRAN requires an NDA and must be requested from AFRL. An example MODTRAN output run from their on-line demo is provided in Figure 2-6.

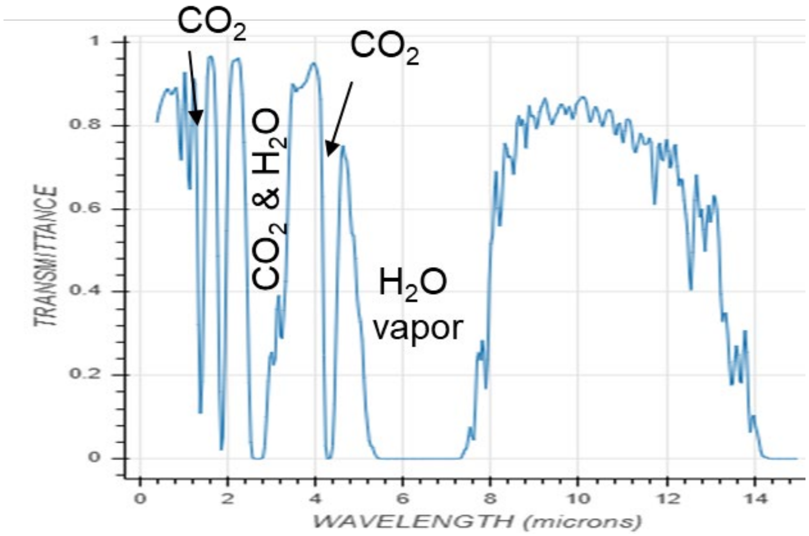

Figure 2-6. MODTRAN output for Mid-latitude summer, rural, 23km Visibility and 1km path length.
http://modtran.spectral.com/modtran_home#plot

While MODTRAN provides spectral transmission over a chosen band, it is sometimes nice to have a single transmission number when doing quick calculations. Simplified Beer-Lambert's Law using the extinction coefficient, α, with path length, R is useful for these calculations.

$$T = e^{-\alpha R} \qquad 2\text{-}10$$

A modified version that includes variation of transmission with path length (added variable β) is:

$$T = e^{-\alpha R^{\beta}} \qquad 2\text{-}11$$

The variables $\alpha \; and \; \beta$ are often derived from MODTRAN for specific bands of interest.

2.2.3 Turbulence

Atmospheric turbulence can significantly impact the ability to visualize an object. In astronomical applications this is called atmospheric seeing. No matter how good your sensor is if the turbulence is bad, you will never be able to focus well. This is because the total resolution limit, known as the point spread function (PSF, see section 2.4.1 for more details on PSF) is the convolution of the PSF of the sensor system with the PSF of turbulence. For many applications, effects of turbulence are insignificant in the estimation of system performance, but it can be very important for:

- Vibrometers & laser-based systems
- Imaging over long-range horizontal paths and
- Astronomical applications.

In the Infrared turbulence is much less a factor than in the visible bands since the strength of turbulence is inversely proportional to $\lambda^{6/5}$. Books and other references are available on the topic of atmospheric turbulence (Kolmogorov, 1941, Tatarski, 1971). This section is limited to simple methods to model turbulence. The split-step propagation approach involves splitting the path into multiple steps and modifying the wavefront (as a Green's function) with a phase screen at each step. The development of the phase screens is based on the Kolmogorov Ansatz such that the three-dimensional power spectral density of the turbulence is:

$$\varphi(\kappa) = \sqrt{2\pi \cdot 0.033 \cdot 6.88/2.91 \cdot r_0^{-5/3} \cdot \kappa^{-11/3}} \qquad 2\text{-}12$$

Where r_0 is the coherence radius and $\kappa = 2\pi/\lambda$ where λ is the wavelength.

Manipulation of this equation, and defining $M \equiv \Delta k_x/\Delta k_y$ such that $\Delta k_x \; and \; \Delta k_y$ are spatial frequency deltas produces the implemented equation:

$$\varphi(m,n) = (2\pi \cdot 0.033 \cdot 6.88/2.91)^{0.5} \cdot M^{-0.5} \cdot (X/r_0)^{5/6} \cdot [(m^2 + n^2) \cdot (2\pi)^2/M^2]^{-11/12} \qquad 2\text{-}13$$

Where m and n are the location in the grid and X is the size of the grid in the same units as the coherence radius. A random seed randomizes the results for every run. An example phase screen generated with this method is shown in Figure 2-7.

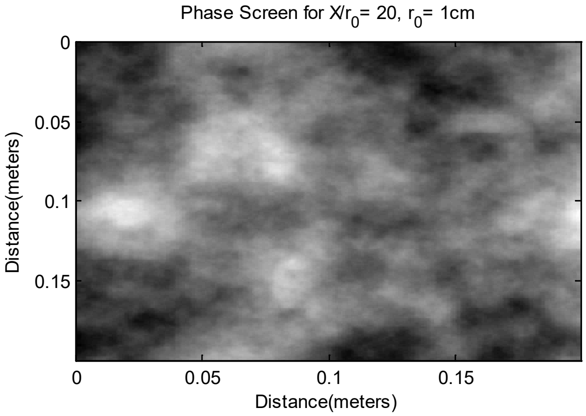

Figure 2-7. Example phase screen. Note that it looks like clouds which are also 'turbulent'.

An example of a Gaussian beam propagated through one kilometer of turbulent path for this same screen is shown in Figure 2-8.

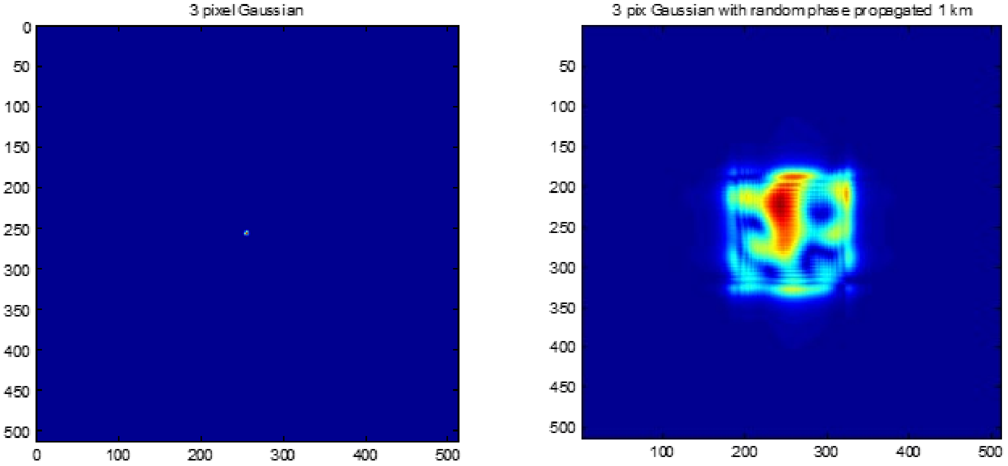

Figure 2-8. An example of a Gaussian laser beam scattering from a target at 50 meters range (left) and at 1000 meters (right) propagated using the split-step method. Note that the turbulence causes extreme scattering.

A simpler and much less computationally intensive method to model the point spread function (PSF) of turbulence was developed by Nelson (2000). For turbulence, the long-time PSF can be modeled as the Fourier transform of the Optical Transfer Function (OTF) of turbulence as:

$$psf_{\text{turb}}(\theta) = \mathcal{F}\left[e^{-3.44\left(\frac{r(\theta)}{r_0}\right)^{5/3}}\right] \qquad 2\text{-}14$$

Scaling the PSF to angle space is based on the relationship between r_0 and the seeing limit, ϕ_{turb}. This PSF can then be convolved with the PSF of the system. See section 4.2 for an implementation of this method.

2.3 INDEX OF REFRACTION AND DIELECTRIC CONSTANT

Section 2.1 described sources including how reflectivity and absorptivity (absorption) impact the received or emitted photons. This section will give the reader a slightly better understanding of material characteristics' relationship to these key optical parameters.

Materials have natural vibrational frequencies related to their structure. If a force disrupts the natural state of an atom or molecule, the restoring force will have a harmonic oscillation with the eigen frequency (the natural frequency of the system) that is the plasma frequency, ω_p. See section 4.8 for more details on this. When the incoming photon energy matches a vibrational frequency, it is absorbed and transitioned to a higher energy state, thus absorbing that energy. Materials behave as conductors, insulators, or liquids. Materials have two key parameters, which ultimately relate back to these natural frequencies and thus back to the optical parameters of interest:

- Permittivity (Farads/meter), ε, describes the ability of a material to hold a charge.
- Permeability (Henry/meter), μ, describes the ability of a material to form a magnetic field.

Permittivity and permeability describe the relationship between the electric and magnetic fields in a material. Permittivity is related to the ability of a material to store charge while permeability is related to the ability of a material to form a magnetic field. Relative permittivity (also known as dielectric constant, ε) is the ratio of the permittivity of the material to that of that of a vacuum ($\varepsilon_0 = 8.8541878188 \times 10^{-12}\mathrm{Farads/m}$). The same is true for relative permeability. For non-magnetic materials where the relative permeability is one, it can be proved that the unitless dielectric constant, is directly related to the index of refraction, as:

$$\varepsilon = \varepsilon' + i\varepsilon'' = (n + ik)^2 \qquad \text{2-15}$$

Where ε' and n are the real parts and ε'' and k are the imaginary parts of the dielectric constant and refractive index. Note that the real and imaginary parts are interdependent and follow a Kramers-Kronig relation.

The imaginary part of these variables results in absorption while the real part describes whether the material will store (capacitive, refraction of light, phase velocity) or resist holding (inductive) electric charge (attenuation of light, extinction). Alternatively, index of refraction is:

$$n + ik = \sqrt[2]{\varepsilon' + i\varepsilon''} \qquad \text{2-16}$$

For a non-magnetic material, the loss tangent that may be available in literature in lieu of ε'' is:

$$\tan(\delta) = \frac{\varepsilon''}{\varepsilon'} \qquad \text{2-17}$$

Work function depends on the configuration of the atoms on the material surface; thus, it has some relationship to dielectric constant. Work function tends to decrease as dielectric constant increases. Materials with a higher dielectric constant have more ability to polarize and distribute charges, thus the electrons can more easily escape, decreasing the work function (Zou, 2020).

Absorption and reflection at an interface can be computed using Fresnel's equation (Paschotta, 2024) which depend on index of refraction, incident angle, and polarization. If polarization effects can be ignored, reflection is be computed as:

$$\rho = \left(\frac{n_1 - n_2}{n_1 + n_2}\right)^2 \qquad \text{2-18}$$

An excellent *n* and *k* database is located at:

https://refractiveindex.info/?shelf=main&book=Al&page=Rakic/. This is useful when looking for spectral response of materials. It provides journal references along with curves for *n* and *k* plus corresponding dielectric constants.

Absorption and emission spectra are available at:

https://www.spectraplot.com/. This database uses HITRAN, HITEMP, ExoMol, and Pacific Northwest National Laboratory (PNNL) spectra.

Atomic spectra can be found at: https://www.nist.gov/pml/atomic-spectra-database.

2.4 Sensor Systems

Optical system components vary depending on the application. Figure 2-9 shows an optical sensor system that consists of an optic (lens, telescope, pinhole) that focuses the energy onto a sensor (focal plane array, FPA). The FPA consists of a detector that converts the incoming photons per second to current (electrons/second) via quantum efficiency, fill factor (QEFF) and a transimpedance amplifier that converts the electrons/second (current) to voltage. Voltage is converted to counts or digital number (dn) via an Analog to digital (A/D) converter. Depending on the application, an optical filter may be included. Optical filters for a visible or Near IR (VNIR) system may be placed in front of the optic, but for IR systems the filter should be placed between the last optical element and the detector (or at a pupil where the rays are parallel) to minimize the halo that occurs from emissions from the filter.

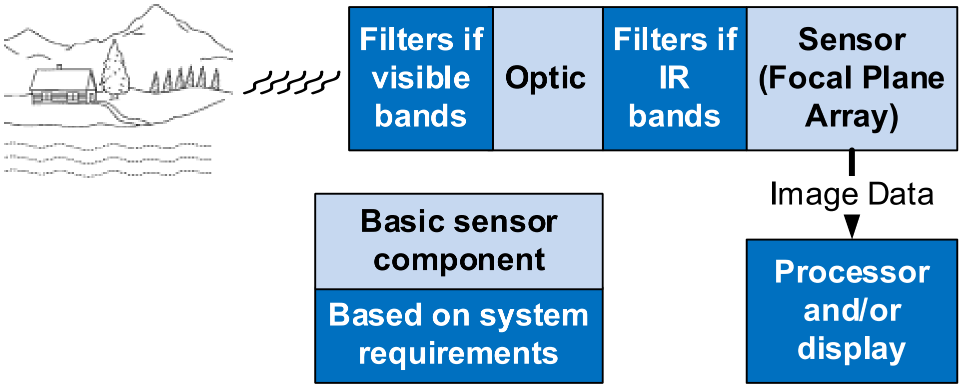

Figure 2-9. Sensor system components discussed in this section. If an optical filter is needed, it may be placed in front of the optic for VNIR applications but must be placed internal to the system for IR applications. This is because the filter will produce photons due to its temperature and emissivity. If in front of the sensor a halo will occur due to the difference in distance to the entrance changing with angle.

Main optical system types are summarized in Table 2-3.

Table 2-3. Sensor types discussed herein.

Technology	Application
Single band imager	Spatial information in a single band. This can be broad band, such as a typical monochrome camera or a selected band by inserting a filter on the camera.
Single pixel Spectrometer	Spectral information per pixel which shows species within that integrated pixel.
Multispectral Imager	Spatial information in 2 or more bands. A cell phone camera with three colors (red, green, and blue) is a multi-spectral imager.
Hyperspectral Imager	Spectral and spatial information for location and identification of selective emitters/reflectors (species).

Specification of the correct system components is critical to both performance and cost. A system may or may not have an optical filter, grating, or other spectral selection component. Imaging system requirements are typically those listed in Table 3-1.

Table 2-4. Key imaging system specifications: Modeling helps determine best components.

Requirement	Description	Determined by
Instantaneous Field of View (IFOV)	Angular resolution of a pixel	Pixel size, effective focal length (EFL)
Field of View (FOV) aka Field of Regard (FOR)	Total angular coverage of an optical system	FPA size, EFL
Signal to Noise Ratio (SNR)	Captured electrons from the desired target divided by the noise electrons	Electrons captured, FPA read noise, FPA dark current, shot noise (sqrt of electrons captured), thermal noise of optics
Angular resolution	The smallest angle that can be resolved	The convolution of the optics blur circle and the IFOV, Rayleigh limit
Frame rate	Rate at which images are captured	Selected detector
Integration (exposure) time range	Amount of time required for the system to integrate the photons	Selected detector, desired SNR, system noise
Dynamic range	Intensity range that can be captured with a desired exposure time	Electrons captured vs detector well depth (maximum electrons)
Crosstalk	Can be optical or pixel to pixel (electrical) bleed through from one pixel to the next	Optical system and detector – often can be ignored.
Depth of field	The amount the object can move with respect to the sensor and still be in focus	Aperture, acceptable blur and distance from the entrance aperture to the object

The line spread function (LSF) of an imaging system is the convolution of the blur circle with the pixel. The point spread function (PSF) is the 2-D version.

It is important to know if you are designing a system for sub-resolution or resolvable targets. A sub-resolution (point) source is a target that does not fill a pixel. A resolvable or extended source overfills a pixel. For a point source, the photons that land on a pixel rely on aperture size. This is why astronomers use large aperture systems with higher f-numbers but imaging systems must have a low f-number. The general expression for photons from a point source that impinge on a pixel is:

$$q_{\text{point}} = \frac{Q \cdot A_s \cdot A_o \cdot T_o \cdot t_{\text{int}} \cdot CE}{\pi R^2} = \frac{Q \cdot A_s \cdot \Omega_{\text{source}} \cdot T_o \cdot t_{\text{int}} \cdot CE}{\pi} = \frac{Q_{\text{tar}} \cdot \phi_{\text{tar}}^2 \cdot T_o \cdot t_{\text{int}} \cdot A_o \cdot CE}{\pi} \qquad \text{2-19}$$

Where:

- q_{tar} is the number of photons on a detector from the target
- Q is the in-band radiant photon flux *from* the source in photons/sec-m^2 (including atmosphere and reflectivity)
- A_o is the area of the entrance aperture
- T_o is the optics transmission,
- t_{int} is the exposure time,
- ϕ_{tar}^2 is thus the steradian subtense of the target,
- CE is the collection efficiency based on the portion of the PSF impinging on a pixel, when optimized based on the Rayleigh limit, this will be about 0.33,
- $A_s\Omega_{\text{source}} = A_s A_o / R^2$ is the etendue of the source.

Etendue ($A_s\Omega_{\text{source}}$) describes the ability of a source to emit light or the ability of an optical system to accept light. It is often used in the development of non-imaging systems such as spectrometers where the etendue of the system should match that of the source. We have split etendue in equation 2-19 to aid the reader in understanding how it impacts the detected photons.

For an extended source, the photons onto the pixel are independent of aperture size and only rely on f-number and pixel area. That is why when you look at a white wall it is the same brightness no matter the distance to the wall. This is because the photons into the pixel for an extended source are limited by the projected area of the pixel at range. Since all the blur circles of the optical system overlap, the collection efficiency for an extended source is 1.0. This means that we replace ϕ_{tar}^2 with the steradian subtense of the pixel in equation 2-19, we can derive the classic inverse proportionality of photons to f-number squared.

$$q_{\text{ext}} = \frac{Q \cdot \phi^2 \cdot T_o \cdot t_{\text{int}} \cdot A_o}{\pi} = Q \cdot \frac{A_p}{\pi f^2} \cdot T_o \cdot t_{\text{int}} \cdot A_o = Q \cdot A_p \cdot T_o \cdot t_{\text{int}} \cdot \frac{\pi \, D^2/4}{\pi f^2} = \frac{Q \cdot A_p \cdot T_o \cdot t_{\text{int}}}{4 f\#^2} \qquad \text{2-20}$$

Where:

- q_{ext} is the number of photons on a detector from an extended source
- f is the focal length of the optical system
- D is the diameter of the entrance aperture s.t. $A_o = \pi \, D^2/4$
- A_p is the pixel area
- $\phi^2 = \frac{A_p}{f^2}$ is the steradian subtense of the pixel
- *f#* is the f-number of the optic
- $A_o\Omega_{\text{pixel}}$ is the maximum etendue of the system.

Note that the maximum etendue of the system is $A_o\Omega_{\text{pixel}}$ is not the same as the etendue of the target, $A_s\Omega_{\text{source}}$.

This section will briefly discuss optics and detectors. This is not a guide to designing optics or detectors, but a guide to what is important in the selection of parts when designing an electro-optical system.

2.4.1 OPTICS

Optical systems can be reflective (telescope) or refractive (single or multi-element lens). Key optical parameters are effective focal length (EFL), aperture size or f-number and point spread function (PSF). These parameters dictate the angular resolution limit, the depth of field and the depth of focus. Depending on the lens, the spatial domain will map to angle differently. Basic lens mappings are:

- F-Theta map where height or width is proportional to field angle – fisheye lens
- Tangent map – produces the flat image we typically see, spatial dimension goes with the tangent of the angle
- Tailored distortion used in some fisheye lenses where the edges are important
- Fovea lenses which mimic the eye with higher resolution in the center than the edges

The PSF is convolved with the detector to determine the total image resolution. For very wide-angle system, the PSF is critical. The optical transfer function (OTF) is the Fourier transform of the PSF. The real part of the OTF is the modulation transfer function (MTF) and the imaginary part is the phase transfer function (PhTF). Lens manufacturers often provide the MTF as it represents the magnitude of the response of an optical system to different spatial frequencies and can be used to identify an optical system's spatial resolution, but it cannot be used directly in a model. It is often difficult to get a PSF from a manufacturer, thus we often estimate the perfect, diffraction limited, case with an Airy disk such the one-dimensional line spread function (LSF) as:

$$l_{\text{diff}}(\theta) = \left[\frac{2J_1(\pi D\theta/\lambda)}{\pi D\theta/\lambda}\right]^2 \qquad \text{2-21}$$

Where:

l_{diff} = the LSF which is the normalized response to the peak at θ=0
θ = angular radius
D = primary aperture diameter
J_1 = order 1 Bessel function of the first kind
λ = wavelength

The Rayleigh criteria for angular resolution is *half* the Airy disk size assuming a system that is relatively aberration free. This provides a about a 20% contrast between spots as is seen in Figure 2-10 (Smith, 1966).

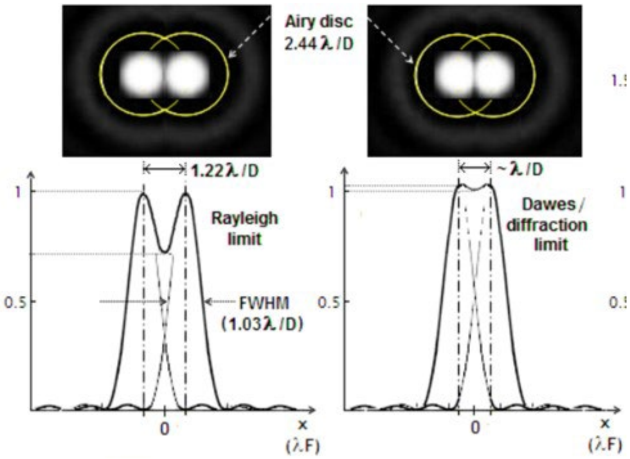

Figure 2-10. Rayleigh criteria. (reused from Sacek, 2018).

These angular resolution criteria are often computed as:

$$\alpha_r = 1.22 \cdot \lambda / D \qquad \text{2-22}$$

where α_r is the Rayleigh angular resolution, D is the aperture diameter and λ is band centered wavelength. The distance between spots, d_r, is computed as

$$d_r = 0.61 \cdot \lambda / NA = 1.22 \cdot \lambda \cdot f\# \qquad \text{2-23}$$

Where *NA* is the numerical aperture and *f#* is the f-number of the optical system.

To resolve two spots on a detector array, we assume the Nyquist criteria such that the pixel width is half the spot size. For an astronomical telescope or long-range horizontal paths, we must consider atmospheric turbulence effects. In astronomical systems, this is called the seeing limit. Understanding the seeing limit is important to not overdesigning a system since the seeing limit can dominate system spatial resolution. If the telescope diffraction limit is smaller than this seeing limit, the selected size of the detector pixel size will be dictated by the seeing limit as.

$$d_{\text{pix}} \sim \max(2 \cdot \mathrm{d}_r, \alpha_s * f) \qquad \text{2-24}$$

Where d_{pix} is the size of the pixel, α_s is the seeing angular resolution, and *f* is the focal length of the optical system. Some detectors can bin pixels to reduce noise. With binning, these sizes should be cut by the binning size.

2.4.2 DETECTORS

There are two basic classes of detectors, *photo detectors and thermal detectors*. Rogalski provides a good summary in his 2004 paper “Optical Detectors for focal plane arrays” (Rogalski, 2004) although new CMOS detector types have been developed since then.

The approximate wavelength range vs detector material and class/type commonly used in spectrometers and imaging systems are shown in Table 2-5 and Table 2-6.

Table 2-5. Detector types commonly used

Detector Material	Wavelength Range	Detector Class/Type
Silicon	200-1100 nm	Photo, PV
InGaAs (technology dependent)	800-1550, 1700 or 2200 nm	Photo, PV
Ge (technology dependent)	800-1550 or 1800 nm	Photo, PV
PbS	1-2.8 µm (typically single pixel)	Photo, PC
PbSe	1-4.5 µm (typically single pixel)	Photo, PC
InSb	2-5.5 µm	Photo, PC
HgCdTe (MCT)	2-20 µm	Photo, PC
Vanadium Oxide (Vox)	7.5-14 µm, but can be tuned	Thermal, Bolometer
Amorphous Silicon	7.5-14 µm	Thermal, Bolometer

Table 2-6. Survey of detector technologies and materials

Detector Type	Method of Operation	Materials
Photo - Intrinsic, inter-band	Photoconductive (PC)	AlGaN, Si, GaAs, PbSe, InSb, HgCdTe
	Photovoltaic (PV)	AlGaN, Si, InGaAs, InSb, HgCdTe
	Capacitance	Si, GaAs, InSb, HgCdTe
	Photoelectromagnetic (PEM)	InSb, HgCdTe
Photo - Extrinsic, Impurity in band	Photoconductive (PC)	Si:In, Si:Ga, Ge:Cu, Ge:Hg
Photo - Free Carriers, intraband	Photoemissive	PtSi, Pt2Si, IrSi Schottky barriers, GaAs/CsO
	Photoconductive (PC)	InSb electron bolometer
	Photon-drag	Ge
Photo - Quantum Wells	Photoconductive (PC)	GaAs/GaAlAs, InSb nipi
	Photovoltaic (PV)	InAs/InGaSb SLS
Thermal - Bolometer	Change in electrical conductivity	Vanadium Oxide (Vox), Amorphous Silicon
Thermal - Thermocouple/ Thermopile	Voltage from change in temperature of the junction of two dissimilar materials	Pt/Rh, Ni/Cr - constantan, F/Constantan, Ni/Cr, Ni/Al, Nicrosil/Nisil, Cu/Rh. Bi/Sb for thermopiles
Thermal - Golay cell/Gas microphone	Thermal expansion of gas	Xe gas with photo detector, often used for THz detection

When dealing with detectors in different wavelength ranges, the specified parameters may differ. The discussion in this book is limited to photo voltaic (PV), photoconductive (PC), and bolometer detectors.

2.4.2.1 *Visible, Near IR and SWIR*

Visible, Near IR (VNIR) detectors will typically have specifications as shown in Table 2-7. These sensors (detectors) are then coupled to the appropriate optic (lens or telescope).

Table 2-7. Key specifications for silicon based (VNIR) detectors

Requirement	**Typical units**	**Notes**
Exposure time range	Seconds	This dictates the photons on the detector
Frames per second (fps)	Seconds^{-1}	Revisit rate is important. For an explosion, must be very fast, for situational awareness can be standard 30fps
Maximum bins	unitless	Binning allows beating down noise, particularly for astronomical applications
Read Noise	electrons	For short exposures, this dominates the noise
Dark Current	Electrons/second	For long exposures, this dominates the noise
Pixel size	µm	Dominates resolution limit
Well Depth	electrons	Determines dynamic range
Number of Bits	unitless	Most detectors' dynamic range is limited to 10 bits, noise bit should be second or third bit, ideally have 12 bits or better.
Spectral Response	Amps/Watt or electrons/photon	A curve that is A/W or electrons/photon vs wavelength
Number of pixels H x V	unitless	1080p is 1920 x 1080 for example
% area fill	Percent	Not all detectors use the full pixel area as the active area. This is important for maximizing the total electrons.
Detector Type	CMOS, Charge coupled device (CCD)	Complementary Metal-Oxide-Semiconductor (CMOS) each pixel is read out directly. CCDs shift the charge per pixel to a read out. CMOS has advantages over CCDs with higher resolution, faster readout speeds, lower power consumption and lower cost. CCDs have lower system noise, higher % area fill, and higher cost.

Color cameras are a special case of visible cameras that create color pictures using a CMOS (or CCD) detector array that has filters (also known as a Bayer filter or mask) on individual pixels. A common RGGB arrangement is shown in Figure 2-11.

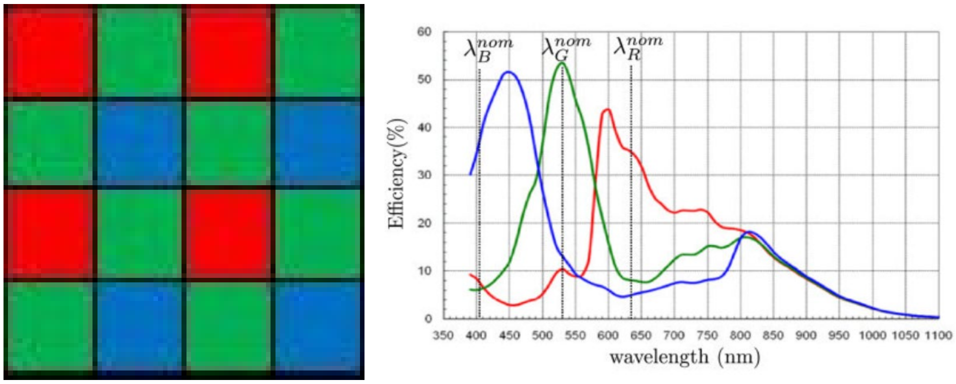

Figure 2-11. Pixels of a Bayer Mask (left), Example spectral response for a Basler camera (right). Note that the response of the detector goes out past 750 nm. Most cameras have an IR cut filter to remove the longer wavelengths to match the eye response.

To make the colors look like the human eye, an IR cut filter is often placed in the camera to remove wavelengths above 750 nm. Figure 2-11 shows the response without the IR cut filter.

Raw Bayer data has the same number of pixels as the equivalent gray scale camera which would be N × M × 1 (rows × columns × number of colors). To create the color image, the raw data is processed using color reconstruction, also called demosaicing. This uses an interpolation method to 'fill in' the missing red, green or blue pixels so that the new image is N x M x 3. An example of a raw image and the corresponding demosaiced image using bi-linear interpolation are shown in Figure 2-12 left and right respectively.

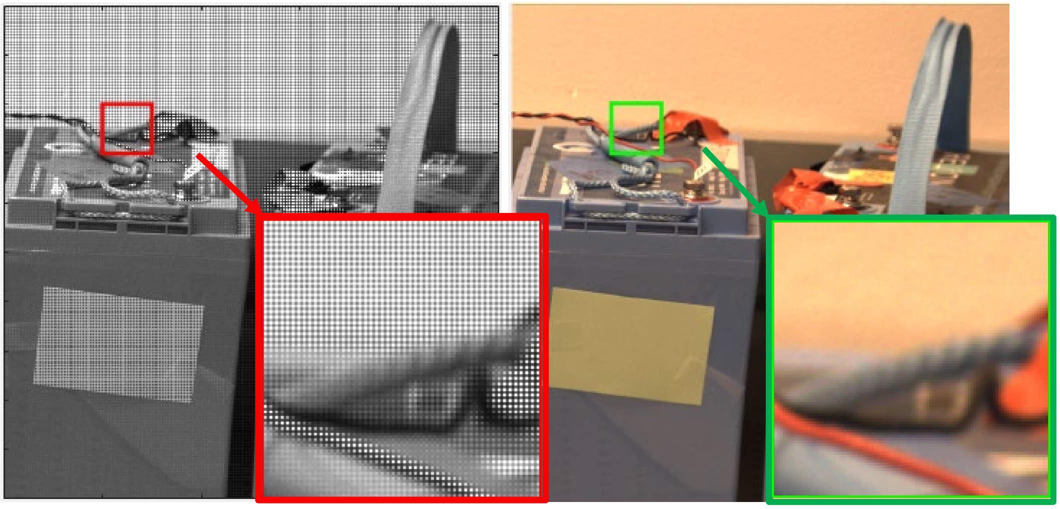

Figure 2-12. Raw image (left); note that the checkerboard pattern in the zoomed-in area indicates the difference in the intensities of the colors. The demosaiced image shows some artifacts at the edges of different color areas to imperfections in the interpolation method.

A trade for the best interpolation method for clarity versus speed is usually done. Custom cameras with more than three bands are available from some manufacturers. While these color cameras have the same number of RGB pixels once processed as their grayscale counterpart, the resolution is about 1.5 times worse instead of two times worse due to the interpolation methods.

2.4.2.2 Thermal (infrared) detectors

Infrared detectors use a different set of variables to specify system performance. These are summarized in Table 2-8.

Table 2-8. Key specifications for Infrared detectors.

Requirement	Typical units	Notes
Exposure time	Seconds	This dictates the photons on the detector
Frames per second (fps)	Seconds^{-1}	Revisit rate is important. For an explosion, must be very fast, for situational awareness can be standard 30fps
Noise NEDT or NEP or Detectivity (D*)	 Kelvin Photons/sec or W cm Hz$^{1/2}$W^{-1}	Noise equivalent delta temperature Noise equivalent irradiance at detector, gives SNR=1 The inverse of noise equivalent power into 1 Hz bandwidth (Δf)
Pixel size	µm	Dominates resolution limit
Well Depth	electrons	Determines dynamic range.
Number of Bits	Unitless	Most detectors can't do better than 10 bits, but you usually want your noise bit to be the second or third bit, so ideally you have 12 bits or better for an instrument.
Relative Spectral Response	Unitless	A curve that is response vs wavelength from 0 to 1.0
Number of pixels H x V	unitless	640 x 512 for example for a microbolometer
Detector Type	unitless	Microbolometer (uncooled), InSb (cooled), HgCdTe (cooled) are examples of imaging IR sensor types, SiGa, thermopile, thermistor are some examples of single for linear detectors.

Sensitivity specifications can be confusing. NEP (Noise Equivalent Power) is the radiant power that produces an SNR of one at the detector output. It Is often defined at a particular chopping frequency, or noise bandwidth Δf and has the units of $W/\sqrt{Hz}$ or Watts if the specified bandwidth is one-Hz. A lower NEP is associated with a more sensitive detector. Noise equivalent irradiance (NEI) at the detector is $\mathrm{NEI} = \mathrm{NEP}/A_p$.

D-Star (D*) can be used to compare performance of different detector types. A higher D* is associated with a more sensitive detector. It is normalized to the detector size such that it has units of $cm\sqrt{Hz}/W$ and is equal to $\sqrt{A_p.\Delta f}/\mathrm{NEP}$ (Keim, 2018). These relationships are summarized in Table 2-9.

Table 2-9. Relationship between specified values and noise equivalent irradiance (NEI)

Sensitivity specification	**Relationship to Noise Equivalent Irradiance (NEI)**
Noise Equivalent (NEP)	$NEI = NEP/A_p$
Detectivity (D*)	$NEI = \frac{\sqrt{\Delta f}}{\mathrm{D}\cdot\sqrt{A_p.}}$
Noise Equivalent Delta Temperature (NEDT)	$NEI = \left(W(T+\mathrm{NEDT}) - W(T)\right)$

3 Uncertainty Analysis

This section briefly discusses uncertainty analysis. Without an understanding of uncertainties, measurements or models are useless since there is no basis to determine if the result is meaningful.

Uncertainties fall into two categories:

- **Systematic uncertainty**: A repeatable error that causes the result (measurement, model output) to be too large or too small. This is effectively a bias and is related to accuracy, or how far a result is from the 'true' value. Drift, lag time, and hysteresis are examples of systematic uncertainties. Parallax between different sensor systems results in pointing error which falls into this category.
- **Random uncertainty**: A variation in a result that occurs without a predictable pattern. This is an error that can usually be derived from statistics and is related to precision or the spread of measured values. This is often assumed Gaussian but may follow other distributions.

There are two basic ways to evaluate uncertainties. **Statistical evaluation** is the simplest as it involves statistical analysis of observations. For optical systems, noise can be evaluated using data that does not have the target in the data. Alternatively, if many observations are made, assuming a Gaussian (or appropriate) distribution, a standard deviation can provide this answer. Number of standard deviations will inform the final uncertainty. If possible, having data with and without the object of interest allows a better estimation of this error. Alternatively, for imaging sensors removing all large objects can provide an estimate of sensor noise without taking dark data (see section 7.2.3 for example filter).

The second method is **other than statistical evaluation**. This is often used for determining the uncertainty of models, a circuit or an instrument and includes systematic uncertainty. For measurements, this involves having some form of truth data.

Most guides describe how to determine uncertainties (or errors) on a measurement, but there are instances where one must determine model or instrument uncertainties that include multiple components. For all methods, error propagation is key.

When modeling a system that is composed of characterized components, the modeler propagates the errors through the system model using the model equations. Often, the uncertainties will combine differently in each direction, which provides an indication of bias. This is also true when characterizing a system where there are uncertainties that propagate to the final result. A simple example of this type of error analysis for a spectrometer system is shown in section 5.2.3.

For physics-based models this may be more difficult since the uncertainties on the input data may not be well known, or assumptions may not be correct. A common method to determine uncertainties is a parametric study, where the input parameters are varied as dictated by the physics. Monte-Carlo simulations that result in an answer for each parametric case are then combined statistically to determine the expected error. These types of parametric studies can also indicate the most important parameters in the model result.

Excellent sources on uncertainty analysis are located in the:

- "Measurement and Uncertainty Analysis Guide" published by UNC Chapel Hill (https://users.physics.unc.edu/~deardorf/uncertainty/UNCguide.pdf) and
- National Institute of Standards (NIST) guide (Taylor, 1994). An uncertainty calculator is located at https://physics.nist.gov/cuu/Uncertainty/index.html.

4 Example Sensor Models

The department of defense has employed a modeling pyramid for years (AFRL, 2023). This pyramid provides a way to model high level missions with systems engineering credibility. An example pyramid is shown in Figure 4-1.

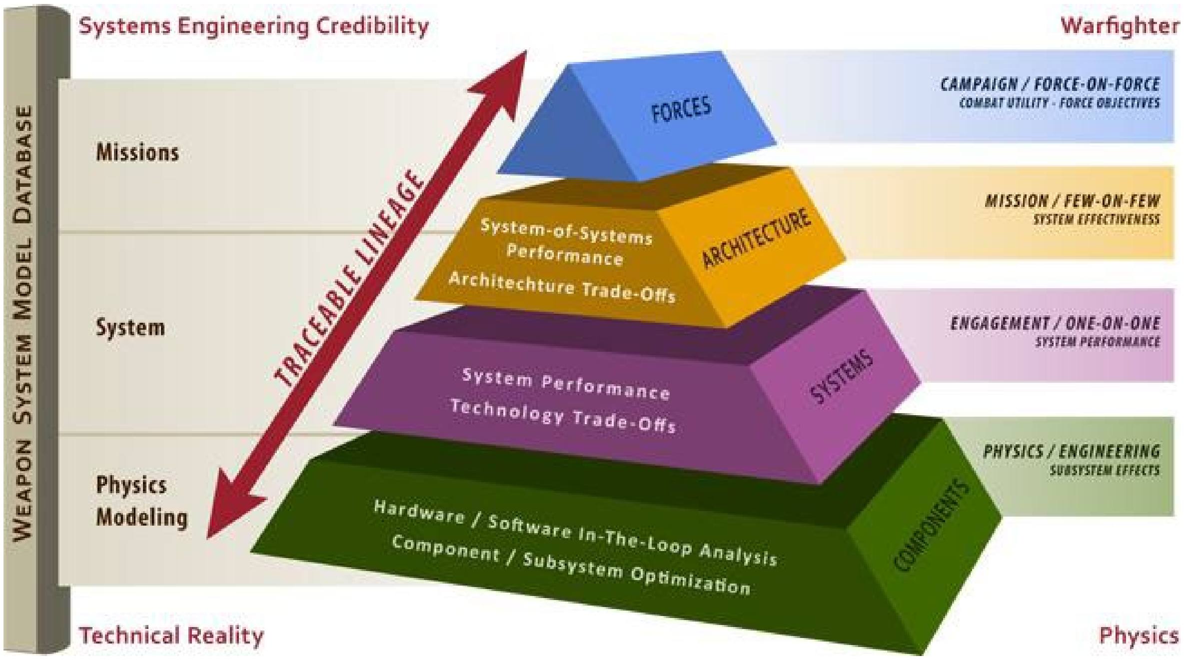

Figure 4-1. Modelling pyramid. Low-level, high-fidelity Engineering physics models create outputs that can be fed into engagement models. The result of a single engagement feeds into a mission model, which goes to the lowest fidelity, highest complexity, campaign model. In this way, the most accurate campaign result can be achieved (AFRL, 2023).

As an example, for aircraft survivability, physics models may include on-board sensors, threats, atmosphere, aircraft, etc. These individual models then feed a system model for a one-on-one scenario. The results of many cases of the one-on-one are combined in the Mission (few-on-few) model. These then feed into a campaign model. When done properly this is a powerful tool for predicting outcomes. Unfortunately, the interfaces between the levels are often not well defined.

In this section we discuss low level physics/engineering models with outputs that are common to most applications. We focus on electro-optical infrared (EO/IR) modeling.

One of the most important things in developing a model is defining inputs and outputs that are traceable to experiments for model validation.

4.1 Infrared Sensor Models

For this model we carefully define the inputs based on the specifications of the sensor components. We then define the three main output parameters of interest which are easily measured:

1. Spatial resolution versus range, the smallest object that can be imaged
2. Total Field of Regard (FOR)
3. Depth of field, which is the amount of distance the object can shift and still be in focus.

4. Signal to noise ratio and contrast ratio versus temperature and range to target

4.1.1 Spatial Resolution versus range

Spatial resolution is the smallest object that can be resolved. It is dependent on the instantaneous field of view (IFOV) of the sensor combined with the optics blur. For this model, we assume that the blur circle of the optic and the detector pixel size match such that the pixel size can be used for the resolution cell. Thus, the spatial resolution for a target at range, R, is:

$$d_{\mathrm{min}} = \frac{R \cdot d_{\mathrm{pix}}}{f} \tag{4-1}$$

Where:

d_{pix}	pixel size
f	optic effective focal length
R	range to source in meters

Note that the IFOV, ϕ_{pix} assuming square pixels and a tangent map lens is simply:

$$\phi_{\mathrm{pix}} = \mathrm{atan}\left(\frac{d_{\mathrm{pix}}}{f}\right) \tag{4-2}$$

When ϕ_{pix} is small or we are using a theta map lens, it can be approximated as d_{pix}/f.

4.1.2 Total Field of Regard (FOR)

Total field of regard (FOR) can also be called field of view (FOV). While some just multiply the number of pixels by the IFOV, this is only suitable for an F-theta lens and can result in errors for a tangent map lens. For a tangent map lens, the FOR horizontal, vertical, and diagonal (φ_h, φ_v and φ_{diag}) are:

$$\varphi_h = \mathrm{atan}\left(\frac{N_x \cdot d_{\mathrm{pix}}}{f}\right) \tag{4-3}$$

$$\varphi_v = \mathrm{atan}\left(\frac{N_y \cdot d_{\mathrm{pix}}}{f}\right) \tag{4-4}$$

$$\varphi_{\mathrm{diag}} = \mathrm{atan}\left(\sqrt{N_x^2 + N_y^2} \cdot d_{\mathrm{pix}}/f\right) \tag{4-5}$$

Where $N_x\ and\ N_y$ are the number of columns and rows. This is projected at range as $d = R \cdot \tan(\varphi)$.

For an F-Theta lens, the relationship is simply:

$$\varphi_h = \frac{N_x \cdot d_{\mathrm{pix}}}{f} = N_x \cdot \phi_{\mathrm{pix}} \tag{4-6}$$

$$\varphi_v = \frac{N_y \cdot d_{\mathrm{pix}}}{f} = N_y \cdot \phi_{\mathrm{pix}} \tag{4-7}$$

$$\varphi_{\mathrm{diag}} = \sqrt{N_x^2 + N_y^2} \cdot d_{\mathrm{pix}}/f \tag{4-8}$$

When placing cameras side by side, if we want a percentage overlap, p_{ol}, horizontally in the FORs, then, the angular overlap is just $\varphi_{ol} = p_{ol} \cdot 0.01 \cdot \varphi_h$ which is also the angle between the two cameras optical axes.

For other lens types, exact mapping of the lens must be obtained from the manufacturer.

4.1.3 Depth of Focus, Depth of Field (DoF)

Depth of focus, δ', is the zone *behind the lens* within which the image sensor can capture an in-focus image. This is related to the right side of Figure 2-2 between the optic and the pixel. If the depth of focus is small, it will be frustrating to focus the sensor since small movements in the lens will cause rapid defocus. Assuming a circle of confusion (or blur circle angular diameter, ϕ, that is limited by the pixel size, and assuming the in-front and behind the image plane are equal we can estimate δ' as:

$$\delta' \approx \frac{2 \cdot f \cdot \phi}{D} = 2 \cdot f\# \cdot d_{pix} \qquad 4\text{-}9$$

Alternately, the Depth of Field (DoF), δ, is the distance between the closest and farthest objects in a *scene* that are acceptably sharp in an image (target/object portion, left side of Figure 2-2). If the DoF is too narrow objects moving in the z-dimension (along the optical axis) will move in and out of focus. Again, we assume a circle of confusion is limited by the pixel size and the in-front and behind the best focus are equal such that:

$$\delta \approx 2 \cdot \frac{R^2 \cdot \phi}{D} = 2 \cdot \frac{R^2}{f^2} \cdot f\# \cdot d_{pix} = 2 \cdot m^2 \cdot f\# \cdot d_{pix} = m^2 \cdot \delta' \qquad 4\text{-}10$$

Note that Depth of focus and Depth of field are related by the longitudinal magnification, m.

For the optical system alone, if we assume the angular blur is the diffraction limited blur size, and the depth of field is less than the range to the source, R, then the depth of field is approximated as (Beckman, 1963):

$$\delta = \frac{R^2 \cdot 2.44 \cdot \bar{\lambda}}{D^2} \qquad 4\text{-}11$$

Where D is the aperture diameter and $\bar{\lambda}$ is the mean wavelength in the sensor response.

4.1.4 Signal to noise ratio (SNR) and contrast ratio

When modeling a sensor signal to noise ratio, we can employ two approaches.

1. **Basic sensor model, at entrance aperture.** Compute the noise electrons and push these backward through the sensor to the entrance aperture to get noise equivalent power density (NEPD) sometimes called noise equivalent irradiance (NEI). NEPD is used in this document to differentiate noise at the entrance aperture from noise at the detector (typically called NEI). We propagate the source photons through the atmosphere to get target irradiance which can be compared directly with NEPD. This makes SNR comparison for point and extended sources much easier, as you only have to compute the source photons once.
2. **IR Sensor model, SNR at detector**: Propagate source photons through the atmosphere and through the sensor to get equivalent electrons and compare these directly with noise electrons. This is useful when you have different spectral regions or filters to compare. It is also more accurate than the first approach as all noise terms can be included in the model.

For SNR we compute the electrons from the target that land on a pixel. SNR helps us understand the total signal, but signal to clutter ratio (SCR) tells us how many electrons above an adjacent pixel we see with respect to noise electrons. There are cases where the target produces a high SNR and no SCR because there is no contrast with the background.

4.1.4.1 Basic IR Model, SNR at entrance aperture

For the basic sensor model, we work at the entrance aperture in irradiance units. This is not as precise as computing electrons at the detector since we do not include noise from the background and the optics. This model assumes that the detector noise measurement was taken at a comparable temperature to the scene temperature, thus the other factors do not significantly impact the result.

The radiant exitance of a target at temperature, *T* is:

$$W(T) = \sum_{\lambda_1}^{\lambda_2} \frac{c_1 \cdot \mathcal{R}(\lambda)}{\lambda^5 (e^{c_2/\lambda T} - 1)} \cdot \Delta\lambda \tag{4-12}$$

Where:

$W(T)$	in-band radiant exitance in *W*-cm^{-2}
c_1	first radiation constant = 3.7415 x 10^4 *W*-cm^{-2} µm^4
c_2	second radiation constant = 1.43879 x 10^4 µm-K
λ	Wavelength in µm, integrated over the filter from λ_1 to λ_2
T	absolute temperature in Kelvin
$\mathcal{R}(\lambda)$	relative spectral response (RSR) vs wavelength
$\Delta\lambda$	the wavelength step used in the model

We allow for rectangular objects, thus the general case for conversion of irradiance at the entrance aperture from the target is:

$$H_{\text{tar}} = W(T) \cdot \varepsilon_{\text{tar}} \cdot \mathrm{T}_a \cdot \frac{A_s}{\pi \cdot R^2} = W(T) \cdot \varepsilon_{\text{tar}} \cdot \mathrm{T}_a \cdot \frac{\phi_h \cdot \phi_v}{\pi} \tag{4-13}$$

And

$$\phi_{\text{pix}} = \frac{d_{\text{pix}}}{f} \text{ and } \phi_h = \min\left[\frac{d_{\text{pix}}}{f}, \frac{y}{R}\right] \tag{4-14}$$

$$\phi_v = \min\left[\frac{d_{\text{pix}}}{f}, \frac{x}{R}\right] \tag{4-15}$$

Where:

H_{tar}	Irradiance at the entrance aperture of the target
T_a	transmission through the atmosphere, assumed to be 1.0
R	range to source in meters
x & y	dimensions of the target
$\phi_h \cdot \phi_v$	Approximate steradian subtense of the source captured by a pixel
ϕ_{pix}	Approximate subtense of the pixel in radians
ε_{tar}	emissivity of the target, set to 0.8

Looking at equations 4-14 and 4-15 we note that if the angular subtense is based on the target, it is a sub-resolution (point) source, if it is based on the pixel/lens combination, it is resolvable or extended source.

The portion of the pixel covered by the target CE_{tar} (collection efficiency of the target), important for the signal to background calculations, is:

$$CE_{\text{tar}} = min\left(\frac{\phi_h \cdot \phi_v}{\phi_{\text{pix}}^2}, 1\right) \tag{4-16}$$

For an extended source, the *CE* is always one and for a sub-resolution source, it is less than one.

For NEDT (noise equivalent delta temperature) we compute the Noise equivalent power density (NEPD) at the entrance aperture including optical transmission (T_o).

$$\text{NEPD} = \frac{\mathrm{A}_p \cdot (W(T + \text{NEDT}) - W(T))}{\mathrm{A}_o \cdot \mathrm{T}_o} \tag{4-17}$$

Where:

A_p area of the pixel, = d_{pix}^2.

A_o area of the entrance aperture

The SNR is thus:

$$\text{SNR} = \frac{H_{\text{tar}}}{\text{NEPD}} \tag{4-18}$$

For contrast ratio, for a sub-resolution target, we must add in the background for the area that is not covered by the target. To get the irradiance that will land on a pixel, we scale the radiant exitance of the background as:

$$H_{\text{bkg}} = \frac{W(T_{\text{bkg}})}{\pi} \cdot \left(\frac{d_{\text{pix}}}{f}\right)^2 \tag{4-19}$$

Thus, the generalized signal to contrast ratio (SCR) is:

$$\text{SCR} = \frac{H_{\text{tar}} + (1 - CE) \cdot H_{\text{bkg}} - H_{\text{bkg}}}{\text{NEPD}} = \frac{H_{\text{tar}} - CE_{\text{tar}} \cdot H_{\text{bkg}}}{\text{NEPD}} \tag{4-20}$$

4.1.4.2 IR Sensor Model, SNR at detector

For SNR we compute the electrons from the target that land on a pixel. SNR helps us understand the total signal, but the signal to contrast ratio (SCR) tells us how many electrons above an adjacent pixel we see with respect to noise electrons. Without sufficient SCR we cannot see the signal. The SNR is computed as:

$$\text{SNR} = \frac{e_{\text{tar}}}{e_{\text{noise}}} \tag{4-21}$$

And contrast ratio (signal pixel to adjacent pixel) is:

$$\text{SCR} = \frac{e_{\text{tar\_pix}} - e_{\text{bkg}}}{e_{\text{noise}}} = \frac{e_{\text{tar}} - CE_{\text{tar}} \cdot e_{\text{bkg}}}{e_{\text{noise}}} \tag{4-22}$$

Where:

e_{tar}	number of electrons from the target
$e_{\text{tar\_pix}}$	number of electrons in the pixel including background electrons not covered by the target, For an extended source, $e_{\text{tar}} = e_{\text{tar\_pix}}$
e_{bkg}	number of electrons from the ambient background
CE	Collection efficiency as the portion of the pixel covered by the target

The following sections will describe the derivation of each component in detail.

4.1.4.2.1 Target electrons ($\boldsymbol{e_{\text{tar}}}$)

For thermal bands, we model emissive targets. Some SWIR bands require adding both emissive and reflective photons, but this simple model is limited to the mid to long wave IR regions.

It is assumed that the source is Lambertian and that the spectral emissivity, $\varepsilon(\lambda)$, is constant with wavelength (graybody) and thus does not need to be in the integral. For earth background in the MWIR and LWIR, a rule of thumb for emissivity is about 0.8-0.85 but if there is a known background it should be considered. The sensor in-band, radiant photon exitance of a black body is computed using Planck's Law (Hudson, 1969) as:

$$Q(T) = \sum_{\lambda_1}^{\lambda_2} \frac{c_1 \cdot \mathcal{R}(\lambda)}{\lambda^4 (e^{c_2/\lambda T} - 1)} \cdot \Delta\lambda \qquad \text{4-23}$$

Where:

$Q(T)$	in-band radiant photon exitance in ph-sec^{-1}cm^{-2}
c_1	first radiation constant = 1.88365 x 10^{23} sec^{-1}cm^{-2} µm^3
c_2	second radiation constant = 1.43879 x 10^4 µm-K
λ	Wavelength in µm, integrated over the filter from λ_1 to λ_2
T	absolute temperature in Kelvin
$\mathcal{R}(\lambda)$	relative spectral response (RSR) vs wavelength
$\Delta\lambda$	the wavelength step used in the model

We allow rectangular objects. The general case for conversion of radiant photon emittance to electrons at the detector, is:

$$e_{\text{tar}} = Q(T) \cdot \varepsilon_{\text{tar}} \cdot T_a \cdot T_o \cdot t_{\text{int}} \cdot A_o \cdot \frac{\phi_h \cdot \phi_v}{\pi} \cdot \text{QEFF} \qquad \text{4-24}$$

And

$$\phi_{\text{pix}} = \frac{d_{\text{pix}}}{f} \text{ and } \phi_h = \min\left[\frac{d_{\text{pix}}}{f}, \frac{y}{R}\right] \qquad \text{4-25}$$

$$\phi_v = \min\left[\frac{d_{\text{pix}}}{f}, \frac{x}{R}\right] \qquad \text{4-26}$$

Where:

e_{tar}	number of electrons from the target
A_o	area of the entrance aperture
T_a	transmission through the atmosphere
T_o	transmission through the optics
t_{int}	integration (exposure) time
d_{pix}	pixel size
f	optic effective focal length
R	range to source in meters
x & y	dimensions of the target
$\phi_h \cdot \phi_v$	Approximate steradian subtense of the source captured by a pixel
ϕ_{pix}	Approximate subtense of the pixel in radians
QEFF	quantum efficiency, fill factor, electrons/photon
ε_{tar}	emissivity of the target

The portion of the pixel covered by the target, CE_{tar} (collection efficiency of the target) is important for signal to background calculations later and is:

$$CE_{\text{tar}} = min\left(\frac{\phi_h \cdot \phi_v}{\phi_{\text{pix}}^2}, 1\right) \tag{4-27}$$

Note that angular symbols are used since these are small angles. Physics dictates that the actual ratios are used. The total electrons in the target pixel including background electrons not covered by the target are thus:

$$e_{\text{tar\_pix}} = e_{\text{tar}} + (1 - CE_{\text{tar}}) \cdot e_{\text{bkg}} \tag{4-28}$$

4.1.4.2.2 Noise ($\boldsymbol{e_{\text{bkg}}}$)

There are three sources for noise. These are:

1. Detector Noise, $e_{\text{det\_noise}}$ - electronics noise including read out, Johnson noise, power supply rejection, shot noise, dark current, etc. This is usually specified by the vendor as NEDT at 300K for an f/1 sensor, as noise equivalent power (NEP) in W/Hz$^{1/2}$ or photons/sec or detectivity (D*) in cm- Hz$^{1/2}$/W.
2. Shot Noise from background, $\sqrt{e_{\text{bkg}}}$ - Photon noise due to scene background temperature.
3. Optics reradiation, $\sqrt{e_{\text{optics}}}$- Photon noise due to optics emissivity

The main noise source is the shot noise with detector noise with optics noise shown for completeness. To combine these, we must convert everything to electrons out of the detector.

The total noise is the root sum square of the three as:

$$e_{\text{noise}} = \sqrt{e_{\text{det \_noise}}^2 + e_{\text{bkg}} + e_{\text{optics}}} \tag{4-29}$$

Computation of each component is described in the following subsections. For a background limited infrared photodetector (BLIP) sensor, the background noise (shot noise) will dominate such that the noise is approximately the square root of the background.

4.1.4.2.2.1 Detector Noise

As discussed in the previous section, noise can be specified as NEDT, NEP, or D*. If we have NEDT (noise equivalent delta temperature) we compute the noise equivalent photon rate at the detector as:

$$\dot{q} = A_p \cdot (Q(T + NEDT) - Q(T)) \tag{4-30}$$

where:

$\dot{q}$	Noise equivalent photon rate in ph-sec^{-1}
$Q(T)$	in-band radiant photon emittance in ph-sec^{-1}cm^{-2}
A_p	pixel area in cm^{2}

Note that the equation 4-23 for $Q(T)$ includes responsivity.

For detectivity or D* we must compute NEP first. There is a case where NEP is just the inverse of D*. We will show the case where it does not include a bandwidth. By definition,

$$NEP = \frac{\sqrt{A_p f_{3\text{db}}}}{D^*} \tag{4-31}$$

We must consider the bandwidth that the manufacturer specified for D*. If the bandwidth is not specified, then use the detector bandwidth. Often only rise time is specified. Using the low pass filter model, the 3dB bandwidth, $f_{3\text{db}}$, is related to rise time, t_{rise}, as:

$$f_{3\text{db}} = 0.35/t_{\text{rise}} \tag{4-32}$$

Thus, from NEP, we compute the noise electrons using the Einstein-Planck relationship as:

$$\dot{q} = hc \sum_{\lambda_1}^{\lambda_2} \frac{\text{NEP} \cdot \Re(\lambda)}{\lambda} \cdot \Delta\lambda \tag{4-33}$$

Where *hc* is Planck's constant times the speed of light = 1.9863x10^{-16} W-sec-nm/photon.

Detector noise electrons are then computed as:

$$e_{\text{det\_noise}} = \dot{q} \cdot t_{\text{int}} \cdot QEFF \tag{4-34}$$

4.1.4.2.2.2 Shot noise

Shot noise or Poisson is associated with the particle nature of light or in electronics, the discrete nature of electrons. It follows Poisson statistics and is thus the square root of the electrons that are produced by the detector from the impinging photons.

We assume that the background is an extended source (larger than a pixel), thus the electrons on one pixel from the background are:

$$e_{\text{bkg}} = \frac{Q(T_{\text{bkg}}) \cdot \varepsilon_{\text{bkg}} \cdot T_o \cdot t_{\text{int}} \cdot A_p \cdot \text{QEFF}}{4f\#^2} \tag{4-35}$$

where:

e_{bkg}	number of electrons from the ambient background
$Q(T_{\mathrm{bkg}})$	in-band radiant photon emittance in ph-sec-1cm-2 at T_{bkg} and ε_{bkg} (equation 4-23)
$f\#$	lens f-number
$\varepsilon_{\mathrm{bkg}}$	background emissivity, typically set to 0.85

The equivalent noise electrons are.

$$e_{\mathrm{shot}} = \sqrt{e_{\mathrm{bkg}}} \qquad 4\text{-}36$$

4.1.4.2.2.3 Photons from optics

The third noise source is comprised of the photon noise associated with re-radiation and reflection from optical component sources. The total electrons collected as a result of the reradiation from the optics are:

$$e_{\mathrm{optics}} = \frac{Q(T_{\mathrm{optics}}) \cdot (1 - T_o) \cdot A_p \cdot t_{\mathrm{int}} \cdot \mathrm{QEFF}}{4f\#^2} \qquad 4\text{-}37$$

We set the approximate emissivity of the optic to $(1 - T_o)$. Optics temperature is often set to 10 C higher than the ambient temperature.

4.1.4.3 IR Sensor Model, Insufficient SCR

There are cases where we cannot see a signal even with sufficient SNR. In the infrared, this is related to temperature, emissivity separation (TES). To demonstrate the concept of TES, we simplify, only looking at proportionalities. From the equations in the previous section, We know that:

$$e_{\mathrm{tar}} \sim \varepsilon_{tar} \cdot Q(T_{tar}) \cdot \left(\frac{d_{pix} \cdot R}{f}\right)^2 \text{ and } e_{bkg} \sim \varepsilon_{bkg} \cdot Q(T_{bkg}) \cdot \left(\frac{d_{pix} \cdot R}{f}\right)^2 \qquad 4\text{-}38$$

We know also can determine that SCR relates to the electrons and the projected pixel size at range, $\left(\frac{d_{pix} \cdot R}{f}\right)$, as:

$$SCR \sim \frac{\left(\varepsilon_{tar} \cdot Q(T_{tar}) - \varepsilon_{bkg} \cdot Q(T_{bkg})\right)}{\sqrt{\varepsilon_{bkg} \cdot Q(T_{bkg})}} \cdot \left(\frac{d_{pix} \cdot R}{f}\right)^2 \qquad 4\text{-}39$$

Consider the numerator, when the emissivity of the target times the photons from the target $(\varepsilon_{tar} \cdot Q(T_{tar}))$ and the emissivity of the background times the photons from the background $(\varepsilon_{bkg} \cdot Q(T_{bkg}))$ are equal, the target will be invisible independent of SNR and all other factors. Selecting the spectral region for the temperatures of interest is the only way to avoid a zero TES case for the scenario of interest.

4.2 Visible/NIR Sensor Model for sub-resolution moving targets

This very detailed model was developed as a menu driven model. It still requires the user to have knowledge of the desired system. It was designed to provide outputs in astronomical units of magnitudes but can also give absolute radiance values. This model includes determining sensitivity for multi-element systems such as the Dragonfly system developed at Yale and University of Toronto (Van Dokkum, 2014).

4.2.1 Radiometric calculations – Astronomical Units, Basics

When doing radiometric calculations, it is best to remember that everything converts from angle space. With few exceptions, each pixel element in an electro-optical system can be projected into an angle related to the size of the pixel and the focal length. Remember that the photons from a point source depend only on the size of the entrance aperture and for an extended source, the area of a pixel and the f-number dominate. Calculations must be done using radiometric units and then converted to astronomical units for comparison to results in literature. For astronomical applications, the sky background is given in surface brightness in mag/arc-sec^2. Sky brightness values are dependent on band and vary based on location and time of year (STScI, 2017, Ohio State, 2025). Standard values for the six standard astronomical bands are provided in Table 4-1.

Table 4-1. Sky Brightness and filter parameters for the six standard astronomical bands

Parameter	**V**	**G**	**r**	**J**	**H**	**K**
Center Wavelength (µm)	0.545	0.483	0.626	1.22	1.63	2.19
Filter Width, FWHM (µm) $\Delta\lambda$	0.085	0.098	0.095	0.16	0.29	0.34
Cut on-Cut off wavelength (µm)	0.502-0.587	0.434-0.532	0.579-0.674	1.17-1.33	1.49-1.78	2.03-2.37
$\boldsymbol{H_V(\lambda)}$ **(10^{-13}W/m^2-nm)**	363.1	363.1	363.1	31.47	11.38	3.96
$\boldsymbol{Msky}$ **(mag/arc-sec^2)**	19.6	19.6	19.6	13.6	13.24	12.34

Conversion of sky surface brightness, M_{sky}, in mag/arcsec2 to spectral irradiance (W/m^2-nm), assuming the sky is a Lambertian extended source is:

$$H_B(\lambda) = H_V(\lambda)\cdot 10^{-\frac{M_{sky}}{2.5}}\cdot a\cdot \pi \tag{40}$$

M_{sky} = sky surface brightness is mag/arc-sec^2
a = arc-secs^2/sr=4.25x10^{10} into π sr for a Lambertian target
$H_b(\lambda)$ = the spectral irradiance (W/m^2-nm) for the sky background
$H_V(\lambda)$ = the spectral irradiance of Vega (Colina, 1996)

Debris in the atmosphere are assumed to be an emissive source, thus a graybody at temperature, T. For a graybody, the integrated in-band radiant exitance in W/m^2 is;

$$W(T) = \sum_{\lambda_1}^{\lambda_2} W(\lambda,\, T)\cdot \varepsilon(\lambda)\cdot T_{filt}(\lambda)\cdot \Delta\lambda = \sum_{\lambda_1}^{\lambda_2} \frac{c_1\cdot \varepsilon(\lambda)\cdot T_{filt}(\lambda)}{\lambda^5\left(e^{c_2/\lambda T}-1\right)}\cdot \Delta\lambda \tag{41}$$

$W(\lambda,\, T)$ = spectral radiant exitance in W/m^2-nm
$W(T)$ = in-band radiant exitance in W/m^2
$\varepsilon(\lambda)$ = spectral emissivity of the target
$T_{filt}(\lambda)$ = spectral transmission of the filter
c_1 = first radiation constant = 3.7415 x 10^{20} W nm^4/m^2
c_2 = second radiation constant = 1.43879 x 10^7 nm-K
λ = Wavelength in nm, integrated over the filter from λ_1 to λ_2
T = absolute temperature in Kelvin

If the target is reflective, then the spectral radiant exitance, $W(\lambda, T)$, is computed for the illumination source, such as $W(\lambda, T_{sun})$ for the sun, and emissivity is replaced by reflectivity, $\rho(\lambda)$. Solar spectrum are available from sources such as (https://www.nrel.gov/grid/solar-resource/spectra):

- MODTRAN
- SMARTS
- ASTM-G173 solar spectrum
- ASTM Standard Extraterrestrial Spectrum Reference E-490-00

Also note that the sun can be approximated by a 5800K graybody, as can be seen in Figure 4-2.

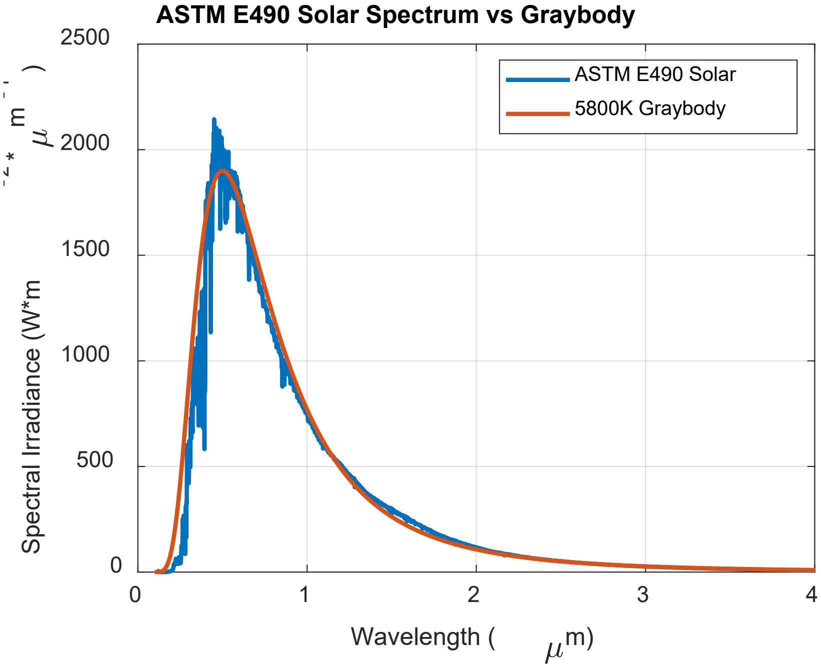

Figure 4-2. ASTM E490 solar spectrum at the surface of the earth compared to a 5800K graybody (normalized to the known peak).

If using a solar spectrum, it should be for the location of the object such as at earth or for debris perhaps Low earth orbit (LEO). This affects the apparent emissivity if using the 5800K approximation.

To have an accurate comparison with the measurements made by the astronomical community, the point source and extended source values must be converted to magnitudes and surface brightness. To get to an equivalent point source magnitude, the conversion must include the area of the scene captured by the pixel since this determines the irradiance at the entrance aperture captured by a pixel. Thus, the spectral irradiance at the entrance aperture for an equivalent point source from an extended source is:

$$H_P(T) = \frac{\phi_{pix}^2 W_B(T)}{\pi} \qquad 42$$

To then get the equivalent point source magnitude this becomes more simply:

$$M_T(T) = -2.5log_{10}\left(\frac{H_P(T)}{H_V(T)}\right) \qquad 43$$

4.2.2 BACKGROUND AND TARGET ELECTRONS TO THE DETECTOR

The electrons on one pixel from an extended source are computed using the discrete integral:

$$e_{bkg} = \frac{\varepsilon_{bkg} \cdot t_{int} \cdot A_p \cdot T_o \cdot c \cdot SF}{4f\#^2} \sum_{\lambda_1}^{\lambda_2} W_B(\lambda, T) \cdot \Re(\lambda) \cdot T_{filt}(\lambda) \cdot \Delta\lambda \qquad \text{4-44}$$

where:

e_{bkg} = electrons collected from the background
ε_{bkg} = emissivity of the background
t_{int} = integration time
A_p = area of the pixel in meters
c = 6.24150975 x 10^{18} electrons/Coulomb
SF = scatter factor computed from adjacent pixel ensquared energy (see section 4.2.3)
$f\#$ = f/number of the optical system
$W_B(\lambda)$ = the background spectral radiant exitance in W/m^2-µm
$\Re(\lambda)$ = Sensor responsivity in Amps/Watt (Coulombs/Watt-Sec)
$T_{\text{filt}}(\lambda)$ = spectral transmission of the filter
T_o = transmission of the optics
$\Delta\lambda$ = the wavelength step in µm

Within the model, it is often convenient to read in the responsivity and the filter curves from a text file. Alternatively, a single value transmission and band center and bandwidth can be input and the corresponding top-hat transmission curve will be used. Example curves for the Dragonfly SBIG detector (Van Dokkum, 2014) and two SDSS filters (also used in the Dragonfly system) are shown in Figure 4-3.

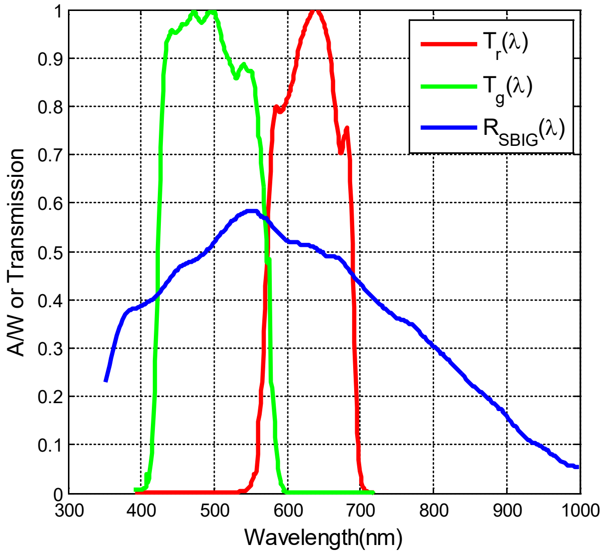

Figure 4-3. Example spectral responsivity of the SBIG detector used by the Dragonfly professional astronomers (blue) and spectral transmission curves for red and green SDSS spectral filters..

The electrons collected from a sub-resolution target are limited by the target area and are computed as

$$\widehat{e_{pt}} = \left\langle \frac{t_{\text{int}} \cdot A_T \cdot A_o \cdot T_o \cdot c \cdot CE}{\pi R^2} \sum_{\lambda_1}^{\lambda_2} W_T(\lambda) \cdot \Re(\lambda) \cdot T_{\text{filt}}(\lambda) \cdot \rho_{pt}(\lambda) \cdot \Delta\lambda \right\rangle_{\text{all elements \& frames}} \tag{4-45}$$

$\widehat{e_{pt}}$ = electrons collected from a point source target
ρ_{pt} = reflectivity; ***for emissive target change to emissivity***
A_T = area of the target in meters
A_o = area of the entrance aperture in meters
CE = collection efficiency computed from ensquared energy; (see section 0)
$W_T(\lambda)$ = the target spectral radiant exitance in W/m^2-nm

Two cases of magnitude versus object diameter are shown in Figure 4-4. Both cases assume a reflectivity of 0.2, but one case uses the full ASTM-G173 spectral irradiance values, the second assumes a sun angle such that 60% of the energy is reflected off the target debris.

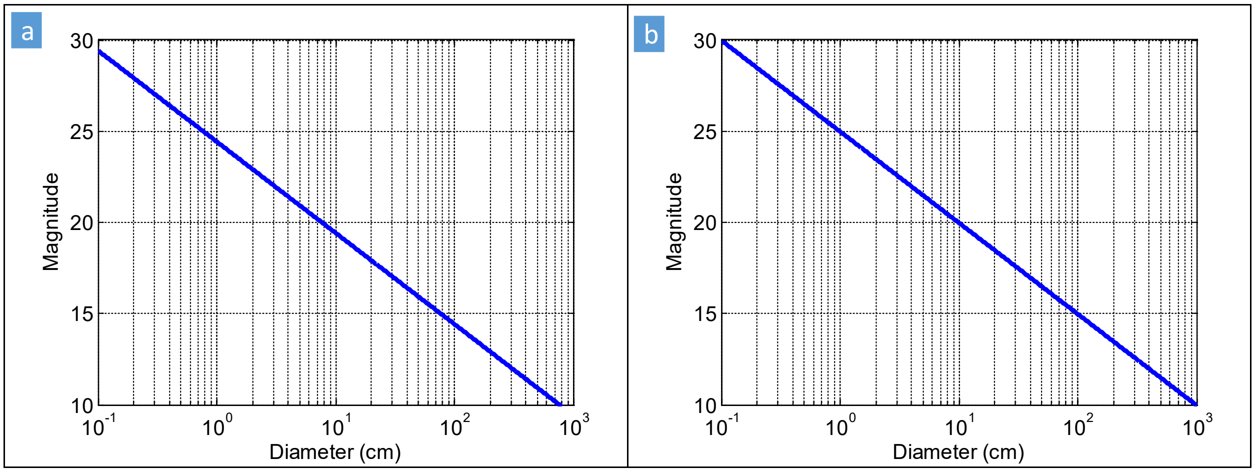

Figure 4-4. Target magnitude versus object diameter for (a) full sun and (b) 60% of full sun. Variations in object size or solar angle will produce a different magnitude for the same size object.

If multiple elements and/or frames are averaged, this results in the average electrons in a frame. Collection efficiency and scatter factor are critical to determining the ability to find a dim target next to a bright one such as planets next to stars, or small debris (space junk) next to a bright (or dim) star.

4.2.3 COLLECTION EFFICIENCY AND SCATTER FACTOR

In order to determine the amount of target energy in the central (peak) pixel(s) and the amount that leaks into the adjacent pixels, thus reducing contrast hence detectability, a point spread function (PSF) analysis is done within the model. While the Rayleigh limit is the simplest method, the central obscuration in the telescope modifies the typical PSF decreasing the energy in the central lobe and increasing the energy in the adjacent rings. Sandin measured the PSF of a number of telescopes including the Dragonfly system (Sandin, 2014). This data was useful in verifying the PSF model.

The model uses PSFs instead of the optical transfer functions (OTF). The OTF is the Fourier transform of the PSF, with the real part being the modulation transfer function (MTF) and the imaginary portion being the phase transfer function (PhTF). Because of the need for accuracy in the wings, the PSF or the OTF must be used. The MTF does not contain the phase information required to determine accurately the amount of energy from a target that ends up in the adjacent pixels. This is critical to determining the ability to separate targets and the effect of scatter on the result. The total PSF is a convolution of the individual component PSFs. The model is initially run in one dimension as line spread functions (LSF) to reduce computation time and includes:

- Diffraction including central obscuration as a modified Airy pattern (Rivolta, 1986)
- Turbulence using point source propagated through a series of phase screens estimated via an equation from Nelson (Nelson, 2000)
- Approximate scattering due to microstructure on the mirror (Hassan, 1995)

Once these components are computed in one dimension, symmetry is assumed to determine the two-dimensional PSF. This is a reasonable assumption for narrow FOV telescope optics. This PSF is then convolved with the pixel and a unit step function in one dimension to get the total smeared PSF. The peak ensquared energy in a pixel or super-pixel (binned pixels) is used to determine the collection efficiency.

Diffraction is computed using a modified Airy function that includes the central obscuration (Rivolta, 1986):

$$l_{\mathrm{diff}}(\theta) = \frac{1}{(1-\epsilon^2)^2}\left[\frac{2J_1(\pi D\theta/\lambda)}{\pi D\theta/\lambda} - \epsilon^2 \frac{2J_1(\epsilon\pi D\theta/\lambda)}{\epsilon\pi D\theta/\lambda}\right]^2 \quad \text{4-46}$$

Where:

l_{diff} = LSF which is the normalized response to the peak at θ=0
θ = angular radius
D = primary aperture diameter
ϵ = ratio of the obscuration diameter to the primary aperture diameter
J_1 = order 1 Bessel function of the first kind
λ = wavelength

Note that with no obscuration, this becomes the standard Airy disk pattern of:

$$l_{\mathrm{diff}}(\theta) = \left[\frac{2J_1(\pi D\theta/\lambda)}{\pi D\theta/\lambda}\right]^2 \quad \text{4-47}$$

A comparison of the LSFs for no obscuration (blue) and with a typical 25% obscuration by diameter (red) is shown in Figure 4-5.

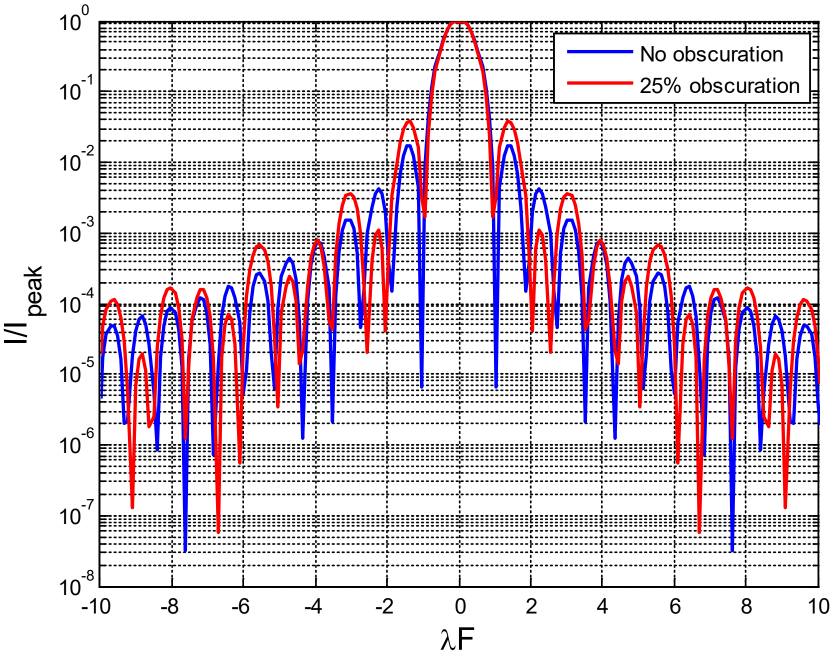

Figure 4-5. Line spread function (LSF) modeled as an Airy disk pattern with respect to λ-F number (λF). Note that the central obscuration increases the energy in the wings with respect to the normalized peak.

Note that the central obscuration increases the energy in the wings with respect to the peak.

For turbulence, the long-time PSF for atmospheric turbulence can be modeled as the Fourier transform of the MTF of turbulence from Nelson (Nelson, 2000)

$$psf_{\text{turb}}(\theta) = \mathcal{F}\left[e^{-3.44(\frac{r(\theta)}{r_0})^{5/3}}\right] \tag{4-48}$$

Where r_0 is the coherence radius, r is the radial distance from the center of the MTF, related to θ. Scaling the LSF to angle space is based on the relationship between r_0 and the seeing limit, ϕ_{turb}.

For telescope systems, the outer LSF profile aureole (corona), is most likely the result of light scattering by atmospheric aerosols or by scratches, micro-ripples or dust on the telescope optics (Van de Hulst, 1981). Hasan provides equations for the scatter due to the mirror micro-roughness, but these are difficult to implement for a general case. Racine speculated that the aureole may also be caused by "the diffusion and reflection of light in the detector assembly" (Racine, 1996). Racine's equation for the surface brightness of the aureole has been modified to provide the line spread function, LSF (l_a)with respect to the seeing limit as

$$l_a = \frac{f}{8\pi d_0^2}\cos^3\left(\text{atan}\left(\frac{\theta}{2d_0\phi_{\text{turb}}}\right)\right) \tag{4-49}$$

The variable d_0 provides the distance between the source and the reflecting surface in half width units of the full point spread function. For this model, it is assumed that this is approximately equal to half of the turbulence seeing limit, ϕ_{turb}. Sandin provides data for the Palomar telescope and Racine had fit parameters for this same telescope in his paper, the model was then run with Racine's parameters (d_0;f=100; 0.03). Figure 4-6 shows the LSF model components and the total model result as compared to the measurements from Sandin for the Palomar telescope with the Schmidt plate (PSF$_{K73}$, 200" aperture) and for the Dragonfly system (PSF$_{A14}$, 4" aperture lens) compared to the model.

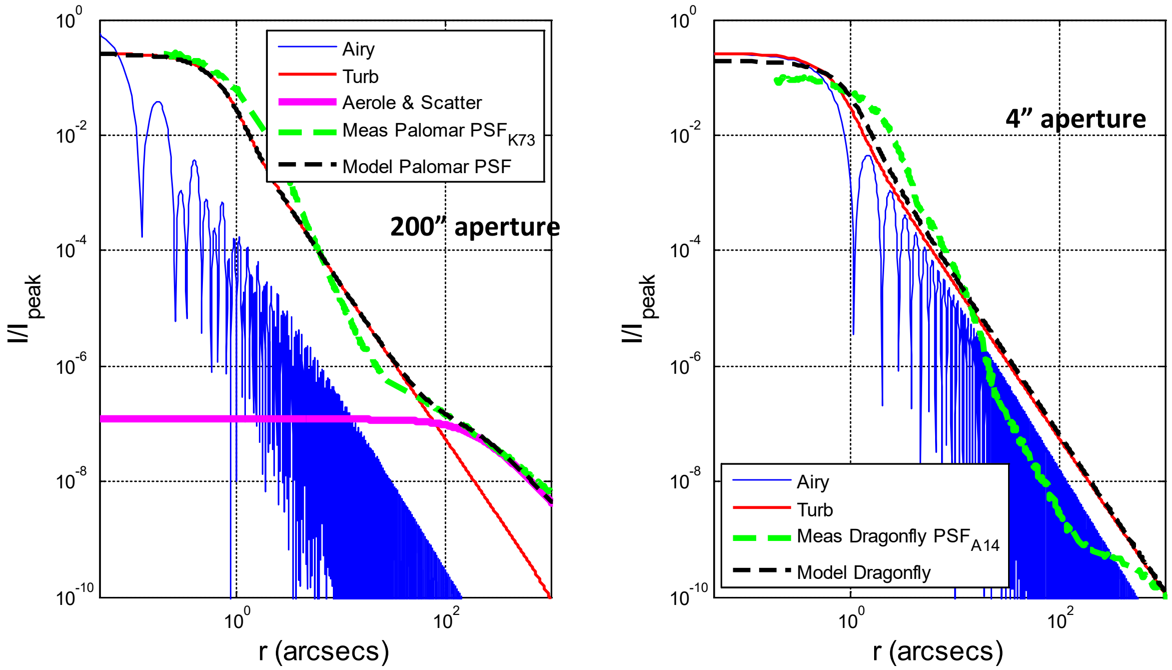

Figure 4-6. Comparison of total LSF model with measurements from Sandin for the Palomar telescope (left). The magenta line is the areole and scatter from the model; the red line is the seeing limit (turbulence) and the blue is the Airy pattern. These are combined in the model to obtain the black line which compares well with the green dashed lined measured by Sandin et al. Note that the larger aperture is dominated by the seeing limit. The right plot shows the same for a 4" canon lens. There is no scatter as this is a lens and not a telescope.

In the left plot the model components are separated as the areole & scatter (magenta), turbulence (red) and the Airy diffraction (blue). They combine to the seeing dominated line spread function (black). This compares well with the measurements. On the right, the same is shown except there is no areole & scatter for a lens. The disagreement with the Dragonfly system Canon 400 mm lens at large angles is most likely measurement error since the system cannot be better than the diffraction limit.

Once the LSF is computed, a two-dimensional PSF is derived assuming that the PSF is symmetric. An example PSF for a Canon 400 mm lens is shown in Figure 4-7.

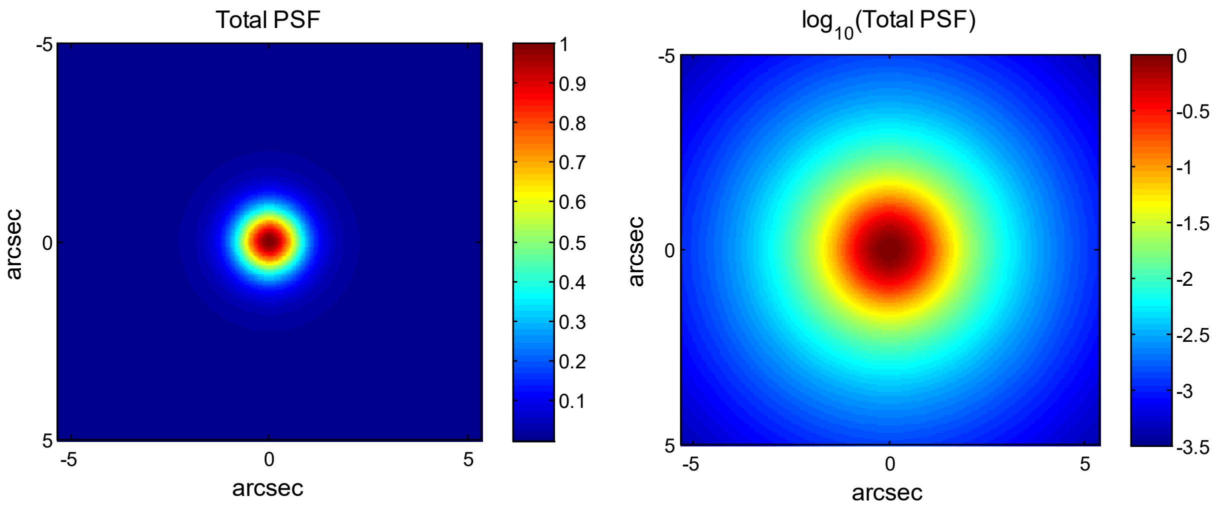

Figure 4-7. 2D PSF derived from 1D LSF for the Canon 400 mm lens with seeing limit at 1 arc-sec. Left shows linear response normalized to the peak, right shows the log of the response normalized to the peak. Note that the right image shows some of the diffraction pattern from the lens.

The image on the right shows this PSF on a linear scale, while the right shows the log base 10 of this same PSF providing additional visualization of the model output.

This PSF is then smeared using uncompensated motion, $\dot{\theta}$. With motion it is assumed that there will be some point where the center of the PSF will smear across a pixel. An example of a portion of the total PSF for a 20 arcsec/sec piece of debris, integrated for 200 milliseconds and with 2 x 2 binned pixels, is shown in Figure 4-8.

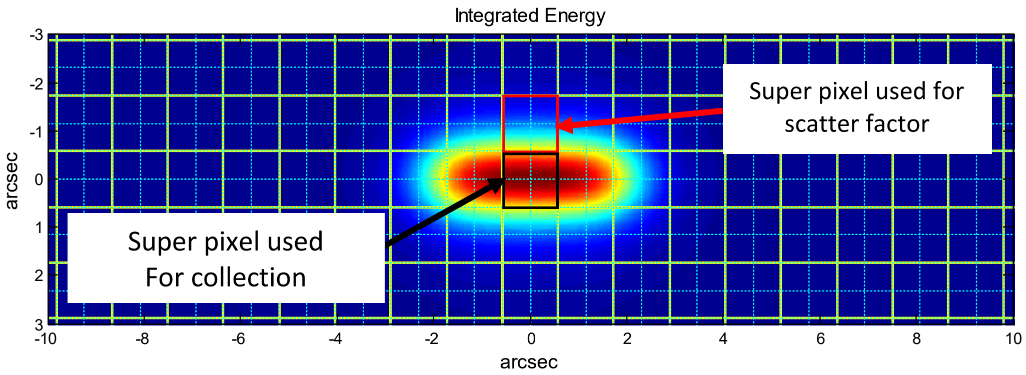

Figure 4-8. Smeared PSF for a 20 arcsec/sec target integrated for 200 milliseconds. The yellow grid indicates binned 2 x 2 super-pixels; the cyan dotted lines are single pixels. For this case, pixel pitch is half the pitch of these super-pixels. The collection efficiency for this target considering the losses in the wings of the PSF is only 15.5% for the center super-pixel.

Note that this figure shows only a portion of the grid that is used within the model. The binned pixels make up a super-pixel. The collection efficiency for this case for the peak pixel is about 15.5%. Because of the smear, the adjacent super-pixels also collect almost the same number of photons. The pixel above the peak pixel is chosen to determine contrast. The integrated percentage of the energy is thus the scatter factor (SF) noted in equation 4-44.

4.2.4 NOISE CALCULATIONS

All noise computations are done in electrons. There are typically three sources for noise, these are:

1. Read noise, e_{read}
2. Shot noise related to Dark current, $e_{\text{dk}} = I_{\text{dk}} \cdot t_{\text{int}}$ with I_{dk} converted to electrons/second
3. Shot noise related to captured scene background temperature or sky radiance

Note that noise is decreased by the square root of the number of elements, n_{Sens}, and the number of frames averaged, n_{Frames}. Binning pixels into a super pixel (n x n binned pixels) improves SNR for CCD detectors by n, not by n-squared since the read noise is only accumulated once. At the time of this writing, CMOS detectors did not have the accumulated prior to read capability. This may become a capability in the future.

Read noise and dark current are specified by the sensor manufacturer. Thermoelectric cooled (TEC) cameras lower the dark current for long exposure time collects. These may also be called Peltier cooler. For example, the Dragonfly system uses a cooled camera that typically has 0.04 e/second dark current. The model assumes 1 decade/5°C dark current reduction for a TEC cooled detector such 0.04 e/second dark current is achieved at about 10° C. Any electrons collected in the well result in shot noise and thus noise is assumed to be the square root of the captured electrons. This is true for the dark, background and the target electrons. The equivalent shot noise electrons from background are $e_{\text{n\_bkg}} = \sqrt{e_{\text{bkg}}}$.

One of the advantages to binning for CCD detectors is that read noise is only added for one 'super' pixel. In the model the one-dimensional bin value is input such that the total number of binned pixels is n_{Bins}^2. This increases SNR up to the point where the super-pixel matches the smear due to exposure time and angular rate. The Dragonfly system (Van Dukkum , 2014) shows the advantage of stacking images from multiple lens/cameras for increasing sensitivity. In this model we allow for multiple sensors as, n_{Sens} and multiple frame averages, n_{frames}. For the sensor only limitations (no target) we start with the first two sources for the number of frame averages and sensors such that:

$$e^{-}_{\text{noise\_lm}} = \sqrt{\frac{e_{\text{read}}^2 + (e_{\text{dk}} + e_{\text{bkg}}) \cdot n_{\text{Bins}}^2}{n_{\text{Sens}} \cdot n_{\text{frames}}}} \tag{4-50}$$

While individual noise components are root-mean-square (RMS) noise, each of these noise components are root-sum-squared to get the total noise. The true noise including the background and target is:

$$e^{-}_{\text{noise}} = \sqrt{\frac{e_{\text{read}}^2 + \widehat{e_{\text{pt}}} + (e_{\text{dk}} + e_{\text{bkg}}) \cdot n_{\text{Bins}}^2}{n_{\text{Sens}} \cdot n_{\text{frames}}}} \tag{4-51}$$

Note that the background noise may include photons from the target.

Unlike CCDs, for CMOS detectors that can bin pixels, the number of bins squared is also multiplied times the read noise (read noise increases with the number of pixels) cancelling each other out, thus there is no advantage to binning for CMOS.

4.2.5 Signal to Noise Ratio (SNR) & Signal to Clutter Ratio (SCR)

The actual electrons in the target pixel include background electrons such that:

$$\widehat{e_{\text{tar}}} = \widehat{e_{\text{pt}}} + e_{\text{bkg}} \cdot (1 - FF) \tag{4-52}$$

Where FF is the fill factor which is the portion of the pixel (as projected at the target) covered by the point source; $\phi_{\mathrm{pt}}^2/\phi_{\mathrm{pix}}^2$, almost always <$10^{-8}$, but implemented for completeness. This typically means that the target minus the background is equal to $\widehat{e_{pt}}$. Signal to noise ratio includes all sources and is computed as

$$\mathrm{SNR} = \frac{\widehat{e_{pt}}}{e_{\mathrm{noise}}^{-}} \qquad 4\text{-}53$$

The signal to clutter ratio (SCR) includes the photons that blur into the adjacent pixel. For this computation, it is the photons on the pixel above the peak pixel that determine the contrast. The adjacent electrons are computed as

$$e_{\mathrm{adj}} = e_{\mathrm{bkg}} + SF \cdot \widehat{e_{\mathrm{tar}}} \qquad 4\text{-}54$$

Where SF is the scatter factor discussed in section 4.2.3. SCR is thus computed as

$$\mathrm{SCR} = \frac{\widehat{e_{\mathrm{tar}}} - e_{\mathrm{adj}}}{e_{\mathrm{noise}}} \qquad 4\text{-}55$$

Note that for both SNR and SCR, the optimal bin size is critical to the best result.

4.2.6 WELL DEPTH

Well depth is important to dynamic range and limits useful exposure time. If the photons from the sky dominate, then the target cannot be seen. With a smaller pixel, we get a correspondingly smaller area of the sky for the same telescope. Consider the case of a 24µm pixel versus a 4 µm pixel. Because the 4 µm pixel captures only 1/36th of the area captured by the larger pixel, it captures that many fewer photons. Thus, well size is related to pixel size (area). The dim point source targets with photon fluxes limited by aperture do not limit the well depth. This means that the 24µm pixel will have to have a well depth 36 times larger than the 4 µm pixel detector to not saturate on the same sky background.

4.2.7 CONVERSION TO ASTRONOMICAL VALUES

4.2.7.1 LIMITING MAGNITUDE

Limiting magnitude is the faintest stellar magnitude which scan be seen by an imaging system for a given exposure time. While a number of different methods exist for computing limiting magnitude, these typically do not consider sky brightness and other factors associated with the system. In our model the limiting magnitude is computed from the noise electrons at the detector. Limiting magnitude thus corresponds the sensor noise equivalent irradiance (NEI) also called noise equivalent power density (NEPD) at the entrance aperture times a detection variation (signal to noise factor), typically set to five. NEPD is the irradiance at the entrance aperture that produces a signal to noise of one. NEPD is an excellent way to compare systems since it is a measure of the minimum detectable target irradiance at the entrance aperture which can be compared from system to system. To compute NEPD for a system with a given filter with center wavelength, λ_{cen}, the noise electrons from equation 4-50 are 'pushed back' through the sensor to the entrance aperture reversing equation 4-45.

$$H(\lambda_{\mathrm{cen}}) = \frac{e_{\mathrm{noise\_lm}}^{-} \cdot {}^{hc}/_{\lambda_{\mathrm{cen}}} \cdot \sigma}{\Delta\lambda \cdot t_{\mathrm{int}} \cdot A_o \cdot T_o \cdot CE \cdot QE} \qquad 4\text{-}56$$

Where:

$H(\lambda_{\mathrm{cen}})$ is the noise equivalent irradiance of the system

σ is the detection variation, corresponding to the equivalent SNR
hc is Planck's constant times the speed of light = 1.9863e-16 W-sec-nm/photon
λ_{cen} is the center wavelength of the filter of the selected band
$\Delta\lambda$ is the filter width for the selected band

Limiting magnitude is thus computed from NEPD as

$$M_L(\lambda) = -2.5\log_{10}\left(\frac{H(\lambda)}{H_V(\lambda)}\right) \tag{4-57}$$

4.2.8 MINIMUM SEPARATION FROM A BRIGHT STAR

For simplicity the LSF is used to determine the separation. It is assumed that both the star and the target are sufficiently sub-resolution that the energy in a pixel is dominated by the LSF of the system. The magnitude scale is logarithmic based on the fifth root of 100. This means that if there is a magnitude difference between stars of *n*, then the ratio of the intensity of the stars is 2.5119^{n}. Since our baseline is a target of magnitude 20 and the star of magnitude, *m*, then the intensity ratio target/star=$2.5119^{(m-20)}$. The angular separation is thus the angle where the total LSF (dependent only on the chosen optical system, not the detector) shown in Figure 4-6 is less than half this ratio. If the angle is less than the seeing limit, the separation defaults to the seeing limit.

4.3 Grating Spectrometer Model

This model is for a spectrometer that consists of a camera coupled to a grating such that, for a homogeneous source, rows from an image can be averaged to improve signal to noise ratio for the spectra.

We assume an extended source, and we are interested in the source spectral radiant exitance at each wavelength as

$$W(\lambda,\, T) = \frac{c_1 \cdot \varepsilon \cdot T_{\mathrm{atm}}}{\lambda^5 (e^{c_2/\lambda T} - 1)} \tag{4-58}$$

Where:

- $W(\lambda,\, T)$ is the spectral radiant exitance in W/m^2-nm,
- *T* is the Temperature in Kelvin,
- ε is the emissivity of the target, assumed to be about 0.8,
- T_{atm} is the atmospheric transmission set to 0.8 for the first estimate,
- c_1 is the first radiation constant = 3.7415 x 10^{20} W nm^4/m^2,
- c_2 is the second radiation constant = 1.43879 x 10^{7} nm-K
- λ is the wavelength in nm.

Because the spectral resolution of the gratings is very narrow, we can simplify each integral at each wavelength by simply multiplying by the spectral resolution of the camera/grating combination. For this case, we are assuming a gain of 1.0 such that the counts in digital number (dn) are equal to the electrons generated. The electrons generated by the detector from the target are computed as:

$$e^-(T,\lambda) = \frac{W(T,\lambda) \cdot t_{\mathrm{int}} \cdot \Re_{\mathrm{det}}(\lambda) \cdot \Re_{\mathrm{gr}}(\lambda) \cdot \Delta\lambda \cdot T_{\mathrm{opt}}(\lambda) \cdot A_{\mathrm{pix}}}{q_e \cdot 4f\#^2} \tag{4-59}$$

Where:

- $e^{-}(T,\lambda)$ is the number of electrons at wavelength, λ, and temperature, T,
- t_{int} is the exposure time in seconds,
- $\mathfrak{R}_{\text{det}}(\lambda)$ is the responsivity of the detector in A/W at wavelength, λ,
- $\mathfrak{R}_{\text{gr}}(\lambda)$ is the grating efficiency at wavelength, λ,
- $\Delta\lambda$ is the spectral resolution of the grating on the detector in nm,
- $T_{\text{opt}}(\lambda)$ is the transmission of the optic at wavelength, λ,
- f# is the f-number of the limiting optic,
- $A_{\text{pix}}$is the area of the pixel in m^2,
- q_e is the elementary charge of an electron=1.602176634×10^{-19} Coulombs.

We also assume that:

$$\mathfrak{R}_{\text{sys}}(\lambda) = \frac{\mathfrak{R}_{\text{det}}(\lambda)\cdot\mathfrak{R}_{\text{gr}}(\lambda)\cdot\Delta\lambda\cdot T_{\text{opt}}(\lambda)\cdot A_{\text{pix}}}{q_e\cdot 4f\#^2} \quad \text{4-60}$$

and

$$e^{-}(T,\lambda) = W(T,\lambda)\cdot t_{\text{int}}\cdot\mathfrak{R}_{\text{sys}}(\lambda)/G \quad \text{4-61}$$

Where:

- $\mathfrak{R}(\lambda)$ is the responsivity of the system in e/(W-sec/m^2-nm) at wavelength, λ,
- G is the sensor gain in dn/electron

We can easily measure $\mathfrak{R}_{\text{sys}}(\lambda)$ in the lab assuming that G is one (i.e. one dn per electron) or use the measurements from the detector and grating manufacturer. This responsivity allows us to easily compute the spectral radiant exitance and convert directly to dn**.**

All noise computations are done in electrons. There are typically three sources for noise (Shumaker, 1993). These are:

1. Read noise, e_{read}
2. Shot noise related to Dark current, $e_{\text{dk}} = I_{\text{dk}}\cdot t_{\text{int}}$ with I_{dk} converted to electrons/second; this is negligible for our short exposures but included for completeness.
3. Shot noise as the square root of the captured scene electrons including solar and target electrons.

The shot noise is:

$$e_{\text{shot}}^2(T,\lambda) = e^{-}(T,\lambda) + \frac{(H_{\text{sun}}(\lambda) + H_{\text{bkg}}(340K,\lambda))\cdot t_{\text{int}}\cdot\mathfrak{R}_{\text{sys}}(\lambda)}{q_e} \quad \text{4-62}$$

Where $H_{sun}(\lambda)$ is either the ASTM-G173 or MODTRAN derived irradiance and H_{bkg} is the spectral irradiance from the earth computed conservatively at 340K.

We can also improve the noise by the square root of the number of rows that we average. The total noise is thus the root-sum-square (RSS) of all noise components and is computed as:

$$e_{\text{noise}}^{-}(T,\lambda) = \sqrt{\frac{e_{\text{read}}^2 + e_{\text{dk}}^2 + e_{\text{shot}}^2(T,\lambda)}{n_{\text{rows}}}} \quad \text{4-63}$$

The SNR is thus computed as:

$$SNR(T,\lambda) = \frac{e^{-}(T,\lambda)}{e^{-}_{\mathrm{noise}}(T,\lambda)} \tag{4-64}$$

The percentage of well is computed from the detector well depth, e^{-}_{well}, as:

$$p_{\mathrm{well}}(T,\lambda) = \frac{e^{-}(T,\lambda)}{e^{-}_{\mathrm{well}}} \tag{4-65}$$

4.4 First order Infrasound Model

This model gives a ballpark estimate of sound pressure allowing optimum setup of microphones for an experiment. When an object is shocked, it displaces the air based on the momentary deformation of the object. If we consider a spherical vessel that is shocked, we can determine the infrasound pressure from the deformation. This deformation may be derived from another model or may be measured using images of the vessel and subsequent processing to get that deformation. This first order model uses the definition of adiabatic bulk modulus, B, as:

$$\Delta P = -B\frac{\Delta V}{V} \tag{4-66}$$

Where ΔP is the pressure (for our case sound pressure), ΔV is the change in volume due to deformation, Δr, and V is the volume of surrounding air. The confinement vessel is assumed to be a sphere of radius, r_{vessel}. It is assumed the room is a cube of size $2(r_{\mathrm{vessel}} + \Delta r_{\mathrm{air}})$. The sound pressure is computed for the air volume surrounding the vessel for minimum distances of Δr_{air} such that we compute the sound pressure as:

$$\Delta P = -B\left[\frac{V_{\mathrm{vessel}} - V_{\mathrm{deformed}}}{V_{\mathrm{room}} - V_{\mathrm{vessel}}}\right] = -B\left[\frac{\frac{4\pi}{3}\cdot r_{\mathrm{vessel}}^{3} - \frac{4\pi}{3}\cdot (r_{\mathrm{vessel}} + \Delta r)^{3}}{8\cdot (r_{\mathrm{vessel}} + \Delta r_{\mathrm{air}})^{3} - \frac{4\pi}{3}\cdot r_{\mathrm{vessel}}^{3}}\right] \tag{4-67}$$

The secondary effects and reflections are not included in this model.

4.5 BASIC LASER MODEL

This basic laser model combines photons from the background with those from the reflected laser energy. In includes a canopy (such as trees) that may block the laser illimitation. The photons from the laser are:

$$q_L(R) = \frac{\lambda_L}{hc}\cdot\frac{E\cdot A_o\cdot T_o\cdot T_a(\lambda_L)\cdot T_c(\lambda_L)\cdot \rho(\lambda_L)\cdot \varepsilon}{R^2} \tag{4-68}$$

Where:

q_L is the laser photon density at the receiver entrance aperture in photons
$\frac{\lambda_L}{hc}$ is the conversion from Joules to photons
E is laser power in Joules
λ_L is the Laser wavelength such as 1.55 µm
A_o is the area of receiving optics
T_a is the transmission through the atmosphere
T_o is the transmission through the receiver optics

T_c is the transmission through an obscurant such as a canopy
ρ is the reflectivity of the target
R is the range to target in meters and
ε is the laser spatial efficiency which is:

$$\varepsilon = \frac{4A_T}{\pi\varphi^2 R^2} \tag{4-69}$$

Where:

A_T is the area of the target
φ is the beam divergence

Background photons can be modeled as a graybody and/or solar energy. For solar, the ASMG-G173 solar spectrum (ASTM Docs, 2020) is convenient and shown in Figure 4-9.

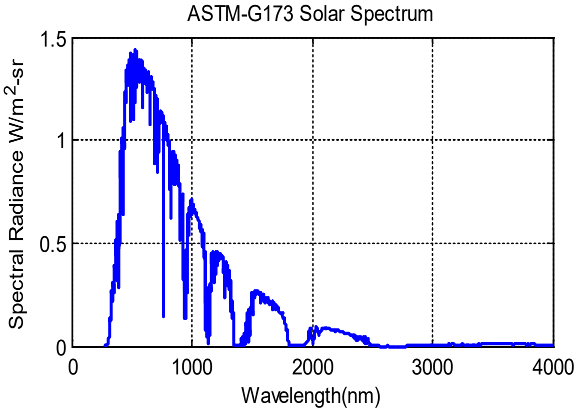

Figure 4-9. ASTM-G173 Solar spectrum used to get background photons.

The background photons are thus:

$$q_b = \sum_{\lambda=\lambda_1}^{\lambda=\lambda_2} L_{\mathrm{bkg}}(\lambda) t_{\mathrm{int}} \left(T_c\rho + (1 - T_c\rho_c)\right) A_o T_o \frac{\lambda}{hc} \tag{4-70}$$

Where:

q_b is the background photon density at the receiver aperture
λ_1 and λ_2 are the receiver wavelength about the laser wavelength, as a top-hat filter
ρ_c is the reflectivity of the canopy =0.1
L_{bkg} is the spectral irradiance of the background on the target in W/m2-sr

We assume that the noise is dominated by background (shot) noise such that:

$$q_{\mathrm{noise}} = \sqrt{q_L + q_b} \tag{4-71}$$

Thus, the signal to noise ratio is:

$$\mathrm{SNR} = \frac{q_L}{q_{\mathrm{noise}}} \tag{4-72}$$

4.6 BIDIRECTIONAL REFLECTANCE DISTRIBUTION FUNCTION (BRDF) MODEL

Bidirectional Reflectance Distribution Function, or BRDF was introduced by Nicodemus (Nicodemus, 1970) as a quantity that completely describes reflectance (or scattering) properties for a diffuse surface. Even smooth surfaces have some degree of roughness. As a result, the apparent reflectance varies with angle of incidences of the illumination source. Understanding BRDF is often critical for satellite and laser-based applications.

This section gives two methods to model BRDF. A special thank you to Liesl Little from Oak Ridge National Laboratory (ORNL) for the models described in this section.

BRDF is defined as the ratio of differential radiance to the differential irradiance, or

$$\mathrm{BRDF} = \frac{\text{differential radiance}}{\text{differential irradiance}} = \frac{\mathrm{dP_s/d\Omega_i}}{\mathrm{dP_i cos\theta_i}} \qquad \text{4-73}$$

BRDFs can be calculated from the power spectral density (PSD) of the surface statistics. The BRDF for a smooth surface based on Rayleigh-Rice relationships is given by (Stover, 1995):

$$\mathrm{BRDF} = \frac{16\pi^2}{\lambda^4}\cos\theta_i\cos\theta_s Q\cdot S(f_x, f_y) \qquad \text{4-74}$$

Where λ = wavelength of the incident and scattered light,

θ_i = the angle of the incident light measured from the surface normal,

θ_s = the angle of the scattered light measured from the surface normal,

Q is a polarization factor dependent on the refractive index, given by the geometric mean of the specular reflectances at θ_i and θ_s for the case of an s-polarized source and plane-of-incidence measurements, and

$S(f_x,f_y)$ is the power spectral density of the surface variation for spatial frequenciesf_x and f_yY.

Several shapes have been suggested for the shape of the surface statistics. The most common shape is the Gaussian, with a height distribution given by

$$P(z) = \frac{1}{\sigma\sqrt{2\pi}}e^{-z^2/2\sigma^2} \qquad \text{4-75}$$

Where z is the distance between points and σ is the surface roughness.

However, fractal (power law) or “Lorentzian-like” distributions are far more common for many polished surfaces. Stover describes several in his book. Each of these power law distributions depends on the autocorrelation length l_c in addition to the surface roughness ⍰. As this model assumes a smooth surface, the bulk of the light is specular with the scattered light as a small fraction of the total.

At the other extreme, Stover presented Beckmann’s Kirchhoff-based relationship for an isotropic randomly rough surface with a normal (Gaussian) height distribution. This yields a BRDF given by

$$\mathrm{BRDF} = \pi R(\theta_i) F_3^2 (L/\lambda)^2 e^{-(\pi f L)^2} \qquad \text{4-76}$$

Where:

$$F_3 = \frac{1 + \cos\theta_i\cos\theta_s - \sin\theta_i\sin\theta_s\cos\phi_s}{\cos\theta_i(\cos\theta_i + \cos\theta_s)} \qquad \text{4-77}$$

$$f = \frac{1}{\lambda}[(\sin\theta_s \cos\phi_s - \sin\theta_i)^2 + (\sin\theta_s \sin\phi_s)^2]^{1/2} \qquad 4\text{-}78$$

$$L = \frac{\ell_c \lambda}{[2\pi\sigma(\cos\theta_i + \cos\theta_s)]} \qquad 4\text{-}79$$

F3 is an obliquity factor, f is the spatial frequency in any orientation, and L is a characteristic length. Both BRDF models described by Stover require measurements of surface roughness, , to calculate the BRDF. For instance, Persson (Persson, 2006) has measured a surface roughness of 10nm for Window glass. Often it is easier to measure a surface than to model it. A multi-axis goniometer is often used to measure BRDF (NIST, 2009). More on surface roughness and light scattering is described by Harvey et al. (1981).

4.7 ATTENUATION MODEL BASED ON SCATTERING THEORY

This model determines the of attenuation due to dust or soot at a given wavelength or frequency. The rule of thumb is that if a particle is the size of the wavelength, it is an obscurant, if it is smaller than the wavelength, the light will pass through the cloud. Firefighters use long wave infrared (LWIR) cameras because the wavelengths are more than twenty times longer than visible and can see through the smoke. This model goes further than this rule of thumb and computes the attenuation through the cloud at the chosen wavelength or frequency.

This section focusses on the millimeter wave, but this model will work for all wavelengths from millimeter wave through ultraviolet as long as the size parameter, x, is less than 100, such that

$$x = k_0 r = 2\pi r/\lambda \qquad 4\text{-}80$$

where k_0 is the wavenumber in a vacuum, r is the particle radius and λ is the wavelength. As always $f = c/\lambda$ where f is the frequency and c is the speed of light.

Most of the scattering models and work are designed to compute particle size distributions. There is some work on attenuation through a cloud in the millimeter wave due to the impact of dust storms on RF transmissions from space. The three models that compute attenuation through a dust cloud in dB/km are:

- A first order Rayleigh model based on the work of Goldhirsh (Goldhirsh 1982, 2001) assuming x<1.
- A Mie model based where the coefficient indices are truncated at maximum of 2 (Islam 2010) for x<100.
- A Mie model based where the Bessel function orders, n, are truncated at a maximum of $n_{\max} = x + x^{1/3} + 2$ as modified from Bohren and Huffman 1983, general case to compute attenuation.

The outputs of these models were compared to the data presented in Islam and Goldhirsh. As expected, the Rayleigh model underestimates the attenuation through the cloud. This section is separated into the following sub-sections:

- General Theory
- Raleigh Approximation

- Mie Approximations
- Model Usage and examples

4.7.1 General Theory

Scattering and extinction of electromagnetic waves is based on Maxwell's equations. Mie scattering theory for spherical particles is a more general case. Detailed derivations are available in two books, Light Scattering by Small Particles (van de Hulst 1957) and Absorption and Scattering of Light by Small Particles (Bohren and Huffman 1983). The bulk of this work is taken from various journal articles and Bohren and Huffman (hereafter referred to as BH). While most work is concerned with measuring particle size distributions from Mie scattering theory, there is limited modeling on attenuation through dust clouds. The basic variables related to attenuation through a dust cloud are the extinction coefficient and the cross-section of the particle. The extinction coefficient, Q_{ext}, is the ratio of the energy absorbed and scattered to the incident energy. The extinction cross section, σ_{ext}, is the equivalent cross section such that:

$$\sigma_{\text{ext}} = \pi \cdot r^2 \cdot Q_{\text{ext}} \tag{4-81}$$

where $\pi \cdot r^2$ is the particle cross sectional area. Integrating the particles in the volume and converting to dB, results in the attenuation due to particles in dB/km as:

$$A = 4.343 \cdot 10^3 \sum_{r_{\min}}^{r_{\max}} \sigma_{\text{ext}} \cdot N(r) \cdot dr \tag{4-82}$$

Where $N(r) \cdot dr$ is the number of particles per unit volume of air with radius between $r_{\min}$ and $r_{\max}$.

The computation of the extinction cross-section differs between the Rayleigh and Mie approximations based on the size parameter, x. The Rayleigh approximation is valid for x<<1 while the Mie approximations are valid for all cases. Materials have two key parameters:

- Permittivity (Farads/meter), ε, describes the ability of a material to hold a charge.
- Permeability (Henry/meter), μ, describes the ability of a material to form a magnetic field.

Permittivity and permeability describe the relationship between the electric and magnetic fields in a material. Permittivity is related to the ability of a material to store charge while permeability is related to the ability of a material to form a magnetic field.

The dielectric constant (typically denoted as κ but denoted in this section as ε for consistency with BH) is the ratio of the permittivity of the material to the permittivity of a vacuum. Relative permeability is the ratio of the permeability of the material to the permeability of a vacuum.

In general Mie theory, the Mie coefficients are dependent on the index of refraction and relative permeability. The simple models used herein assume that relative permeability is one. With this assumption, it can be proved that the unitless dielectric constant, ε, is directly related to the index of refraction, m, as:

$$\varepsilon = \varepsilon' + i\varepsilon'' = (m + ik)^2 \tag{4-83}$$

Where ε' and m are the real part of the dielectric constant and refractive index and ε'' and k are the imaginary part of the dielectric constant and refractive index. The imaginary part of these variables results in absorption while the real part describes whether the material will store (capacitive) or resist holding (inductive) electric charge. Note that m is used for the refractive index instead of n since the referenced literature used n for the Bessel function orders.

4.7.2 Rayleigh Approximation

The Rayleigh approximation can be derived from the more general Mie approximation with the assumption that the particles are much smaller than a wavelength. For millimeter waves, Goldhirsh (1982) derived a Rayleigh approximation for the attenuation ignoring the particle size distribution.

$$A = \frac{2.457 \cdot 10^5 \cdot \varepsilon'' \cdot v_r}{\left[(\varepsilon' + 2)^2 + \varepsilon''^2\right] \cdot \lambda} \tag{4-84}$$

Where v_r is the relative volume of dust particles per cubic meter of air. Since v_r is not readily available, mass loading, M in kg/m^3 is input for a cloud with starting radius, R_0. The relative volume of dust particles is computed using the material mass density, ρ, as:

$$v_r = \frac{M}{\rho} = \frac{9.43 \cdot 10^{-9}}{V_0^{\gamma}} \tag{4-85}$$

Where V_0 is the visibility at the beginning of the event and γ is the visibility exponent. For comparison with the Goldhirsch results, we also computed visibility. The starting visibility is:

$$V_0 = \left(\frac{9.43 \cdot 10^{-9}}{v_r}\right)^{1/\gamma} \tag{4-86}$$

As the cloud grows assuming the same number of particles, visibility is computed as:

$$V(R) = V_0 \cdot e^{(R - R_0)/R_0} \tag{4-87}$$

In the Goldhirsh's model, the cloud can grow, thus reducing the mass density and volume using a simple exponential form where:

$$v_r = \frac{M}{\rho \cdot e^{\gamma \cdot (R - R_0)/R_0}} \tag{4-88}$$

The results from equations 4-84 and 4-86 as compared to the results from Goldhirsh's 2001 paper are shown in Figure 4-10.

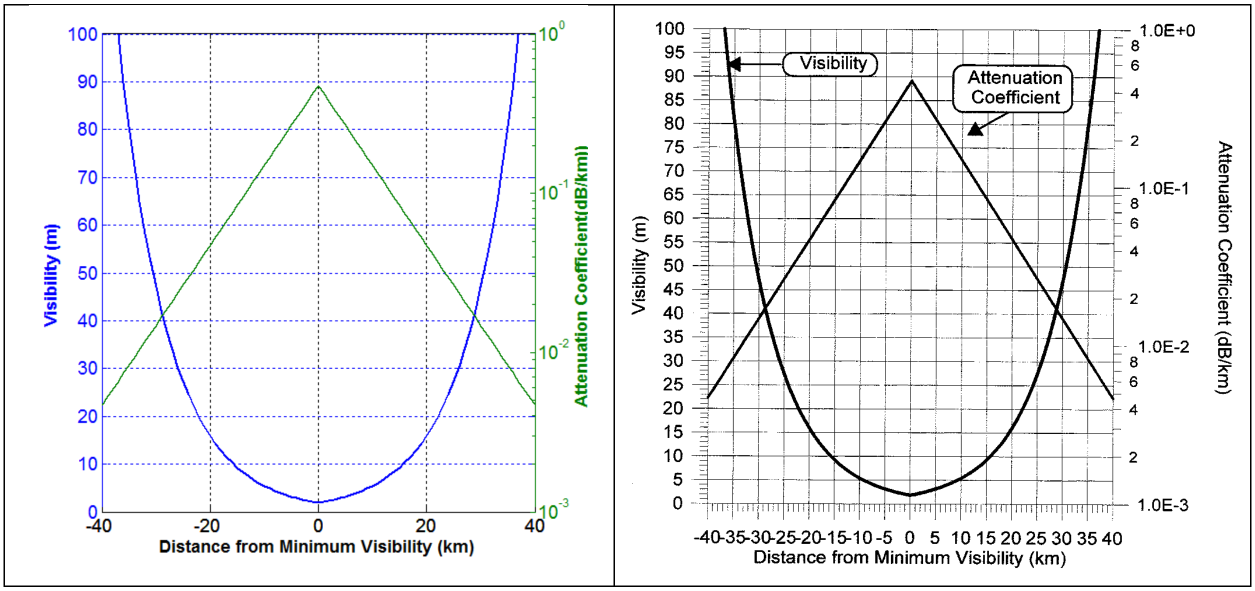

Figure 4-10. Model output (left) and Goldhirsh 2001 (right).

4.7.2.1 Mie Approximations

There were two methods to compute the Mie approximation. The more general Mie approximation method in BH model computes the extinction coefficient, Q_{ext} as

$$Q_{\text{ext}} = \frac{2}{x^2} \sum_{n=1}^{n_{max}} (2n+1) \cdot Re(a_n + b_n) \qquad \text{4-89}$$

From BH, page 100 and assuming that the relative magnetic permeability, µ=1, the Mie coefficients, a_n and $b_n$simplify to (Matzler, 2002):

$$a_n = \frac{m^2 j_n(mx)[x j_n(x)]' - j_n(x)[mx j_n(mx)]'}{m^2 j_n(mx)\left[x h_n^{(1)}(x)\right]' - h_n^{(1)}(x)[mx j_n(mx)]'} \qquad \text{4-90}$$

$$b_n = \frac{j_n(mx)[x j_n(x)]' - j_n(x)[mx j_n(mx)]'}{j_n(mx)\left[x h_n^{(1)}(x)\right]' - h_n^{(1)}(x)[mx j_n(mx)]'} \qquad \text{4-91}$$

The functions $j_n(z)$ and $h_n^{(1)}(z) = j_n(z) + y_n(z)$ are spherical Bessel functions of order n (n=1, 2, …) and of the arguments z=x or mx, respectively. The prime indicates a differentiation with respect to the argument in parentheses, x is the size parameter, and m is the refractive index. In the BH model the summation is truncated at

$$n_{\text{max}} = x + 4 \cdot x^{\frac{1}{3}} + 2 \qquad \text{4-92}$$

The implementation was taken directly from the Matzler implementation of the BH Mie equations. More detail can be found in the two Matzler papers (2002).

As described previously, the extinction coefficient is computed as:

$$\sigma_{\text{ext}} = \pi \cdot r^2 \cdot Q_{\text{ext}} \qquad \text{4-93}$$

and the attenuation due to particles in dB/km as:

$$A = 4.343 \cdot 10^3 \sum_{r_{\min}}^{r_{\max}} \sigma_{\text{ext}} \cdot N(r) \cdot dr \qquad \text{4-94}$$

This more general first method is noted as BHMie. The second method always truncates after two terms ($n_{\max} = 2$). Islam et al. show the approximation for this truncation removing the spherical Bessel functions (Islam 2010) as:

$$\sigma_{\text{ext}} = \frac{\lambda^2}{2\pi} \cdot x^3 (c_1 + c_2 \cdot x^2 + c_3 \cdot x^3) \qquad \text{4-95}$$

Where:

$$c_1 = \frac{6\varepsilon''}{(\varepsilon' + 2)^2 + \varepsilon''^2} \qquad \text{4-96}$$

$$c_2 = \frac{6}{5} \frac{\varepsilon'^2 + 7\varepsilon''^2 + 4\varepsilon' - 20}{\left[(\varepsilon' + 2)^2 + \varepsilon''^2\right]^2} + \frac{1}{15} + \frac{5}{3\left[(2\varepsilon' + 3)^2 + 4\varepsilon''^2\right]} \qquad \text{4-97}$$

$$c_3 = \frac{4}{3}\left[\frac{(\varepsilon' - 1)^2(\varepsilon' + 2) + [(\varepsilon' - 1)(\varepsilon' + 2) - 9] + \varepsilon''^4}{\left[(\varepsilon' + 2)^2 + \varepsilon''^2\right]^2}\right] \qquad \text{4-98}$$

4.7.3 Typical Model steps

An attenuation model may contain the following steps

1. Read material and scenario characteristics from worksheet
2. Set constants and compute related variables
3. Compute Rayleigh per Goldhirsh 1982 & 2001
4. Compute Mie per Bohren & Huffman modified from Matzler 2002
5. Compute Mie per Islam 2010
6. Plot or display output

Table 4-2 shows input file for this model for the Goldhirsh scenario.

Table 4-2. Goldhirsh input file

Menu Title	Variable name	value
Operating frequency (GHz)	f	10.5
Real part of dielectric constant	e_real	5.73
Imaginary part of dielectric constant	e_imag	0.415
Average measured density (kg/m^3)	rho	2440
Mass Loading, M (kg/m^3)	M	0
Visibility	V0	0.00184
Mass loading exponent, gamma	gamma	1.07
Characteristic radial distance (km)	R0	9.26
Particle size distribution file name	PartName	GoldHirshDist.csv
Mean Particle size (μmeters)	r_mean	100

Note that the either visibility or mass loading can be input as a space delimited vector or as a scalar. If both fields are in the spread sheet, Mass loading takes priority over visibility unless mass loading is set to zero. If the **particle size distribution file name** is "none" then the mean particle size (r_mean) is used, if not, then the program will read the distribution file. The distribution file is a comma delimited file with two columns. The second column is the particle size, and the first column is the probability of that particle size. This first column should add up to 1.0 but is rescaled automatically in the program if there are errors in the input file. The attenuation results for this input file are shown in Figure 4-11.

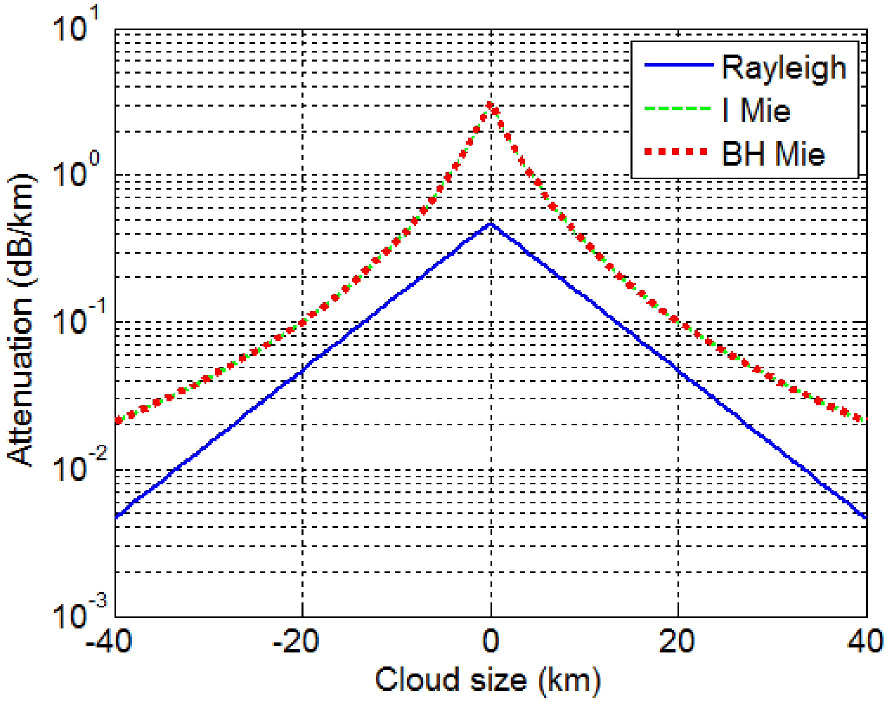

Figure 4-11. Comparison of three models using inputs as described in GoldHirsh 2001.

Table 4-3 shows the input file values for the Islam scenario.

Table 4-3, Islam input file

Menu Title	**Variable name**	**value**
Operating frequency	f	4.00E+10
Real part of dielectric constant	e_real	4
Imaginary part of dielectric constant	e_imag	1.325
Average measured density (kg/m^3)	rho	2440
Mass Loading, M (kg/m^3)	M	0
Visibility	gamma	1.07
Mass loading exponent, gamma	V0	0.625 1.25 1.42 3.75 5.56
Characteristic radial distance (km)	R0	0
Font size	fntSz	14
Particle name	PartName	n/a
Mean Particle size (µmeters)	r_mean	30

Note that the visibility values are a set of space delimited numbers. The output of this model compared with the Islam published values is shown in Table 4-4.

Table 4-4. Comparison of models with data published in Islam et al.

	Islam 2010		**Model**		
Visibility	Raleigh	Mie	Rayleigh	I Mie	BH Mie
0.625	0.02	0.13	0.018	0.1272	0.1273
1.25	0.01	0.064	0.009	0.0636	0.0636
1.42	0.007	0.06	0.0075	0.0560	0.0560
3.75	0.003	0.021	0.0026	0.0212	0.0212
5.56	0.002	0.014	0.0017	0.0143	0.0143

4.8 DISPERSION MODELS

In the previous section, we discussed an attenuation model. Often, dielectric constant is available at only a few frequencies. If that frequency is not the one of interest, the dispersion models allow determination of the dielectric constant for the sensor frequency. There are three models described herein. Two are based on Bohren and Huffman (BH).

The single oscillator Lorentz Dispersion model is applicable to insulators and describes the behavior of a transparent or weakly absorbent material. The single oscillator Drude dispersion model is applicable to metals and heavily doped semiconductors. The Single Debye relaxation fit considers polarization and can be applicable to liquids and non-conductors. A Two-Debye relaxation fit applicable specifically to water can be implemented from work by Meissner et al. (2004) and is not covered herein.

All of these models rely on the plasma frequency. If a force disrupts the natural state of an atom, the restoring force will have a harmonic oscillation with the eigen frequency that is the plasma frequency, ω_p.

$$\omega_p = \sqrt{\frac{e^2 \cdot n}{\varepsilon_0 \cdot m_e}} \qquad 4\text{-}99$$

Where e is the charge of an electron, m_e is the mass of an electron, ε_0 is the permittivity of free space and n is the charge carrier number density computed as:

$$n = \frac{N_a \cdot \rho \cdot x}{M} \tag{4-100}$$

Where

ρ is the density of the material in grams/m^3
x is the number of free electrons per atom
M is the molar mass in grams/mol
N_a is the Avogadro constant = 6.0221 x 10^{23}/mol

The models rely on the dielectric constant, which is directly related to the index of refraction, n, as:

$$n = \sqrt[2]{\varepsilon' + i\varepsilon''} \tag{4-101}$$

Where ε' and ε'' are the real and imaginary parts of the dielectric constant. The relationship between the real and imaginary parts of the dielectric constant is an example of the Kramers-Kronig relations. The interdependence of the parts dictates a dependence of both on frequency. Figure 9.16 from BH (repeated as Figure 4-12 herein) shows the frequency variation of the dielectric function for a non-conductor.

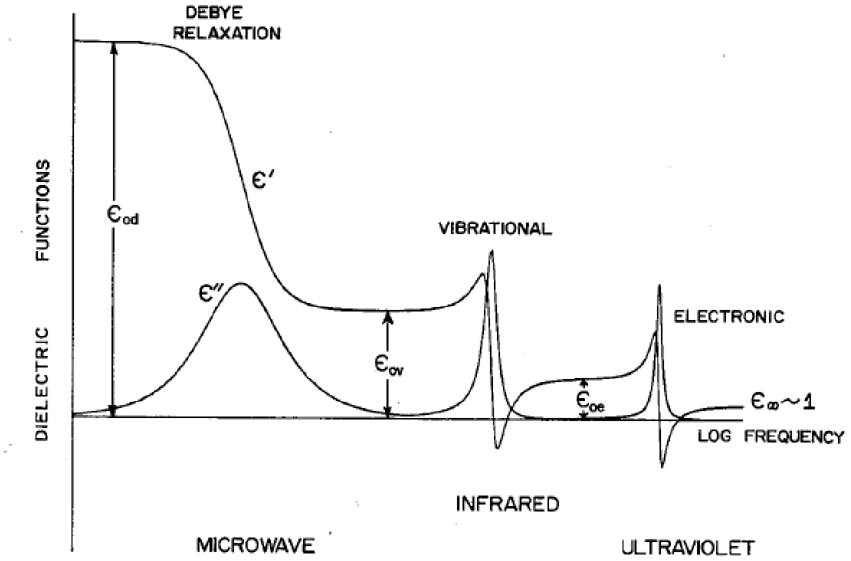

Figure 4-12. Figure 9.16 from BH, frequency variation of the dielectric function for an ideal non-conductor. Note that both the Debye and Lorentz models are applicable depending on the frequency.

Note that the relationship between the two parts is very different depending on the frequency. In this case, the vibrational and electronic modes shift with plasma frequency. This means that there is a limitation on the frequency distance from the known dielectric constant and the predicted one.

These models are the simplest form that give reasonable results for most work. These models thus have limited spectral range and may not apply to every scenario. This section describes the models as modified, how they are integrated, and some examples of attenuation vs frequency.

While the models are taken from other sources, the modifications described herein allow data from a single frequency (wavelength) to be extrapolated to other frequencies. Comparison of new frequency versus old frequency and plasma frequency determine the validity of this implementation. The models were validated against plots and data from literature. The frequency in BH is in angular frequency. In the implementation, the frequency at which the dielectric constant was originally measured can be in eV, Hz (cycles/sec), angular frequency (rad/sec) or wavenumber (cm-1). This is because the equations are modified to allow for consistency within the calculations. For the Lorentz and Drude models, the conversion factors cancel out when deriving the resonant frequency, damping constant and/or plasma frequency which will be in the units of the input to the model.

4.8.1 Single Oscillator Lorentz Model

The single oscillator Lorentz model treats electrons and ions in matter as simple harmonic oscillators (springs). Details are contained in BH section 9.1 are not repeated herein. The real and imaginary parts of the dielectric constant are described in BH equations 9.8 and 9.9 and are repeated below.

$$\epsilon'(\omega) = 1 + \chi'(\omega) = 1 + \frac{\omega_p^2(\omega_0^2 - \omega^2)}{(\omega_0^2 - \omega^2)^2 + \gamma^2\omega^2} \qquad \text{4-102}$$

$$\epsilon''(\omega) = \chi''(\omega) = \frac{\omega_p^2\gamma\omega}{(\omega_0^2 - \omega^2)^2 + \gamma^2\omega^2} \qquad \text{4-103}$$

Where:

χ'	is the real part of susceptibility
χ''	is the imaginary part of susceptibility
ω_p	is the plasma frequency
γ	is the frequency due to the damping constant
ω_0	is the resonance frequency due to the spring constant

If we assume we have a single data point, $\epsilon'_{\omega_{in}}$, $\epsilon''_{\omega_{in}}$ for a known ω_{in} and we have the plasma frequency for the material, we can compute the two unknowns.

$$\gamma = \frac{\omega_p^2\epsilon''_{\omega_{in}}/\omega_{in}}{\left(\epsilon'_{\omega_{in}} - 1\right)^2 + {\epsilon''_{\omega_{in}}}^2} \qquad \text{4-104}$$

$$\omega_0^2 = \frac{\omega_p^2\left(\epsilon'_{\omega_{in}} - 1\right)}{\left(\epsilon'_{\omega_{in}} - 1\right)^2 + {\epsilon''_{\omega_{in}}}^2} + \omega^2 \qquad \text{4-105}$$

The model then computes the dielectric constant for the desired frequencies. To validate this model, a single point on the curve from the Horiba technical Note, “Lorentz Dispersion Model” (Horiba Tech Note, 2020) was selected. It was input into the MATLAB function with the full range of desired frequencies to be computed. Figure 4-13 shows a representation of the Lorentz absorbing function from the Horiba tech note(left), compared to the output of the model (right). Note the precise match.

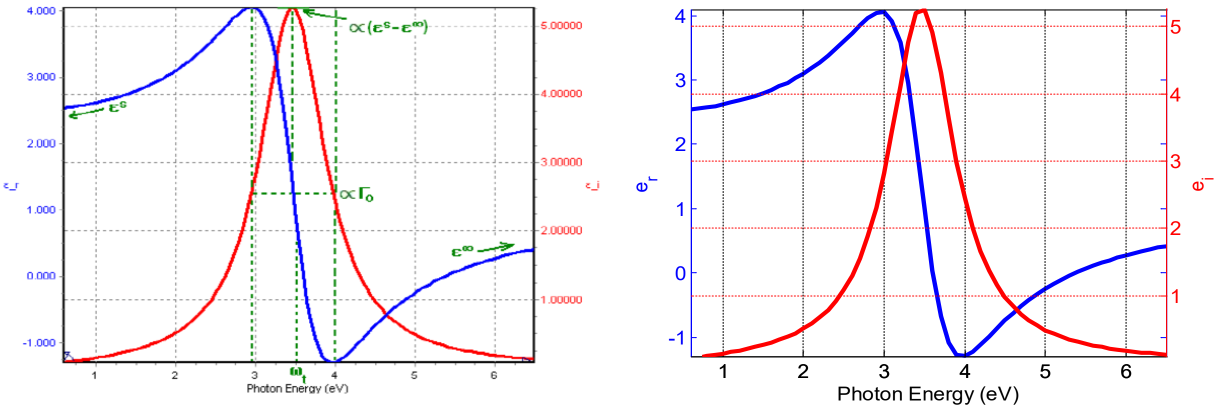

Figure 4-13. Lorentz model, single frequency dielectric constant used to derive parameters (Right). Verified with Test case from Horiba technical note (Left).

This model has limitations. If the dielectric constant is for a millimeter wave frequency, it may not extrapolate properly to visible and IR. To mitigate this, a second dielectric constant is needed in the visible/IR region. An example case for diamond from 300nm to 10 µm based on Phillip et al. was found at the refractiveindex.info site (Polyansky, 2020, Phillip, 1964). A single data point from the curve was used as the basis for comparison. In fact, this data allowed the determination of a more accurate plasma frequency than was found previously. Figure 4-14 shows the excellent agreement between the implemented Lorentz dispersion model compared to measured data.

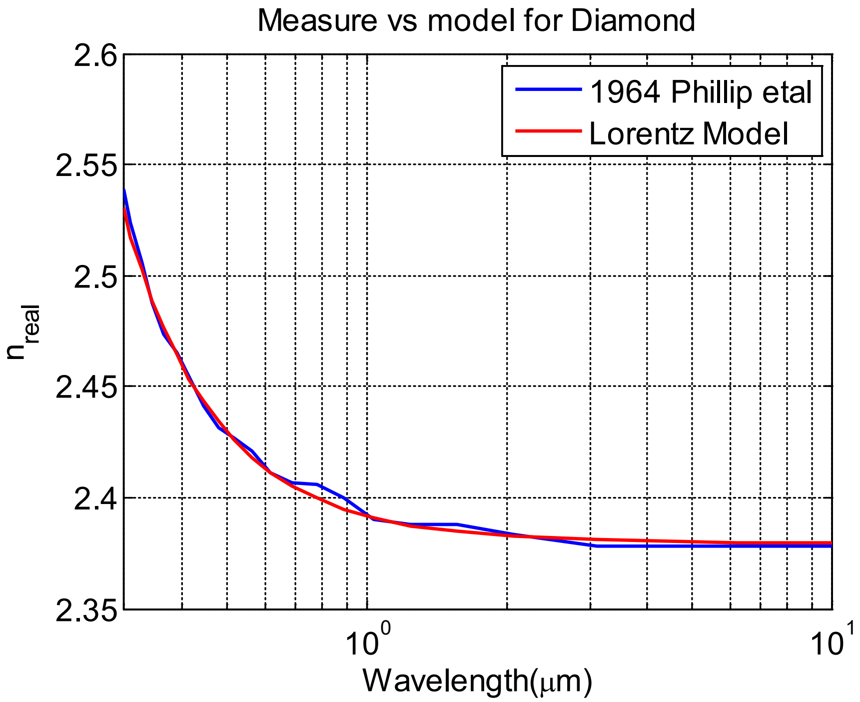

Figure 4-14. Comparison of Phillip Etal data (Blue) with implemented Lorentz model output (red). Selection of the correct plasma frequency resulted in very close agreement.

4.8.2 Drude Model

The Drude dispersion model is applicable to metals and heavily doped semiconductors. The constants for this simplified model can be easily solved for with a single data point ($\epsilon'_{\omega_{in}}$, $\epsilon''_{\omega_{in}}$ for a known ω_{in}). Equation 9.27 from BH is repeated as the two equations below.

$$\epsilon'(\omega) = 1 - \frac{\omega_p^2}{\omega^2 + \gamma^2} \qquad \text{4-106}$$

$$\epsilon''(\omega) = \frac{\omega_p^2 \gamma}{\omega(\omega^2 + \gamma^2)} \qquad \text{4-107}$$

After some manipulation, using the single known data point, ω_p and γ are computed as:

$$\gamma = \frac{\epsilon''_{\omega_{in}} \omega_{in}}{1 - \epsilon'_{\omega_{in}}} \qquad \text{4-108}$$

$$\omega_p^2 = \sqrt{\left(1 - \epsilon'_{\omega_{in}}\right)\left(\omega_{in}^2 + \gamma^2\right)} \qquad \text{4-109}$$

Again, to verify this implementation, a single point on the curve from the Horiba technical Note, “Drude Dispersion Model” (Horiba, 2020) was selected. Figure 4-15 shows the Starting values of a classical Drude function from the Horiba tech note (left), compared to the model output (right). Note the precise match.

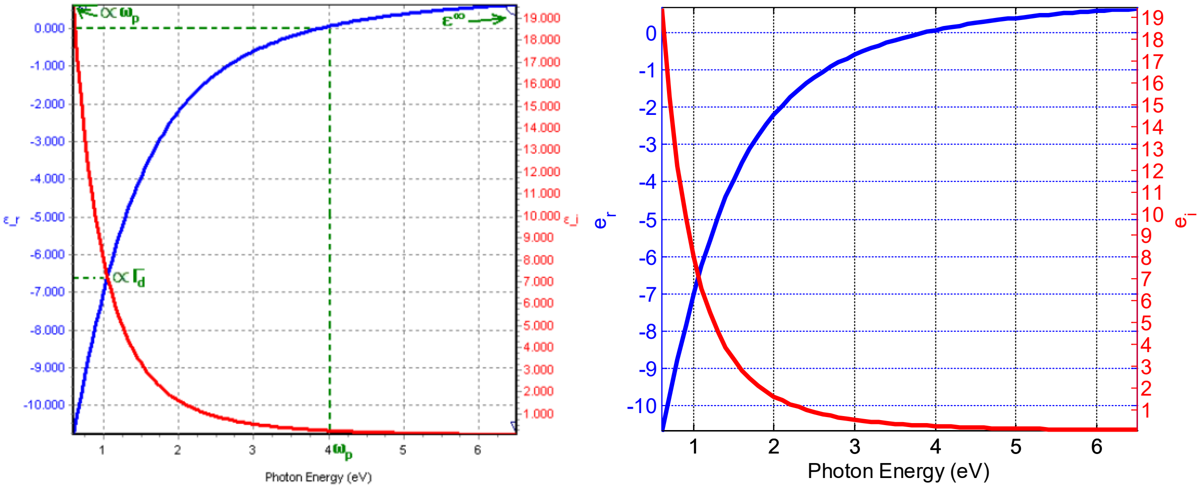

Figure 4-15. Drude model, single frequency dielectric constant used to derive parameters (Right). Verified with Test case from Horiba technical note (Left).

4.8.3 Debye Relaxation Models

The single Debye relaxation fit considers polarization in liquids. It allows determination of attenuation through aerosols and reflectance from liquids. The basis for the implementation is section 9.5 of BH. The real and imaginary parts of the dielectric constant are:

$$\epsilon'(\omega) = \epsilon_{0v} - \frac{\Delta}{1 + \omega^2\tau^2} \qquad \text{4-110}$$

$$\epsilon''(\omega) = \frac{\omega\tau\Delta}{1 + \omega^2\tau^2} \qquad \text{4-111}$$

$$\tau = \frac{4\pi\eta a^3}{K_b T} \qquad \text{4-112}$$

Where

τ	is the relaxation time of a sphere
Δ	is the susceptibility difference in the dominant mode
a	is the radius of the sphere
η	is the viscosity of the fluid
K_b	is Boltzmann's constant = $1.38064852\text{x}10^{-23}$ kg-m^2/s^2-K
T	is the temperature in Kelvin

This model requires that η, a and T are known allowing computation of τ. As before, single data point ($\epsilon'_{\omega_{in}}$, $\epsilon''_{\omega_{in}}$ for a known ω_{in}), we compute the unknowns as:

$$\Delta = \frac{\epsilon''_{\omega_{in}}\left(1+\omega_{in}^2\tau^2\right)}{\omega_{in}\tau} \tag{4-113}$$

$$\epsilon_{0v} = \epsilon'_{\omega_{in}} - \frac{\Delta}{1+\omega^2\tau^2} \tag{4-114}$$

Figure 9.15 of BH served as the basis for verification. A single data point was used to compute the unknowns. The full range of values were then computed. Figure 4-16 shows this verification with the BH figure (left) and the model implementation (right).

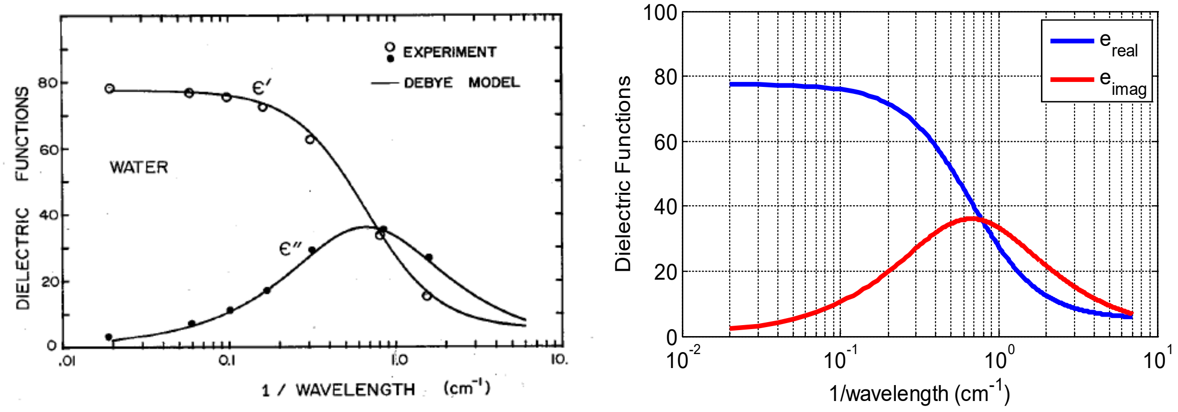

Figure 4-16. Debye single relaxation model with input being a single Frequency Dielectric constant, liquid viscosity, Molecule radius and Temperature. Model Results (Right) compared to Figure 9.15 in BH (Left).

To more accurately model water in the millimeter wave, a Two Debye relaxation fit applicable specifically to water in the millimeter wave can be directly implemented from work by Meissner (2004) and is not included herein.

4.9 Basic Millimeter Wave Sensor Model (frequency) -Signal to Noise & Contrast

As is done in the infrared, we compute the SNR and signal to clutter ratios (SCR). This is done by computing the scene and target irradiance at the entrance aperture and computing the noise equivalent power density at the entrance aperture using the sensor parameters. We add in Mie scattering to get cross sections for sub-resolution debris.

4.9.1 Scene and Target Irradiance

We are assuming all objects are graybody in nature, no selective emissions in the waveband of interest. For a blackbody, the spectral radiance in W-m^{-2}-sr^{-1}-Hz^{-1} is (Planck, 1900) is:

$$L(f,\,T) = \frac{2 \cdot h \cdot f^3}{c^2(e^{hf/kT} - 1)} \qquad \text{4-115}$$

$L(f,\,T)$ = spectral radiance in W-m^{-2}-sr^{-1}-Hz^{-1}
f = frequency in Hz
h = Planck's constant = 6.6260693x10^{-34} W-s^2
c = speed of light = 2.99792458x10^8 m/s
k = Boltzmann's constant = 1.380658x10^{-23} J/K

For our purposes, we are assuming the energy is integrated uniformly into a relatively narrow bandwidth, f_{bw}. Passive RF sources are not Lambertian and radiate into 4π steradians. Thus, M, the radiant exitance in W/m^2 (power density leaving the reflecting and/or emitting object) is:

$$M(f,T) = 4\pi \cdot f_{\text{bw}} \cdot L(f,T) \qquad \text{4-116}$$

The photons into the pixel for an extended (resolvable) source are limited by the steradian subtense of a pixel whereas the photons from a point source are limited by the steradian subtense of the target (Beckman, 1986). A typical model will project the energy through the sensor, but for this model, we will use the irradiance that can be collected by a pixel from the entrance aperture, not including typical sensor parameters used to convert to photons since these cancel out in the final SNR equations. This allows computation of SNR and contrast more directly using only the sensor resolution and target subtense. The irradiance collected by a pixel, E, for an emissive target is:

$$E = \varepsilon \cdot \frac{\min\left(\phi^2, \phi_{\text{pix}}^2\right)}{4\pi} \cdot M(f,T_b) = \min\left(\phi^2, \phi_{\text{pix}}^2\right) \cdot f_{\text{bw}} \cdot \varepsilon \cdot L(f,T_b) \qquad \text{4-117}$$

Where ε is the emissivity of the target, ϕ_{pix}^2 is the steradian subtense of the pixel, and ϕ^2 is the steradian subtense of the source equal to:

$$\phi^2 = \frac{A_s}{R^2} \qquad \text{4-118}$$

Where R is the range to target in meters and A_ss is the area of the source object. We use the target reflectivity and or emissivity computed from the Mie scattering model.

If ϕ^2 is smaller than the sensor instantaneous field of view (IFOV) squared, ϕ_{pix}^2, the object is unresolvable, and the limit is the true area of the source. If not, the source is resolvable or extended and the limit is the area captured by the detector pixel. The background is assumed to be an extended source, thus irradiance at the entrance aperture captured by a pixel is:

$$E_b = \phi_{\text{pix}}^2 \cdot f_{\text{bw}} \cdot \left[\varepsilon_b \cdot L(f,T_b) + \rho_b \cdot L\left(f,T_{\text{sky}}\right)\right] \qquad \text{4-119}$$

Where ε_b is the emissivity of the background, ρ_b is the reflectance of the background, T_{sky} is the sky temperature and T_b is the temperature of the background. It is assumed that $\rho_b = 1 - \varepsilon_b$. The object may be an extended or a point source. It is assumed that the object reflects half sky and half background thus

$$E_o = \min\left(\phi^2, \phi_{\text{pix}}^2\right) \cdot f_{\text{bw}} \cdot t_{\text{cloud}} \cdot \left[\varepsilon \cdot L(f,\,T_o) + \rho \cdot 0.5 \cdot \left[L(f,\,T_b) + L\left(f,\,T_{\text{sky}}\right)\right]\right] \qquad \text{4-120}$$

4.9.2 Targets - Debris Reflectivity, Emissivity and Attenuation

For large pieces of debris, we assume that the surface is specular since it is smooth via Rayleigh criteria d<λ/(8cos(θ)) (Beckman, 1963). This means that for debris larger than the wavelength, the simple reflectance and transmission calculation using refractive index will suffice. For smaller objects, we return to the Mie model.

The debris reflectivity and emissivity can be computed leveraging the Mie model implemented for computation of attenuation as described in section 4.7, attenuation model. Reflectivity and emissivity use some of the same equations which are repeated for convenience.

From BH, page 100 and assuming that the relative magnetic permeability, μ=1, the Mie coefficients, a_n and $b_n$simplify to (Matzler, 2002),

$$x = k_0 r = 2\pi r/\lambda \qquad \text{4-121}$$

$$m = \sqrt[2]{\varepsilon' + i\varepsilon''} \qquad \text{4-122}$$

$$a_n = \frac{m^2 j_n(mx)[xj_n(x)]' - j_n(x)[mxj_n(mx)]'}{m^2 j_n(mx)\left[xh_n^{(1)}(x)\right]' - h_n^{(1)}(x)[mxj_n(mx)]'} \qquad \text{4-123}$$

$$b_n = \frac{j_n(mx)[xj_n(x)]' - j_n(x)[mxj_n(mx)]'}{j_n(mx)\left[xh_n^{(1)}(x)\right]' - h_n^{(1)}(x)[mxj_n(mx)]'} \qquad \text{4-124}$$

where k_0 is the wavenumber in a vacuum, r is the particle radius and λ is the wavelength. As always $f = c/\lambda$ where f is the frequency and c is the speed of light.

The functions $j_n(z)$ and $h_n^{(1)}(z) = j_n(z) + y_n(z)$ are spherical Bessel functions of order n (n=1, 2, …) and of the arguments *z=x* or *mx*, respectively. The prime indicates a differentiation with respect to the argument in parentheses, *x* is the size parameter, and *m* is the refractive index. In the BH model the summation is truncated at:

$$n_{\max} = x + 4 \cdot x^{\frac{1}{3}} + 2 \qquad \text{4-125}$$

Using these coefficients, the backscattering efficiency, Q_b, is directly related to the reflectance at normal incidence (Bohren, 1983) (BH page 122, 123) and is computed as:

$$\rho = Q_b = \frac{1}{x^2}\left|\sum_{n=1}^{n_{\max}}(2n+1)\cdot(-1)^n\cdot(a_n - b_n)\right|^2 \qquad \text{4-126}$$

It can be proved that the emissivity, *e*, of a graybody is equal to the absorption efficiency, Q_{abs}, (BH page 123) which is computed as:

$$\varepsilon = Q_{\text{abs}} = Q_{\text{ext}} - Q_{\text{sca}} \qquad \text{4-127}$$

$$Q_{\text{sca}} = \frac{2}{x^2}\sum_{n=1}^{n_{\max}}(2n+1)\cdot\left(|a_n|^2 + |b_n|^2\right) \qquad \text{4-128}$$

$$Q_{\text{ext}} = \frac{1}{x^2} \sum_{n=1}^{n_{\max}} (2n+1) \cdot Re(a_n + b_n) \tag{4-129}$$

Where Q_{ext} is the extinction efficiency and Q_{sca} is the scattering efficiency. The implementation was taken directly from the Matzler implementation of the BH Mie equations.

We now have reflectance and emissivity for our larger debris. We compute the error on these values from the uncertainty of the radius of the debris. This uncertainty propagates to the target irradiance and thus the SNR and SCR values.

Section 4.7 provides expressions for the attenuation through the cloud in dB in dB/km. The expression for transmission through the cloud as a number from 0 to 1.0 is thus:

$$t_{\text{cloud}} = e^{-R_z \cdot \sum_{r_{\min}}^{r_{\max}} \sigma_{\text{ext}} \cdot N(r) \cdot dr} \tag{4-130}$$

$$\sigma_{\text{ext}} = \pi \cdot r^2 \cdot Q_{\text{ext}} \tag{4-131}$$

4.9.3 Noise equivalent Irradiance

For these millimeter wave sensors, the NEDT takes into account the spreading of the point spread function over multiple pixels, thus the limit between resolvable and unresolvable source still rests with the spatial resolution limit.

Assuming emissivity of 1.0, the noise irradiance collected by a pixel is

$$E_n = f_{\text{bw}} \cdot \phi_{\text{pix}}^2 \cdot [L(f,\, T_{\text{nedt}} + \Delta T) - L(f,\, T_{\text{nedt}})] \tag{4-132}$$

4.9.4 Signal to Noise and Contrast Ratios

The signal to noise ratio provides information on whether the scene is above the noise and is simply:

$$E_o / E_n \tag{4-133}$$

The signal to contrast ratio (SCR) is:

$$(E_o - E_b)/E_n \tag{4-134}$$

SCR can be positive or negative. For sub-resolution targets, only a positive SCR is meaningful since a negative SCR indicates there are not enough photons from the object. For scenes with extended sources, both positive and negative SCRs indicate the ability to see objects that have SNRs above a minimum required for algorithms, which is typically around five. A negative SCR for an extended source indicates a dark object on a light background; a positive SCR indicates a light object on a dark background.

5 Sensor Calibrations and Characterizations

A sensor is only as good as its calibration and/or characterization. In this section we will cover how to:

- Radiometrically calibrate an imaging sensor
- Measure sensor responsivity - a value used in many of the models
- Spectrally and radiometrically calibrate a spectrometer

5.1 Imaging Sensor – extended source

Sensor calibrations are best done at the entrance aperture of the sensor using an extended source or a point source depending on the application. A good calibration allows an educated guess for sensor settings in the field minimizing (and possibly eliminating) trial and error in setup.

For reflective systems, Spectralon or an integrating sphere with a calibrated light source works well. Instead of a calibrated lamp, the measurement of the lamp with a calibrated spectrometer is excellent. For IR system, a blackbody source is required. The response of the system is computed as the digital number (dn) per second per Watt-sec/m^2 at the entrance aperture. Said another way, this is the counts per unit time per in-band irradiance into the optical system. To verify exactly the response of the system, the camera, lens and filter are calibrated with the setup shown in Figure 5-1.

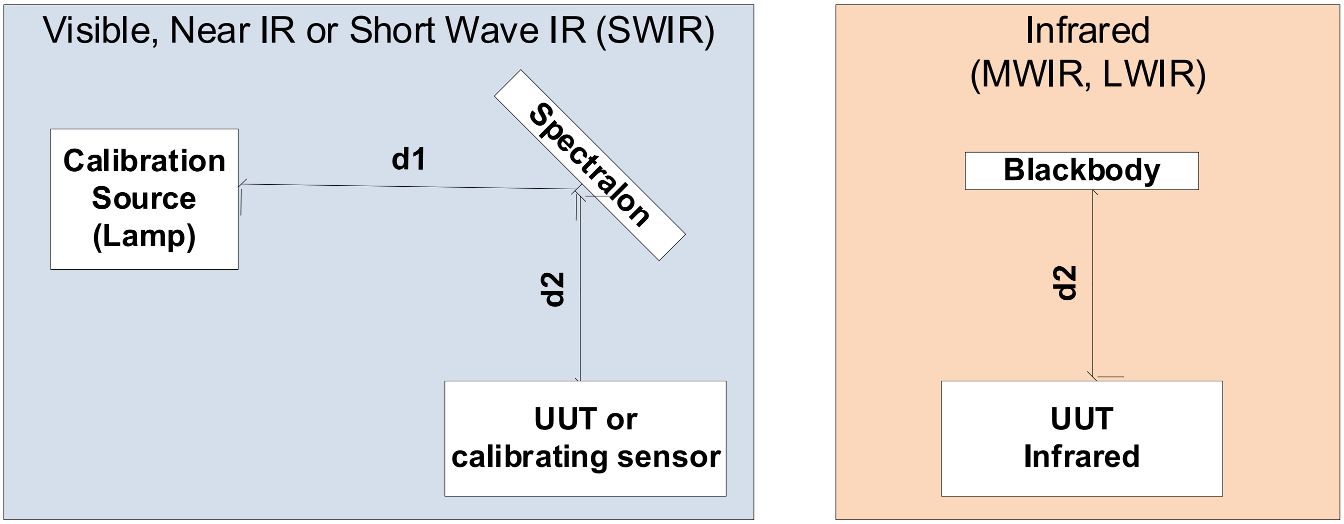

Figure 5-1. Calibration test setup for VNIR and SWIR (left). Illumination from the calibrated source is reflected off the diffuse Spectralon surface into the optical system. If no calibration data is available for the illumination source, a calibrated spectrometer such as an ASD can be placed where the Unit under Test (UUT) is located. It is important to note distance d1. Distance d2 needs to be far enough back to ensure enough of the sensor image plane is illuminated. For infrared calibrations, only a blackbody is needed. Note that Dark frames with the same exposure time are taken by covering the lens to remove variations in the focal plane. For infrared sensor calibrations, a cold source provides the dark data.

The illumination from a calibration source is uniformly reflected off the Spectralon surface for reflective systems, and a blackbody source is used for emissive systems. This illumination is captured by the camera system. Dark frames are captured to remove detector variability. A calibration curve may be provided by the calibration source (lamp) manufacturer for a distance (typically 50 cm) from a

Lambertian surface (Spectralon). The ratio of the square of the actual distance, d1 to this distance will determine the actual irradiance. When using a lamp that is not calibrated, the spectral irradiance off the Spectralon can be measured with a spectrometer such as an ASD FieldSpec. Having the lamp source normal to the Spectralon provides a more uniform illumination source since tilt will cause one side or the other to be brighter due to the distance to the Spectralon being longer at one side of the illumination spot. The camera will see this illumination off the Spectralon as an extended Lambertian source, thus the angle between the camera and the Spectralon is not critical. Centering of the camera on the spot produced by the lamp is important. The analysis steps executed are:

1. Compute the in-band calibration source irradiance
2. Compute the average and standard deviation of the counts from the camera system for the given test set up
3. Determine the Responsivity, dn/(W-sec/m^2), using the exposure time and the lamp source irradiance

The lamp irradiance off the Spectralon is computed as:

$$H_{\text{Lamp}} = \frac{d_{\text{cal}}^2}{d_1^2}\int_{\lambda_1}^{\lambda_2} W_{\text{Lamp}}(\lambda)\cdot T_{\text{filt}}(\lambda)\cdot d\lambda \qquad \text{5-1}$$

Where $T_{\text{filt}}(\lambda)$ is the filter transmission and d_{cal} is the distance for the calibration source data. If the spectral radiance is measured or the source is a blackbody d_{cal}^2/d_1^2 = 1. Notice the square law.

To determine the mean counts, at least one hundred frames should be analyzed to create a statistically significant sample. This includes subtracting a mean background frame taken at the same exposure time. If the source does not fully fill the field of view, the most uniform region of interest (ROI) should be selected. For this ROI, each pixel is averaged to produce a single average image such that the average dn is:

$$dn_{\text{mean}} = \langle dn_{\text{meas}}\rangle_{\text{all } x,y \text{ \& frames}} - \langle dn_{\text{dark}}\rangle_{all\ x,y \text{ \& frames}} \qquad \text{5-2}$$

Each of these pixels are averaged and the standard deviation of all pixels is computed to allow uncertainty analysis. The in-band responsivity is then computed as

$$\Re = \frac{dn_{\text{mean}} \pm dn_{\text{std}}}{H_{\text{Lamp}}\cdot t_{\text{int\_meas}}} \qquad \text{5-3}$$

Where $\Re$ is the responsivity in counts/(W-sec/m^2), and H_{Lamp} is the in-band irradiance of the lamp and t_{int_meas} is the exposure time during the measurement. Using multiple exposure times allows a better estimate of the responsivity. Having this responsivity for the sensor as fielded allows an estimate of the expected counts for an experiment. This allows determination of exposure times that allow the best SNR without saturation. Using the responsivity, the expected dn from an experiment can now be computed for a target temperature, *T*, and exposure time, t_{int}, as:

$$\widehat{dn}(T, t_{\text{int}}) = \Re\cdot H(T)\cdot t_{\text{int}} \qquad \text{5-4}$$

The in-band irradiance for the graybody, $H(T)$, is thus computed as:

$$H(T) = \int_{\lambda_1}^{\lambda_2} \frac{c_1\cdot\varepsilon(\lambda)}{\lambda^5\left(e^{c_2/\lambda T}-1\right)}\cdot T_{\text{filt}}(\lambda)\cdot T_{\text{atm}}(\lambda)\cdot d\lambda \qquad \text{5-5}$$

Where:

$H(\lambda,\ T)$ = spectral radiant exitance in W/m^2-nm

T = Temperature in Kelvin

ε = emissivity of the cloud, assumed flat over the spectral region of interest

c_1 = first radiation constant = 3.7415 x 10^{20} W nm^4/m^2

c_2 = second radiation constant = 1.43879 x 10^7 nm-K

λ = Wavelength in nm

5.1.1 SINGLE PIXEL OR SUB-RESOLUTION CALIBRATION

This is typically done for single pixel radiometers or for systems that look for small targets at range such as missile warning systems. The response of a detector in volts is related to the irradiance at the entrance aperture, H, in W/cm^2. To calibrate a sensor as a measurement device, the radiance of the source, N, in W/cm^2-sr is known. Figure 5-2 shows the basic setup for a point source calibration.

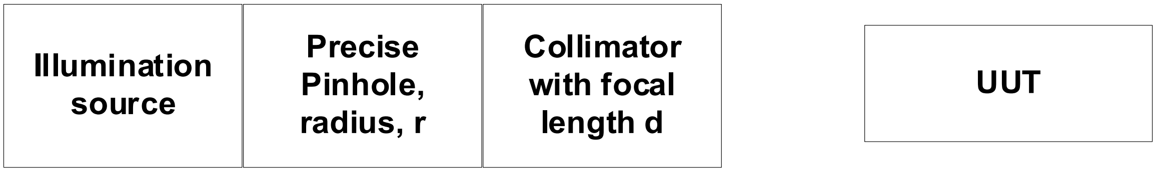

Figure 5-2. Basic setup for point source calibration. The use of a collimator makes the distance between the setup and the unit under test (UUT) unimportant.

A collimator changes a diverging beam to parallel rays making the point look like it is at infinity and setting the angular subtense of the pinhole to a known constant size. This makes the irradiance independent of the distance to the unit under test (UUT), but the alignment angle with respect to the collimator is extremely important and can be difficult. While not optimum, a poor man's collimator can be made by turning a telescope backwards and avoiding the secondary mirror. Radiance is a measure of radiant flux per unit area of source. It is related to radiant intensity in W/sr, J as:

$$H = \frac{J}{d^2} = \frac{W \cdot \pi \cdot r^2}{d^2} \tag{5-6}$$

After measuring the corresponding voltage, we get conversion factor, or response, R, in Volts per W/m^2.

$$R = \frac{V}{H} \tag{5-7}$$

5.2 Spectral Responsivity and Relative Spectral Response (RSR) of a camera

As indicated in the modeling section, we often need the relative spectral response (RSR) and ideally the responsivity of a camera or sensor. Most infrared sensor manufacturers will provide this with the sensor. Visible and near infrared commercial cameras often do not have calibration data other than a quantum efficiency (QE) at a specific wavelength. A single wavelength QE combined with the measured relative spectral response (RSR) will provide a full QE (spectral responsivity) curve. To characterize a sensor versus wavelength, we use an illumination source and a monochromator as shown in Figure 5-3**.**

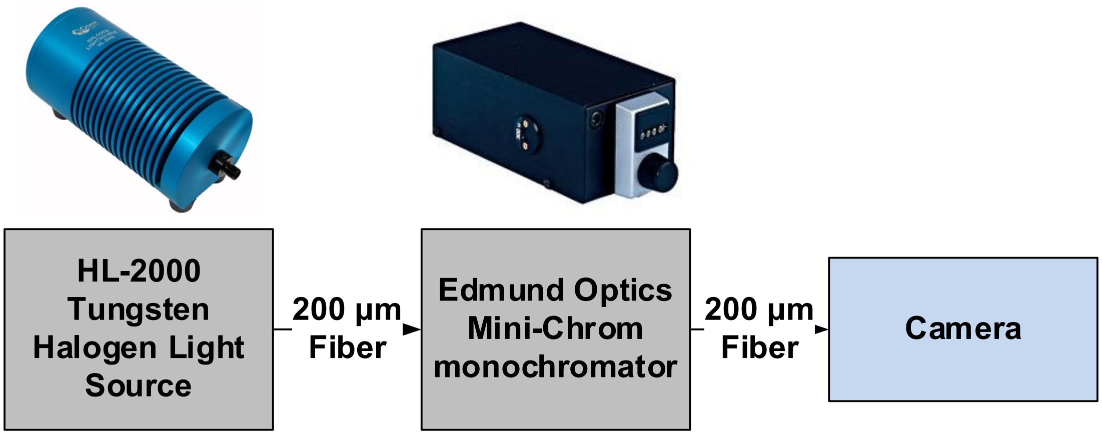

Figure 5-3. Camera RSR measurement setup.

A monochromator is an optical device that separates polychromatic light (such as sunlight or light coming from a lamp) into a range of individual wavelengths (monochromatic light) and allows a narrow individual wavelength to be selected. The dial on the monochromator is set to the desired wavelength, The broadband illumination from the lamp is fed into the monochromator which only allows that single wavelength to be seen by the camera. A set of frames from the camera are recorded and this is repeated for a set of wavelengths. There are programmable monochromators, but the process is the same as for the manual one shown.

The steps to do this calibration are:

1. Measure the dn of the camera with the setup
2. Characterize the monochromator vs wavelength using a spectrometer
3. Calculate the RSR

5.2.1 Camera Measurement

To measure the dn from the camera, we collected a series of images of the fiber end, one for each wavelength. For color cameras, extra care must be taken in collecting each frame since it is easy to end up with one color being saturated since the imaged displayed often does not indicate the actual data intensity collected. To extract the average counts for the fiber end, the user should select the fiber region of interest (ROI) and a background ROI from the collected image as shown in Figure 5-4.

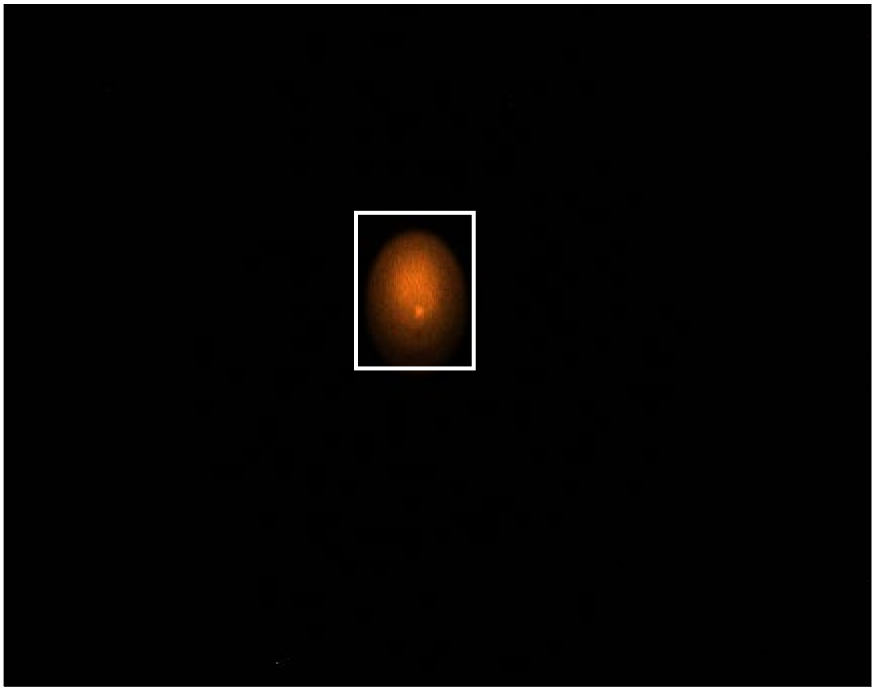

Figure 5-4. Selected ROI for sample color camera image. The background ROI was selected in the upper right corner of the image away from the fiber image.

The mean value of that ROI for all pixels greater than the background mean (in the selected dark ROI) is computed. The background mean is subtracted from this mean dn to determine the dn value for that wavelength used in this calculation as:

$$dn(\lambda) = \langle dn_{\text{meas}} \rangle_{\text{ROI}} - \langle dn_{\text{dark}} \rangle_{\text{ROI\_dk}} \qquad \text{5-8}$$

This is measured for each monochromator wavelength required to characterize the sensor. Following the path of photons to electrons through this setup, the measured dn from the camera will be equal to:

$$dn(\lambda) = L_{\text{lamp}}(\lambda) \cdot T_{\text{fiber}}^2(\lambda) \cdot T_{\text{mono}}(\lambda) \cdot R(\lambda) \cdot t_{\text{int}} \qquad \text{5-9}$$

Where:

- $L_{\text{lamp}}(\lambda)$ is the spectral irradiance of the lamp
- $T_{\text{fiber}}^2(\lambda)$ is the spectral transmittance of the fiber
- $T_{\text{mono}}(\lambda)$ is the spectral transmittance of the monochromator
- $\Re(\lambda)$ is the spectral responsivity of the camera including aperture effects
- t_{int} is the integration (or snapshot time) of the collect

Rearranging this equation we get:

$$\Re(\lambda) = \frac{dn(\lambda)}{L_{\text{lamp}}(\lambda) \cdot T_{\text{fiber}}^2(\lambda) \cdot T_{\text{mono}}(\lambda) \cdot T_{\text{fiber}}(\lambda) \cdot t_{\text{int}}} \qquad \text{5-10}$$

For relative spectral response, we only care about curve shapes and not absolute values. From this the RSR is just responsivity normalized to the maximum of responsivity. For the purpose of this section, we will continue to use absolute units.

There are four unknowns in the denominator of this equation. The transmission of the fiber is provided by the manufacturer. The lamp curve for the case of a tungsten lamp is derived based on a blackbody temperature and the spectral emissivity of tungsten assuming a temperature of about 2300K. When a Deuterium lamp is used, either a measurement or a calibration file from the manufacturer is required. This leaves the monochromator which can be calibrated as described in the next section.

5.2.2 Monochromator response measurement, including spectrometer calibration

The monochromator response is measured using a spectrometer in the basic setup shown in Figure 5-5.

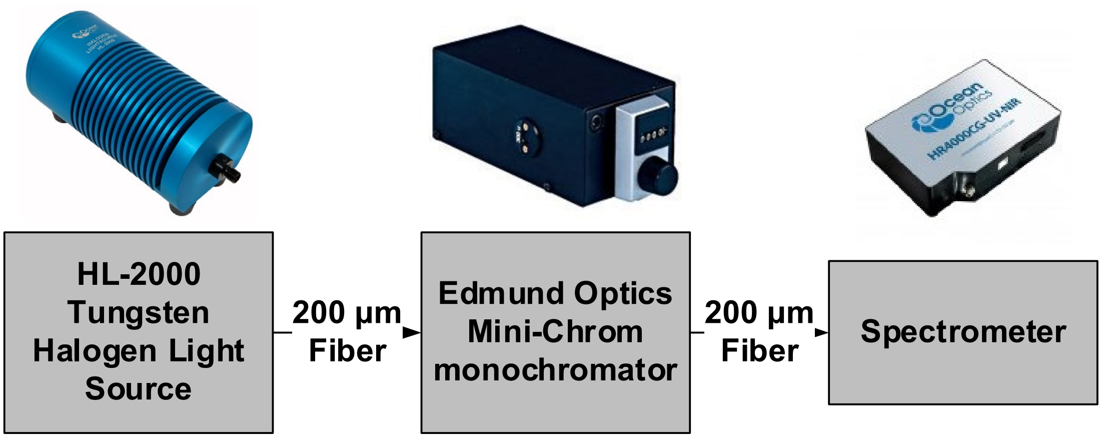

Figure 5-5. Monochromator spectral response measurement setup.

Following the path of photons to electrons and rearranging the equation, the monochromator transmission is computed as:

$$T_{\text{mono}}(\lambda) = \frac{dn_{\text{spect}}(\lambda)}{L_{\text{lamp}}(\lambda) \cdot R_{\text{Spect}}(\lambda) \cdot T_{\text{fiber}}^{2}(\lambda) \cdot t_{\text{int1}}} \qquad \text{5-11}$$

This now leaves one unknown, the response of the spectrometer itself. This is measured using the setup shown in Figure 5-6.

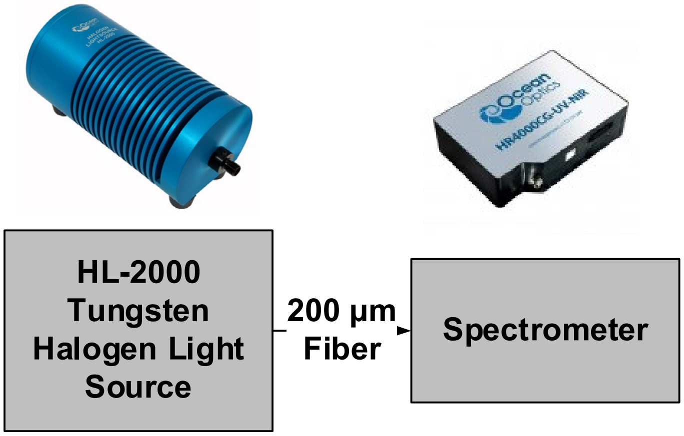

Figure 5-6. Spectrometer spectral response measurement setup.

This results in equation 5-12:

$$dR_{\mathrm{Spect}}(\lambda) = \frac{dn_{\mathrm{cal}}(\lambda)}{L_{\mathrm{lamp}}(\lambda) \cdot T_{\mathrm{fiber}}(\lambda) \cdot t_{\mathrm{int2}}} \qquad \text{5-12}$$

This response for the spectrometer is useful and can be normalized to an RSR for future use. An example for a USB 2000 spectrometer response (black line) from 350 to 1000nm using a tungsten lamp (blue line) with the measured dn_{cal} (red line) is shown in Figure 5-7.

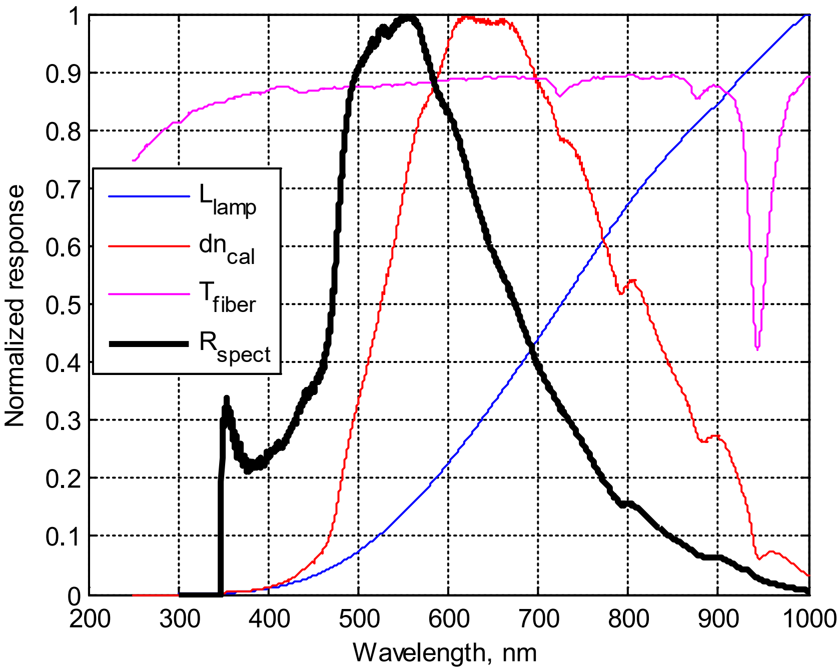

Figure 5-7. USB2000 spectrometer spectral response (black) derived from the lamp (blue), the measured dn (red), and the fiber (magenta).

5.2.3 Compute RSR

For the RSR of the camera, we substitute equations 5-11 and 5-12 into equation 5-10 and simplify to get:

$$R(\lambda) = \frac{dn(\lambda)/t_{\mathrm{int}} \cdot dn_{\mathrm{cal}}(\lambda)/t_{\mathrm{int2}}}{L_{\mathrm{lamp}}(\lambda) \cdot T_{\mathrm{fiber}}(\lambda) \cdot dn_{\mathrm{spect}}(\lambda)/t_{\mathrm{int1}}} \qquad \text{5-13}$$

The 3-sigma positive and negative errors on this measurement are computed using statistical noise as follows:

$$\mathrm{err}_p(\lambda) = R(\lambda) - \frac{(dn(\lambda)+3*std(dn(\lambda))/t_{\mathrm{int}} \cdot (dn_{\mathrm{cal}}(\lambda)+std(dn_{\mathrm{cal}}(\lambda))/t_{\mathrm{int2}}}{L_{\mathrm{lamp}}(\lambda) \cdot T_{\mathrm{fiber}}(\lambda) \cdot (dn_{\mathrm{spect}}(\lambda)-std(dn_{\mathrm{spect}}(\lambda))/t_{\mathrm{int1}}} \qquad \text{5-14}$$

$$\mathrm{err}_n(\lambda) = R(\lambda) - \frac{(dn(\lambda)-3*std(dn(\lambda))/t_{\mathrm{int}} \cdot (dn_{\mathrm{cal}}(\lambda)-std(dn_{\mathrm{cal}}(\lambda))/t_{\mathrm{int2}}}{L_{\mathrm{lamp}}(\lambda) \cdot T_{\mathrm{fiber}}(\lambda) \cdot (dn_{\mathrm{spect}}(\lambda)+std(dn_{\mathrm{spect}}(\lambda))/t_{\mathrm{int1}}} \qquad \text{5-15}$$

The curves for each color are corrected for equipment via equation 5-13. The results for a sample color camera with an IR cut filter removed are shown in Figure 5-8.

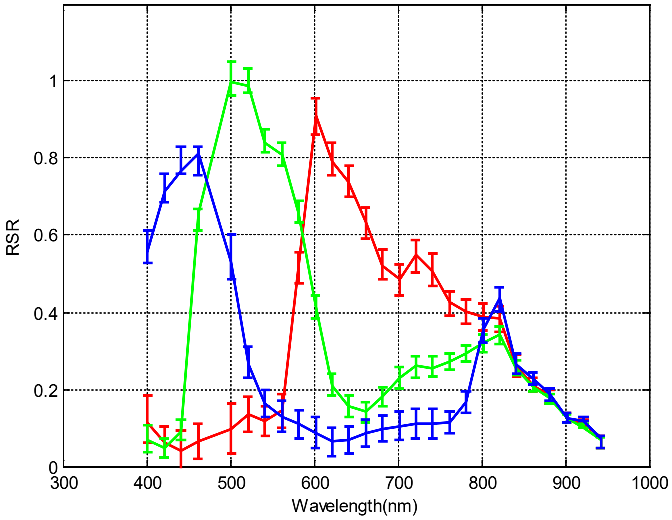

Figure 5-8. Relative spectral response for an example color camera.

To convert RSR to a quantum efficiency (QE) versus wavelength

$$QE(\lambda) = R(\lambda) \cdot \frac{QE(\lambda_{\text{spec}})}{R(\lambda_{\text{spec}})} \tag{5-16}$$

Where λ_{spec} is the wavelength where the manufacturer specified the single value of QE.

5.3 Spectrometer Calibration

Calibrating a spectrometer assembled with a camera or line detector and a grating requires care accurate measurements of both wavelength versus pixel location and radiance versus digital number (dn). A detailed collection procedure is available (O'Neill, 2023), only the basics are provided herein. It is critical that data be corrected for noise. This is included in this section. For a spectrometer calibration, the setup is nearly the same as that for a sensor and is shown in Figure 5-9.

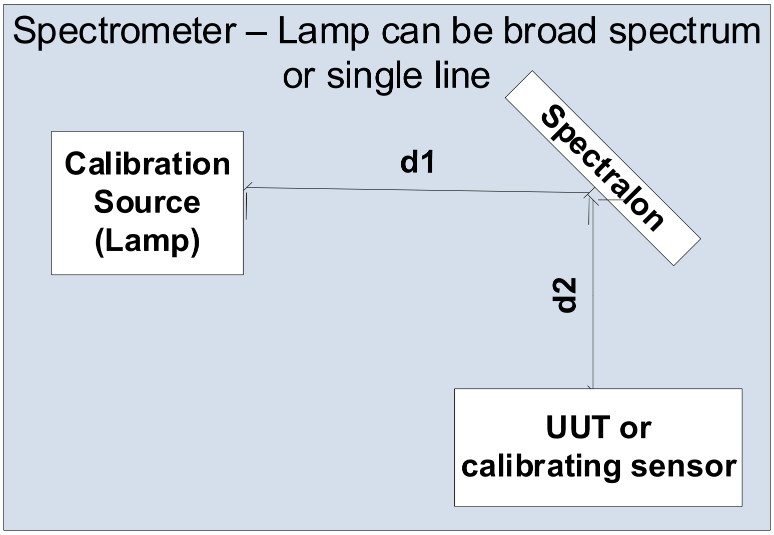

Figure 5-9. Calibration setup for Spectrometer, the lamp is either a spectral line source (Hg or Ar) or a broad source (W).

Spectrometer calibration data are:

1. Spectral calibration with a line lamp such as Hg-Ar lamp or Deuterium lamp
2. Radiometric calibration data with a broad-spectrum lamp such as Tungsten (bright) and corresponding dark frames for multiple exposure times.

Analysis of this data are provided in the following sections:

5.3.1 Spectral calibration (wavelength)

Using the data collected with line lamp (such as an Hg-Ar lamp) we determine the spectral resolution and wavelength versus pixel location. This example is for a camera with M x N (rows, columns) of pixels coupled to a grating. It is recommended that a minimum of 100 frames of data are recorded.

The average dark counts in digital number (dn) for integration time, t_{int}, versus wavelength dispersion position (x) is:

$$\overline{dn}_{\mathrm{dark}}(x, t_{\mathrm{int}}) = \frac{\sum_{y=1}^{M} \sum_{k=1}^{K} dn_{\mathrm{dark}}(x, y, t_{\mathrm{int}}, k)}{K \cdot M} \quad 5\text{-}17$$

Where

k is the frame number and K is the total number of frames.
x is the pixel location for each wavelength (column)
y is the pixel location for each row
t_{int} is the exposure time

Compute the mean spectral data as:

$$\overline{dn}_{\mathrm{spect}}(x, t_{\mathrm{int}}) = \frac{\sum_{y=1}^{M} \sum_{k=1}^{K} dn_{\mathrm{spect}}(x, y, t_{\mathrm{int}}, k)}{K \cdot M} \quad 5\text{-}18$$

Compute the mean measured spectrum corrected for dark pixels as:

$$dn_{\mathrm{spect}}(x, t_{\mathrm{int}}) = \overline{dn}_{\mathrm{spect}}(x, t_{\mathrm{int}}) - \overline{dn}_{\mathrm{dark}}(x, t_{\mathrm{int}}) \quad 5\text{-}19$$

We find the x locations (columns) for the highest values of $dn_{\mathrm{spect}}(x, t)$, ideally, we get three peaks. These should correspond to known wavelengths from our line lamp to correlate x to wavelength, λ. We assume the dispersion is linear such that the estimated wavelength is:

$$\hat{\lambda} = a \cdot x + \lambda_0 \quad 5\text{-}20$$

If we take the differences between known wavelengths, 1 to *n* (*n* is the number of wavelengths we found), and the x where we saw them, we can solve for a and λ_0 as:

$$\hat{a} = \left\langle \frac{\lambda_n - \lambda_{n-1}}{x_n - x_{n-1}} \right\rangle \text{ and } b = \langle \lambda_n - \hat{a} \cdot x_n \rangle \quad 5\text{-}21$$

The average error on the wavelength is thus:

$$\lambda_{\mathrm{err}} = \langle \lambda_n - \widehat{\lambda_n} \rangle \quad 5\text{-}22$$

Thus, the measured wavelength is computed with equation 5-20.

5.3.2 Radiometric calibration

As with the sensor calibration, we must either have a calibrated lamp or measure the spectral irradiance of the lamp at the sensor location. A calibration curve may be provided by the calibration source (lamp) manufacturer for a distance (typically 50 cm) from a Lambertian surface (Spectralon). The ratio of the square of the actual distance, d1 to this distance will determine the actual irradiance. When using a lamp that is not calibrated, the spectral irradiance off the Spectralon can be measured with a spectrometer such as an ASD FieldSpec. Having the lamp source normal to the Spectralon provides a more uniform illumination source since tilt will cause one side or the other to be brighter due to the distance to the Spectralon being longer at one side of the illumination spot.

5.3.3 UUT gain (DN/flick)

For each integration time, the UUT gain (responsivity) will be computed using bright and dark frames in conjunction with the spectral irradiance measured by the ASD. For each integration time, the dark field image will be computed for all frames, K, collected as:

$$\overline{dn}_{\text{dark}}(x, t_{\text{int}}) = \frac{\sum_{y=1}^{M} \sum_{k=1}^{K} dn_{\text{dark}}(x, y, t_{\text{int}}, k)}{N \cdot M} \qquad 5\text{-}23$$

The average bright image is computed as:

$$\overline{dn}_{\text{bright}}(x, t_{\text{int}}) = \frac{\sum_{y=1}^{M} \sum_{k=1}^{K} dn_{\text{bright}}(x, y, t_{\text{int}}, k)}{N \cdot M} \qquad 5\text{-}24$$

We use the spectral calibration from section 5.3.1 to convert x to $\hat{\lambda}$ so that we can compute the average bright image corrected for dark field is:

$$dn(\lambda, t_{\text{int}}) = \overline{dn}_{\text{bright}}(\lambda, t_{\text{int}}) - \overline{dn}_{\text{dark}}(\lambda, t_{\text{int}}) \qquad 5\text{-}25$$

Note that some wavelengths will be saturated at some exposure times which allows the tails of the response to be more accurately determined. The analysis must use the portions that are not saturated and not in the noise designated as λ_{valid}.

The average gain unit exposure time, removing saturated and noisy wavelengths, thus using only the validated wavelengths (λ_{valid}) is:

$$\Re_t(\lambda) = \sum_{t_{\text{int}}=t_0}^{t_{\max}} \frac{dn(\lambda_{\text{valid}}, t_{\text{int}})}{L_W(\lambda_{\text{valid}}) \cdot t_{\text{int}}} \qquad 5\text{-}26$$

Where:

$\Re_t(\lambda)$ is the spectral responsivity in dn/(W-sec/cm^2-sr-nm)

L_W is the spectral irradiance in W/cm^2-sr-nm of the tungsten lamp

5.3.4 UUT noise characterization and Noise Equivalent Spectral Radiance (NESR)

Dark cubes will be used to characterize the UUT noise and dark field. From this darkfield image plots of integration time versus dark field dns for image center and brightest and darkest areas will be done. In these equations, it is assumed that x has been converted to wavelength.

The noise will be computed as the standard deviation (unbiased estimator) for each integration time over all frames.

$$\sigma_{dn}(\lambda, t_{\text{int}}) = \left(\frac{1}{N-1}\sum_{i=1}^{i=N}\left(dn_{\text{dark}}(\lambda, t_{\text{int}}, i) - \overline{dn}_{\text{dark}}(\lambda, t_{\text{int}})\right)^2\right)^{0.5} \qquad 5\text{-}27$$

This is converted to NESR using the responsivity computed in section 5.3.3 for unsaturated data.

$$\text{NESR}(\lambda,\ t_{\text{int}}) = \sigma_{dn}(\lambda, t_{\text{int}})/\left(t_{\text{int}} \cdot \Re(\lambda)\right) \qquad 5\text{-}28$$

5.4 Focusing a camera in high turbulence

Often in the field we struggle to focus our sensor system in high turbulence. We can use a trick that astronomers use to focus. A Scheiner disc (2 holes) or a Hartmann mask (3 or more holes) takes advantage of the fact that light rays from different areas of the entrance aperture will be in front or behind the image plane. In other words, the holes separate the wavefront into different bundles. Examples of a Hartmann mask and Scheiner disc are provided in Figure 5-10.

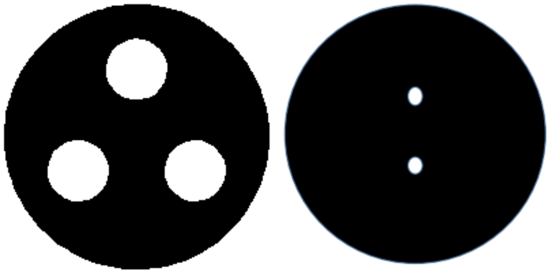

Figure 5-10. Three-hole Hartmann Mask (left) and Scheiner disc (right). When out of focus, there will be as many images as there are holes in the mask. These converge to a single image when in focus.

These are easily constructed with almost any material you can find. The key is that the holes must be equally spaced with respect to the optical axis (center of the entrance aperture). If we follow the ray bundles through a Scheiner disc and optics, when out of focus, the rays will be in front or behind the image plane showing two images instead of one as illustrated in Figure 5-11.

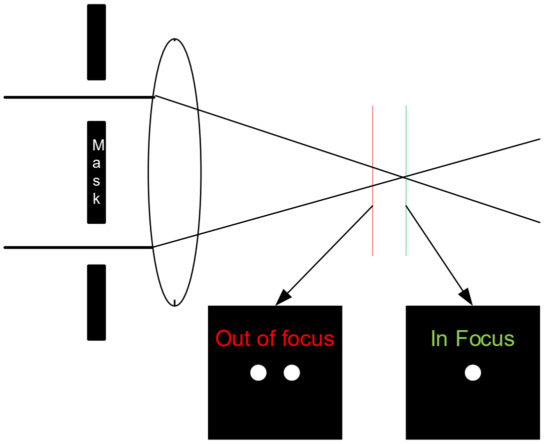

Figure 5-11. Example of Scheiner disc (mask), the rays go through the two holes. When the image plane is in front of the focus, the rays from each hole land on a different part of the image plane making two dots (red) and when at focus, the rays converge to the same point making a single image (green).

For every hole in the mask, there will be that many images. For a scene with structure, it becomes easy to make one image instead of multiples to achieve focus. This is how a Shack-Hartmann wavefront sensor detects the de-focus due to turbulence. An example of an in focus and out of focus glint when viewed through a 3-hole Hartmann mask is shown in Figure 5-12.

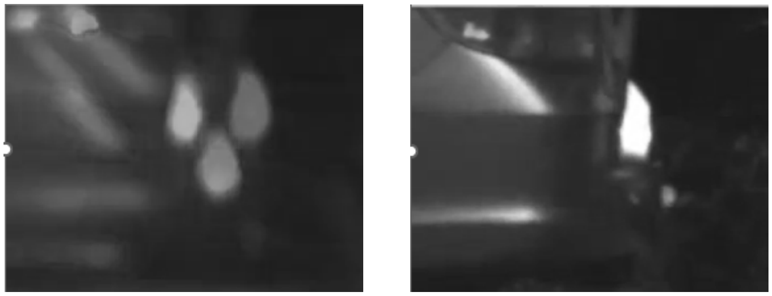

Figure 5-12. Out of focus when viewed through a Hartmann Mask (left) and in focus through that same mask.

6 Transformation from 3-D Image space to 2-D image plane

We live in a three-dimensional spatial world. Transforming from one coordinate system (platform) to earth can be challenging. It requires keeping track of up and down which can feel like standing on one's head. In theory it should be trivial, but it often requires more thought than expected. There are excellent references on transforms for each situation (Cai, 2024, Olsen, 1996, Zhu, 1994).

This section focusses on how to transform from image space to the image plane of a sensor and how the mapping of a sphere to a flat surface impacts the detected image. How a lens maps a shape on the object plane to the image plane while assuming other aberrations are negligible is described as distortion. Once the lens mapping function is known the distortion characteristics are fully determined. There are multiple types of lens mapping, so knowing which one is important for determining your total field of regard. Most cameras have rectilinear mapping. Common mapping functions are:

- Rectilinear -Maps the object space nearly linearly with the image space such that the field of regard is approximately the number of pixels times the IFOV. This function is used in most photographic lenses, including smartphone lenses. The pixels near the edge are stretched with respect to those in the center.
- Stereographic - Both tangential and sagittal magnification increase with the field angle at the same rate. The aspect ratio for the image plane and the object plane is constant across the field of view.
- F-θ or theta-map: Aspect ratio decreases with increasing field angle. This is useful for applications that require knowledge of angle with respect to a platform.
- Fovea distortion: Like our eye, resolution is higher in the center of the field of view and less at the edge. This type of lens mapping function is useful for applications that need to detect objects far away while also having a wide field of view.

Figure 6-1 shows the 3-D area being mapped by a sensor (left) with a theta map or fisheye lens. The optical axis is in line with the z-axis. The right figure shows the image plane coordinate system.

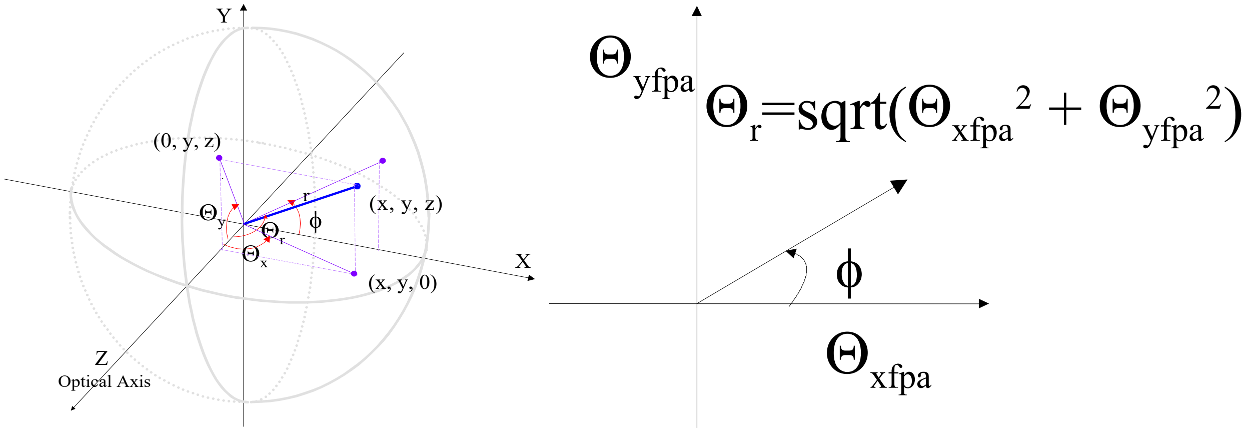

Figure 6-1. Image location with respect to the optical axis of a sensor (left), projected onto the image plane (right). The magnitude of Θ_r (left) is equal to the value of Θ_r in object space (right) and ϕ is the same in both pictures.

The standard transformation from spherical to cartesian coordinates in Figure 6-1 (left) is:

$$x = \cos(\phi)\sin(\Theta_r) \qquad 6\text{-}1$$

$$y = \sin(\phi)\sin(\Theta_r) \qquad 6\text{-}2$$

$$z = \cos(\Theta_r) \qquad 6\text{-}3$$

To project onto the image plane, we know that the magnitude of Θ_r in object space is equal to Θ_r on the image plane. We also know that the angle ϕ in object space is equal to the rotation angle, ϕ on the image plane. Thus

$$\cos(\phi) = \frac{\Theta_{xfpa}}{\Theta_r} \qquad 6\text{-}4$$

$$\sin(\phi) = \frac{\Theta_{yfpa}}{\Theta_r} \qquad 6\text{-}5$$

Substituting for $\sin(\phi)$ and $\cos(\phi)$ into equations 6-1, 6-2, and 6-3, the relationship between the image plane and object space in cartesian coordinates is:

$$x = \frac{\Theta_{xfpa}}{\Theta_r} \cdot \sin(\Theta_r) \qquad 6\text{-}6$$

$$y = \frac{\Theta_{yfpa}}{\Theta_r} \cdot \sin(\Theta_r) \qquad 6\text{-}7$$

$$z = \cos(\Theta_r) \qquad 6\text{-}8$$

If projecting the spherical surface onto a plane tangent to the sphere at the optical axis, the x, y projections on this surface (i.e. what does the image plane see) are:

$$\mathrm{x_{proj}} = \mathrm{x}/\cos(\Theta_r) \qquad 6\text{-}9$$

$$y_{\mathrm{proj}} = \mathrm{y}/\cos(\Theta_r) \qquad 6\text{-}10$$

Figure 6-2 shows the points of the image plane mapped onto the sphere (left) and how they actually map on a flat surface such as the earth (right). Note that the pixels size varies significantly as the field of regard increases.

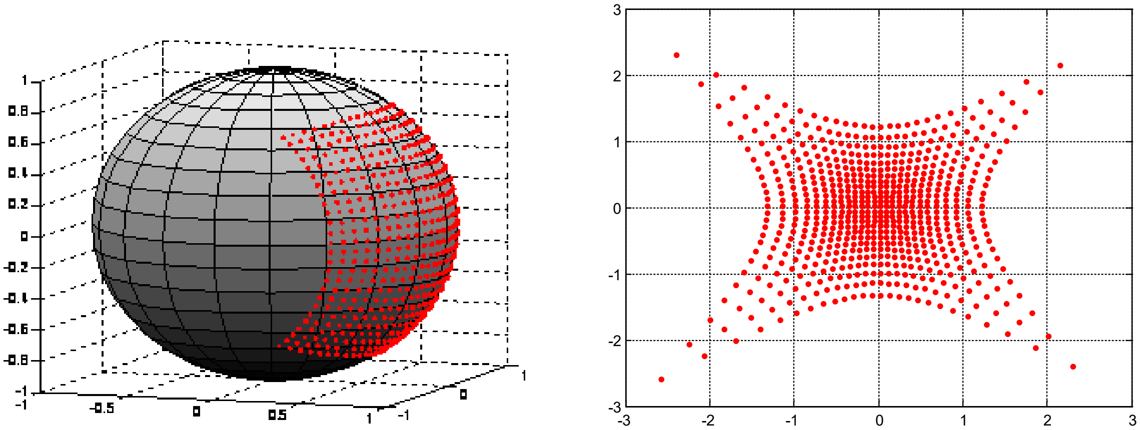

Figure 6-2. Wide angle lens, points seen on the focal plane, shown on the sphere (left) and projected onto a flat surface as would be provided in the image (right). Note the distortion on the edges. This shows the cosine law that dictates the change in pixel size from center to edge of the field of regard.

This becomes important as the field of regard (FOR) increases and can make a target location erroneous if not mapped properly. It also illustrates why computing an instantaneous field of view (IFOV) for a single pixel and multiplying by the number of pixels may provide an erroneous total field of regard if the lens type is uncertain.

7 Signal & Image Processing

This section discusses physics-based signal and image processing algorithms. Algorithms developed for RF signals can often be adapted for imagery and visa-versa. The developer needs to try to 'see' the object from the sensor perspective. This requires a basic understanding of both the physics of the electromagnetic energy and the sensor path and how this results in the counts (dn) on the detector. For many applications, algorithms to condition data are needed for optimizing machine learning (ML) and Neural Networks (NN) algorithms. Particularly in the case of images, ML may not actually be the best solution since the size of the training set for identification of target of interest may be extremely large. Often a simple physics-based algorithm can provide the answers including uncertainties. If not, it can vectorize the data is such a way as to be much more computationally light weight than ML alone. Figure 7-1 shows a basic algorithm flow diagram. This can be adapted for almost all detection and declaration cases.

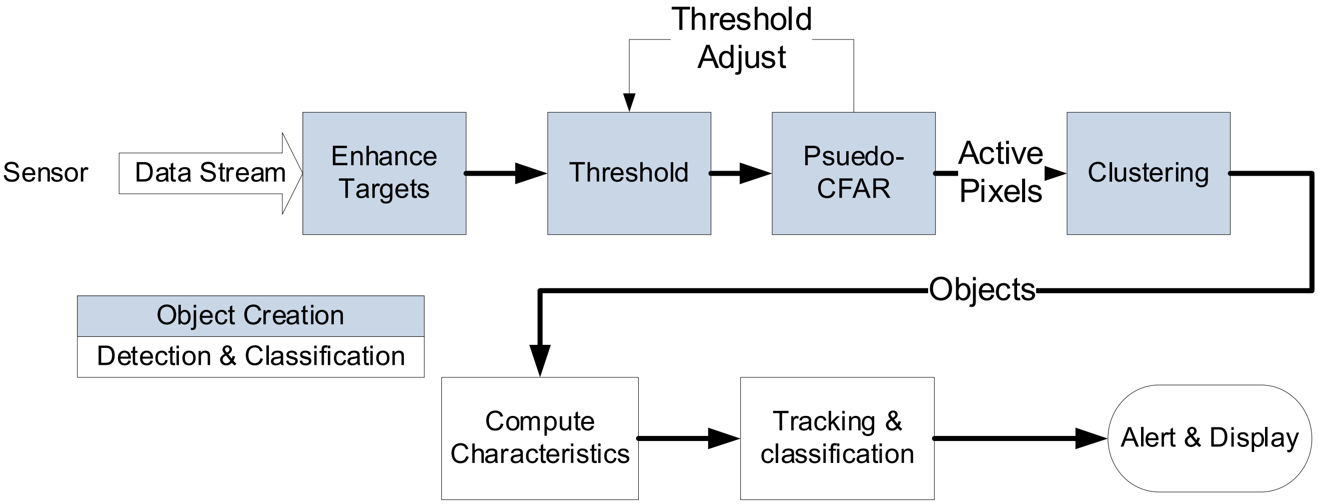

Figure 7-1. Basic algorithm flow diagram. This diagram can be adapted for almost all cases.

Once the electromagnetic energy is received by the sensor, it creates a data stream. This may be a time series (single detector), a series of images (single band imaging sensor) or a series of data cubes (multi-spectral or hyperspectral images). The target is enhanced such that when a threshold is applied, only those objects of interest and a limited number of false positives are seen. Threshold determination is critical to the algorithm result. Often a constant false alarm rate (CFAR) is applied which changes the threshold to limit the number of active pixels or detections that are clustered into objects based on computational power available. For a time series (single dimensional data) clustering may not be needed. At this point, the objects can be put into a ML or other algorithm. If not, computing characteristics which can be analyzed with a Bayesian classifier and tracker will reduce the number of objects to only those of interest. Typical trackers are Kalman or Particle filters. A simple tracker for moving objects can also be created by unique methods such angular rate and linearity of motion.

Alerts can be true or false positives. A good algorithm developer will have standards by which to evaluate the true and false positive rates of the algorithm.

Non-standard usage of convolutions, Fourier Transforms and Wavelet transforms are the methods discussed herein. Other dimensionality reduction methods such as principal components analysis (PCA) are readily available elsewhere.

7.1 ROC CURVES AND CONFUSION MATRICES

When evaluating an algorithm, it is important to understand the relationship between true and false positives. This requires truth data. Truth data used for training should not be used for evaluation of the algorithms as this will bias the evaluation results.

For a given set of truth data, Let N be the number of known true detections. For a given threshold (V_{thresh}), let *M* be the number of algorithm detections. The statistical definitions from the Rensselaer Polytechnic Institute (RPI) website (Newberg, 2006) have been modified. A confusion matrix or an error matrix shows the truth data against the algorithm results. The four fundamental numbers in a confusion matrix are shown in Table 7-1.

Table 7-1. True Conditions and Detected States, confusion matrix basis

	True target	**Clutter or Noise**	**Total**
Detected by Algorithm	True Positive, TP	False Positive, FP	M
Not detected by Algorithm	False Negative, FN	True Negative, TN	FN+TN
Total	N	FP+TN	

If there is more than one class of objects, the table grows. From these four fundamental numbers and their totals, all probabilities can be determined. Using the data in the 'True Object' column, true positive rate (probability of detection or sensitivity) which is the probability that an object will be detected by the algorithms can be computed as:

$$P_d(V_{\text{thresh}}) = \frac{TP(V_{\text{thresh}})}{TP(V_{\text{thresh}}) + FN(V_{\text{thresh}})} = \frac{TP(V_{\text{thresh}})}{N} \qquad \text{7-1}$$

True positive rate is the probability that a detected object is a target.

$$P_{TP}(V_{\text{thresh}}) = \frac{TP(V_{\text{thresh}})}{TP(V_{\text{thresh}}) + FP(V_{\text{thresh}})} = \frac{TP(V_{\text{thresh}})}{M(V_{\text{thresh}})} \qquad \text{7-2}$$

The counterparts to these numbers may also be computed if desired. The false negative rate is the probability that a target will be missed by the algorithms.

$$P_{FN}(V_{\text{thresh}}) = \frac{FN(V_{\text{thresh}})}{TP(V_{\text{thresh}}) + FN(V_{\text{thresh}})} = \frac{FN(V_{\text{thresh}})}{N} = 1 - P_d(V_{\text{thresh}}) \qquad \text{7-3}$$

The false positive rate is the probability that a detected object is clutter or noise.

$$P_{FP} = \frac{FP(V_{\text{thresh}})}{TP(V_{\text{thresh}}) + FP(V_{\text{thresh}})} = \frac{FP(V_{\text{thresh}})}{M} = 1 - P_{TP}(V_{\text{thresh}}) \qquad \text{7-4}$$

Receiver Operating Characteristic (ROC) curves characterize performance of a system and algorithm for varying thresholds. These were developed during World War II for detecting enemy objects in battlefield conditions. For each threshold there will be a false positive and true positive rate. This is an excellent visualization tool that allows setting of thresholds to meet the system requirements. The ROC curve compares true positive and false positive rates for varying thresholds. Figure 7-2 shows three possible ROC curve shapes.

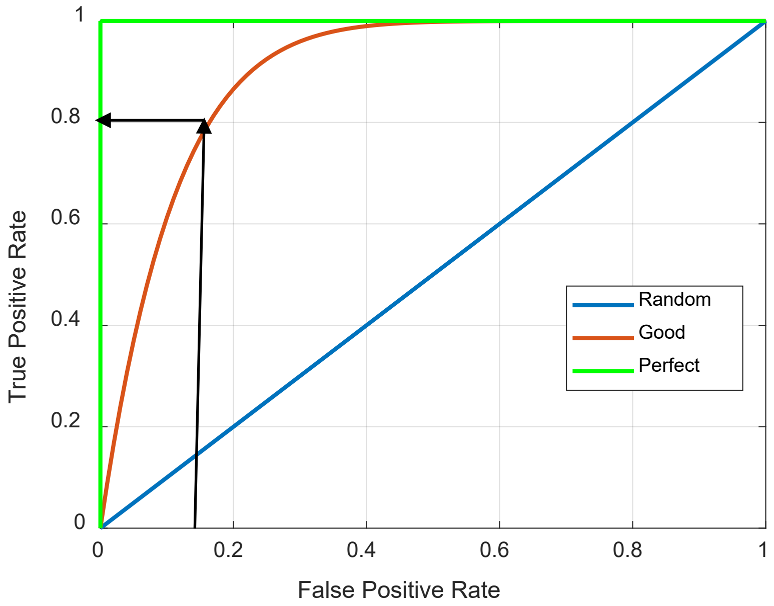

Figure 7-2. ROC curve shape. The blue line indicates a random classifier. As the curve shapes move towards the upper left. A perfect classifier would be in the top, left corner of the plot as indicated in green. Note that for the Good classifier, if the requirement is 80% true positives (probability of detection), the false positive rate will be 15%.

A random classifier has equal true and false positive rates (blue line), a perfect classifier finds all the true positives and not false positives (green line). A perfect classifier is not achievable, but a good classifier might get the orange curve. A designer will have requirements on true and false positive rates. For the orange curve, if the requirement is 10% false positive rate and 80% true positive rate, the algorithms will have to be further optimized to shift the curve left since the false positive rate for this algorithm is too high. This curve thus allows the system engineer to optimize the design and subsequently pick the threshold that meets the requirements for multiple scenarios.

7.2 TARGET ENHANCEMENT

Target enhancement algorithms minimize the amount of data to be processed. For instance, if we know that we are looking for small objects, we can apply a spatial filter. If we are looking for moving objects, we apply frame subtraction.

We will discuss:

- Target enhancement via convolution
- Wavelet transforms
- True Spatial filter
- Histogram stretch
- Frequency domain algorithms

7.2.1 Target enhancement via convolution

In image processing, a kernel or convolution matrix or operator is used to enhance, blur or further modify the image to enhance objects of interest or remove structure improving noise statistics. To enhance an image or object, a kernel is developed specific to the need. The convolution of the kernel operator, h, with an image, A, will produce the filtered output, B, such that:

$$B = h * A \tag{7-5}$$

Edge enhancement is typically done with edge filter kernels that are convolved with the image or the data stream. While typically used on 2-dimensional images, the extension of this to one-dimensional time series data is also useful. Kernels developed for specific cases should be normalized such that the sum of the energy in the kernel is one. Some simple and useful kernels are listed in Table 7-2.

Table 7-2. Some basic Kernels

Kernel name	3 x 3 Kernel
Gaussian blur	$\frac{1}{16}\begin{bmatrix}1&2&1\\2&4&2\\1&2&1\end{bmatrix}$
Box blur	$\frac{1}{9}\begin{bmatrix}1&1&1\\1&1&1\\1&1&1\end{bmatrix}$
Sharpen	$\frac{1}{9}\begin{bmatrix}0&-1&0\\-1&5&-1\\0&-1&0\end{bmatrix}$
Sobel Edge	X- dimension $\frac{1}{9}\begin{bmatrix}1&0&-1\\2&0&-2\\1&0&-1\end{bmatrix}$ Y-dimension $\frac{1}{9}\begin{bmatrix}1&2&1\\0&0&0\\-1&-2&-1\end{bmatrix}$

The Gaussian blur kernel can approximate the blur circle of an imager, and it is useful to compute this for a larger kernel. For a blur size of σ, the 2-D kernel of any size can be computed as:

$$g(i,j) = e^{-\frac{x(i)^2+(x(i)^2}{2\cdot\sigma^2}} \text{ and } h(i,j) = \frac{g(i,j)}{\sum_i \sum_j g(i,j)} \tag{7-6}$$

For a more accurate blur, an Airy disk kernel of a line spread function is useful as is shown in equation 4-47 of this document. Computationally, it may be more efficient to use the product of the Fourier transforms instead of a convolution.

7.2.2 Wavelet transforms

Wavelet transforms are used in many areas of science and engineering for both feature enhancement and data compression. Common examples of wavelet transform applications are; data compression such as JPEG 2000 images (Usevich, 2001), Signal to Noise (SNR) enhancements for AVIRIS and other satellite imagery (Qian, 2011), fusion of multispectral and hyperspectral images(Zhang, 2009) and study and characterization of atmospheric turbulence (Domingues, 2005).

A wavelet transform is simply the convolution of a function (or data stream) with a wavelet for multiple scaling and weighting factors, derived from a scaling or dilation function (Cody, 1992, Ghaderpour, 2021). These different scaling factors provide ‘frequency’ information. Wavelets allow targeting of specific ‘shapes’ whereas Fourier transforms pull the frequency content associated with both the repetition and the sharpness of edges. Basically, wavelets decompose the original signal into a linear combination of shifted and scaled versions of the mother wavelet. Implementation is typically done as a discrete wavelet transform (DWT). The remainder of this section describes the application of a DWT to spectral libraries for hyperspectral imaging.

In the LWIR, the vibrational transitions produce features. The overtones of these transitions may or may not manifest themselves in the VNIR/SWIR region. Although the shape of these features may change with particle size, the position in wavenumber is relatively fixed. Conversion of spectral libraries to the spectral frequency domain via a DWT enhances these features.

Figure 7-3 shows the ASTER library spectra for Calcite for three different particle sizes along with the spectra for solid concrete showing the similarities between these spectra.

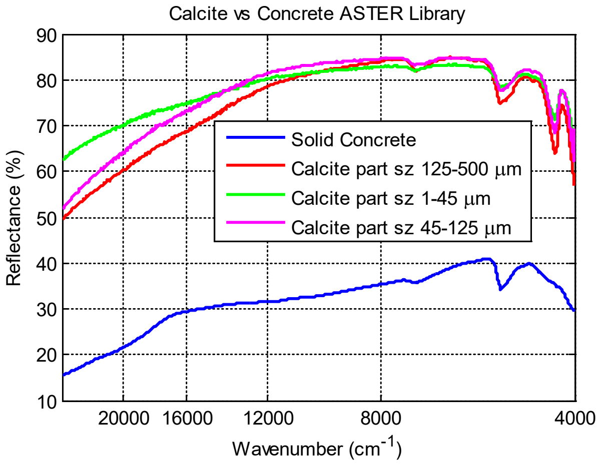

Figure 7-3. ASTER library spectra for Calcite for three different particle sizes compared to concrete.

A very simple transform designed to select specific spectral widths was applied to these spectra, with the cell size varying for each convolution. The simple wavelet for this example is shown in Figure 7-4.

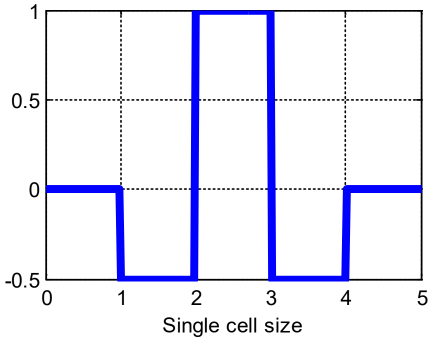

Figure 7-4. Filter shape used to enhance concrete from natural background. The shape naturally attenuates.

By varying the width of this wavelet, we can enhance spectral features of multiple widths and create a two-dimensional spectra. When the wavelet width matches the width of the features, a strong feature emerges. Figure 7-5 shows the wavelet spectra versus the log of the wavenumber (x-axis) for concrete (left) and Calcite (right) for varying filter sizes (y-axis).

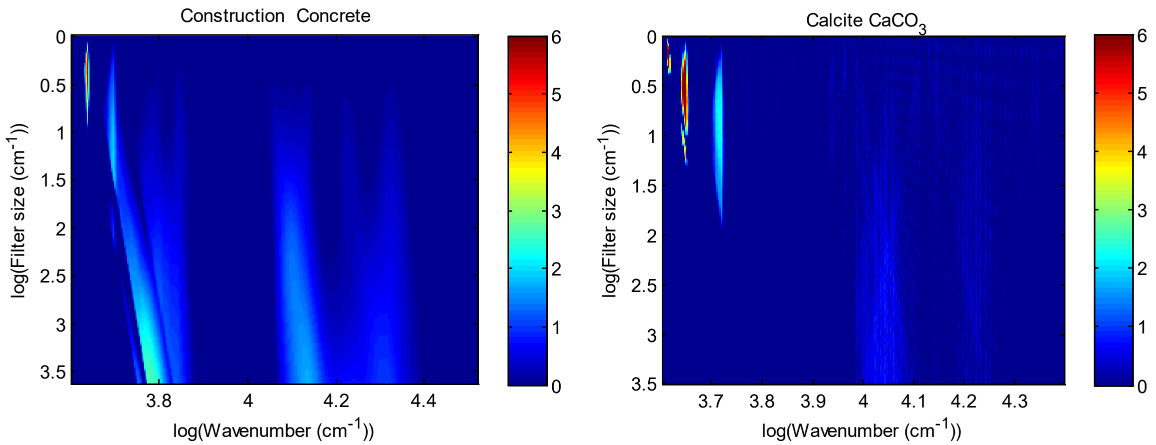

Figure 7-5. A simple wavelet transform amplifies the differences between the Calcite and concrete library spectra (from Figure 7-3). Calcite shows very different features in this domain. This is not an optimum wavelet, but even this simple wavelet amplifies differences in the library spectra.

This simple wavelet transform amplifies the differences between the Calcite and concrete library spectra since the features associated with the overtones are extracted off the slowly moving background. A one-dimensional library spectrum is created by averaging data for all filter sizes as shown in Figure 7-6.

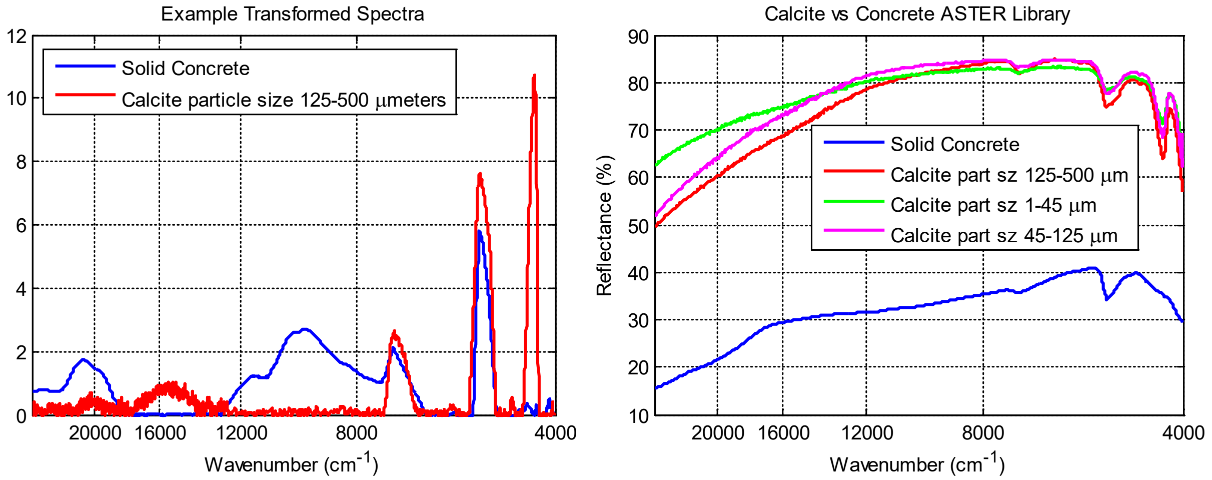

Figure 7-6. A simple wavelet transform (left) amplifies the differences between the Calcite and concrete library spectra (right). Calcite shows very different features in this domain. The amplification of the overtone at about 4300 wavenumbers makes the calcite spectra very distinct from concrete. This is not an optimum wavelet, but even this simple wavelet can help to amplify differences in the libraries.

In this figure, the amplification of the overtone at about 4300 wavenumbers makes this Calcite spectrum very distinct from concrete and much less susceptible to noisy data collection.

7.2.3 True Spatial filter

Consider an image with a large amount of clutter. To detect objects that are less than a certain size, a classic edge filter will not work, and a true spatial filter is needed. The size of the filter depends on the object size, the range to target and the sensor characteristics. This filter is computationally lightweight, and, unlike convolution methods, the number of operations is independent of the object size. For efficiency, instead of a 2-D spatial filter, two 1-D spatial filters can be applied. In this example, rows are filtered first. For a spatial filter size of 2*k+1, the equation for the row filter applied at row, m, and column, n is:

$$dn_{\mathrm{row}}(\mathrm{m,n}) = -\frac{\mathrm{dn(m-k,n)}}{2} + \mathrm{dn(m,n)} - \frac{dn(\mathrm{m+k,n})}{2} \tag{7-7}$$

Where, as before, dn is the counts as a digital number and thus the pixel intensity value. For instance, for a sensor with an instantaneous field of view of one milliradian, looking for a target at one kilometer, that is 3 meters in size, the number of pixels subtended would be 3 pixels and we would set k equal to 3.

The equation for the column filter that is applied at row, m, and column, n is:

$$\mathrm{dn_{filt}(m,n)} = -\frac{dn_{\mathrm{row}}(\mathrm{m,n-k})}{2} + dn_{\mathrm{row}}(\mathrm{m,n}) - \frac{dn_{\mathrm{row}}(\mathrm{m,n+k})}{2} \tag{7-8}$$

To demonstrate the utility of this filter to extract small signals on large variations, a small pulse (original signal) was placed on a slowly varying signal with random noise added to both signals as shown in Figure 7-7 (left). Figure 7-7 (right) shows the original signal without noise that was placed on the slowly varying background (blue) and the output of the filter including noise. Note the inverted 'rabbit ear' shape for the output signal (red).

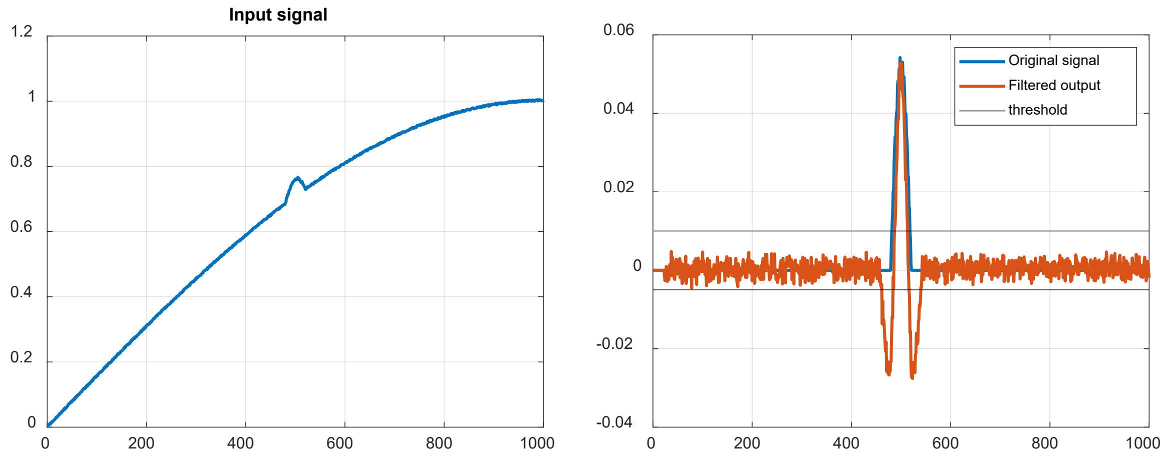

Figure 7-7. Slowly varying signal with small narrow peak on top(left). On the right, the original small signal that was added (blue) is compared to the filter output. Note that the signal maintains the original peak value. Also note the inverted rabbit ear shape. A threshold on this signal can add improved rejection of larger objects.

Note that this algorithm maintains the peak amplitude and shape until it approaches the filter size. Applying this filter and looking for signals above a positive threshold is sufficient for many applications but can leave anomalous detections when objects are close to each other. In this example the target is brighter than the background but for a target that is darker than the background, the image or data can be inverted as $2^{nBits} - dn$ and then processed digging out signals below background.

To truly detect only those objects that are the size chosen or smaller, applying a second stage to look for the rabbit ear shape will remove some anomalous features that may come through. Looking at Figure 7-7 right side, the threshold chosen was two-sigma of the noise (black). Methods to get a threshold are discussed in section 7.3.

We create a positive and negative mask for the data as:

$$M_P(m,n) = \begin{cases} 1\ for\ \mathrm{dn_{filt}(m,n)} \geq \mathrm{thresh} \\ 0\ for\ \mathrm{dn_{filt}(m,n)} < \mathrm{thresh} \end{cases} \tag{7-9}$$

$$M_N(m,n) = \begin{cases} 1\ for\ \mathrm{dn_{filt}(m,n)} < -0.5 \cdot \mathrm{thresh} \\ 0\ for\ \mathrm{dn_{filt}(m,n)} \geq -0.5 \cdot thresh \end{cases} \tag{7-10}$$

Shifting these by the filter size lines up the rabbit ears such that the mask for the valid pixels (losing the edges) is:

$$M_{\mathrm{row}}(m,n) = M_P(m,n) \cdot M_N(m-k,n) \cdot M_N(m+k,n) \tag{7-11}$$

$$M_{\mathrm{col}}(m,n) = M_P(m,n) \cdot M_N(m,n-k) \cdot M_N(m,n+k) \tag{7-12}$$

$$M(m,n) = M_{\mathrm{row}}(m,n) \cdot M_{\mathrm{col}}(m,n) \tag{7-13}$$

$$dn_{\mathrm{out}}(m,n) = M(m,n) \cdot dn_{\mathrm{filt}}(m,n) \tag{7-14}$$

Using our simple one-dimensional example, we see in Figure 8-8 that the filter extracts the original signal including the amplitude above the slowly varying signal. This is considered a pulse-on-pulse method. For a pulse under pulse such as a dark spot on a bright background, the image is inverted prior to applying the filter.

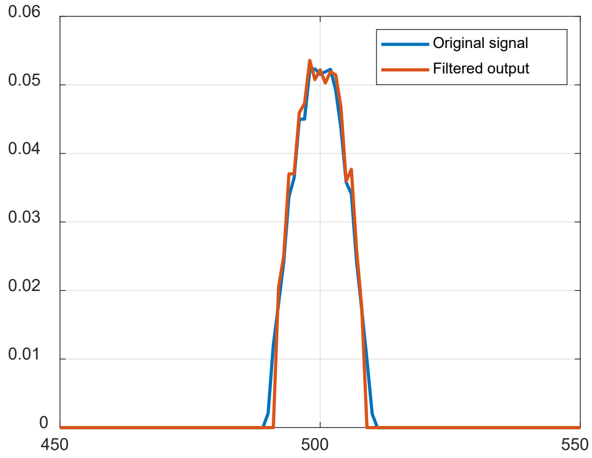

Figure 7-8. Example filter output vs the synthesize input.

The filter works best for areas that do not have a lot of overlapping peaks (or active pixels) but can still be beneficial in most images or in one dimension, time domain signals.

7.2.4 Histogram stretch

A histogram stretch is extremely useful in setting levels for visualizing image data or setting thresholds. When displaying images, a very bright object can obscure the data buried in the noise. A histogram stretch is a form of equalization. Using a lower limit, dn_{low}, and upper limit, dn_{up}, for display based on the histogram percentage values can produce images that make objects of interest more visible. A common stretch is a 2-98% stretch where h_{low}= 2% is the lower limit and h_{up}=98% is the upper limit. In addition, these values can be used to get a threshold for dim targets and maximums for bright target rejection.

Histograms bin or bucket (in our case dn) provide a distribution of values. If plotted, the x-axis is the bin value and the y-axis is the number of occurrences in that bin. Histogram functions are common in computing software (MATLAB, Python numpy.histogram). The number of bins is important for the accuracy of this method. For N bins and minimum and maximum values of digital number from the data (dn_{min} and dn_{max}), the bin width is

$$\Delta\mathrm{dn} = \frac{dn_{\mathrm{max}} - dn_{\mathrm{min}}}{N-1} \tag{7-15}$$

The histogram, $h(n)$, bins every dn_i for i=0 to M-1 (M samples or pixels), into bins from n=0 to N-1 such that:

$$\text{if } dn_{\mathrm{min}} + n \cdot \Delta dn \le dn_i < dn_{\mathrm{min}} + (n+1) \cdot \Delta\mathrm{dn} \text{ then } h(n) = h(n) + 1 \tag{7-16}$$

For the stretch, a cumulative sum for each point, n, is computed as:

$$h_{\mathrm{sum}}(n) = \sum_{i=0}^{n} h(i) \tag{7-17}$$

Note that $\sum_{n=0}^{N-1} h_{\mathrm{sum}}(n)$ must equal M. For stretching, the cumulative sum is normalized to a peak of one such that:

$$h_{\mathrm{norm}}(n) = \frac{h_{\mathrm{sum}}(n)}{M} \tag{7-18}$$

Using this normalized cumulative sum, for an upper and lower stretch, the display minimum (dn_{low}) and maximum (dn_{up}) are:

$$\begin{gathered} dn_{low} = dn_{min} + (k_{low} + 0.5) \cdot \Delta x \; \mathit{where} \; h_{norm}(k_{low}) \ge h_{low} \\ dn_{up} = dn_{min} + \left(k_{up} + 0.5\right) \cdot \Delta x \;\; \mathit{where} \; h_{norm}\left(k_{up}\right) \ge h_{up} \end{gathered} \tag{7-19}$$

Other logic can be applied. In addition, the minimum and maximum histogram thresholds can be varied. An example of a stretched image is shown in Figure 7-9 with much more detail being seen in the stretched image.

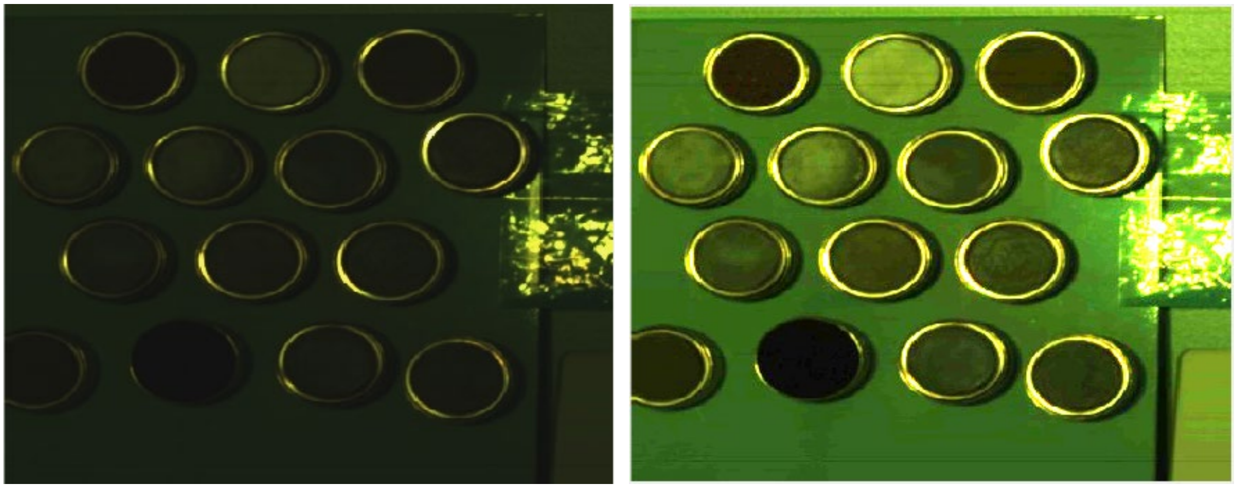

Figure 7-9. Original color image as displayed by MATLAB (left), stretched image (right). Note that more detail is seen.

7.2.5 Frequency domain algorithms

While the previous section discussed methods implemented in the time or spatial domain, frequency domain methods can improve detection significantly. In this section we discuss frequency domain processing for time series such as RF, photodiodes, seismic and acoustic/infrasound. This can also be applied to spatial dimensions in imagery.

We know that the Fourier transform of a convolution is just the product of the Fourier transform of the functions that were convolved. As a result, it is often useful to work within the frequency domain.

A linear time-invariant (LTI) system is a system that is defined as time-invariant and linear. Linear means the response of the system output responds directly to both addition and multiplication on the input signal. Time invariant means that if a signal is input into the system and time, t and again at time t+τ, the output will be the same. An LTI can be represented as a set transfer functions (MATLAB SIMULINK does this). A transfer function is the Fourier Transform of the spatial or time domain function that describes a portion of a system. Electronic circuits are LTI systems. Optical systems can sometimes be modeled this way as was done for fluorescence (Trainham, 2015).

Figure 7-10 is an example of a laser-based system for measuring fluorescence lifetimes where all Fourier Transforms are on time varying signals. If we take the Fourier Transform of the input signal (laser), $X(z)$, the output signal, $Y(z)$, is impacted by the intervening transfer functions shown in Figure 7-10.

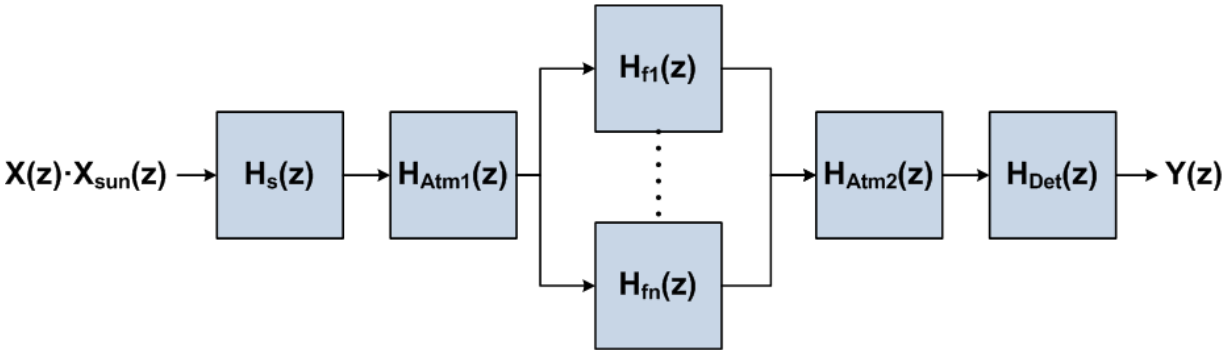

Figure 7-10. System diagram shows transfer functions for different components.

This is mathematically represented as:

$$Y(z) = X(z) \cdot \left[X_{\text{sun}}(z) \cdot H_L \cdot H_{\text{Atm}} \cdot \left(\sum_{n=1}^{n} H_{\text{fn}} \right) \cdot H_{\text{Det}} \right] \qquad \text{7-20}$$

Where:

$X_{\text{sun}}(z)$ is the Fourier transform of the solar irradiance
H_L is the System transfer function for the Laser and associated electronics
H_{Atm} is the atmospheric turbulence transfer function
$(\sum_{n=1}^{n} H_{\text{fn}})$ is the sum of all fluorescing materials reflecting the laser illumination
H_{Det} is the transfer function for the detector receiving the laser signal return

It is clear from the simplicity of this equation that frequency domain analysis is efficient and effective. It also offers an excellent noise mitigation methodology.

Most detectors have some form of 1/f noise meaning the noise at lower frequencies is higher than that at higher frequencies. This means, when looking for narrow peaks on a broad spectrum, a single threshold will not work. Using LTI, we can remove the transfer function of the data collection system along with background signals. The assumption is that the instruments and the background noise are the result of linear time-invariant systems. This is only an approximation since it does not consider the additive nature of background signals that propagate but compensates as if they are convolved with the target signal in the time domain. This ends up being a conservative removal of background signals while effectively removing the response of the electronic systems. This analysis method assumes non-coherent signals such that the phase information does not contribute to the analysis other than in computing the power spectral density (PSD) of the signal. The PSD allows us to see the power at each frequency more clearly. For a given FFT length, N, the PSD (S) is defined as:

$$S(f,k) = \left.\frac{|\mathcal{F}(V(n)\cdot W)|^2}{N}\right|_{k\ to\ k+N/2} \tag{7-21}$$

Where n are the samples from k-N/2 to k+N/2, $\mathcal{F}(V(n))$ indicates the fast Fourier transform (FFT) of the data signal, V(n), and W is a chosen window of length N. Typically, a Hanning or Hamming window will work with most signals. Windowing is important as it reduces the spectral leakage (unwanted frequency components) associated with sampling (National Instruments, 2024). Because this method overlaps each Fourier transform in time, loss of signal outside the window is handled.

The result of equation 7-21 is a two-sided spectrum thus, we only take the samples from k to k+N/2. The frequency range associated with this spectrum is computed as:

$$f = \frac{1}{N\cdot\Delta t} : \frac{1}{N\cdot\Delta t} : \frac{0.5}{\Delta t} \tag{7-22}$$

Where Δt is the time increment for the captured data. Note that the maximum frequency is the Nyquist frequency. This method most closely matches the Welch method (Welch, 1967).

When collecting data, it is important to collect an equal amount of data before the event trigger as after the trigger although any amount of data before the trigger can be useful. If implemented in a real time system, this should be done in the desired length (time), shifting by a small amount of length (time) for each calculation.

We assume that the data prior to the event trigger can be used to create a transfer function that represents the spectral content associated with the instrument and background sources. To reduce noise, we averaged the Fourier transforms over the chosen FFT interval. The system designer should choose the FFT interval carefully based on expected frequency content. The sample time will determine the highest frequency and the length of the FFT, the lowest frequency to be mapped.

The normalized (background corrected FFT) for each slice is thus computed as:

$$\mathrm{S}_{\mathrm{Norm}}(f,k) = \frac{\mathrm{S}_{sig+noise}(f,k)\big|_{k\geq k\_\mathrm{start}}}{\langle \mathrm{S}_{\mathrm{noise}}(f,k)\rangle_{k<k\_\mathrm{start}}} \tag{7-23}$$

Figure 7-11 demonstrates the power of this methodology on a collected data.

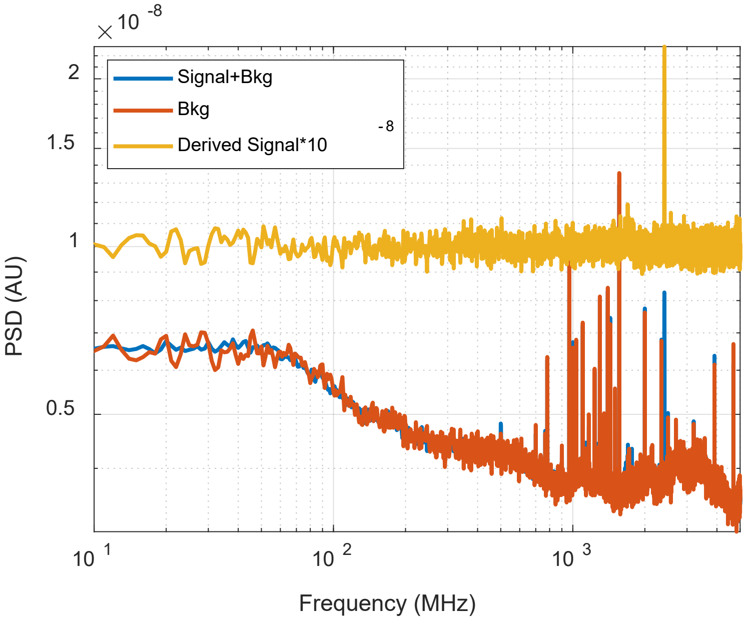

Figure 7-11. Example background and noise removal. The blue line is the PSD of the signal plus background (after the trigger),. red is background PSD of signal before trigger, yellow is the derived signal shifted down for easier visualization. Note that all the background frequencies along with any system noise are removed.

The blue trace is the PSD of the raw collected data that includes signal, background and noise after the trigger. The orange trace is the PSD of the signal collected before the event trigger representing the background and noise. The yellow trace shows the result of using LTI. The simple non-conventional application of LTI removes the 1/f noise and removes most of the periodic background signals from radios and other RF sources. It is not a perfect method but allows all very small signals to be detected in a large amount of clutter. It also allows a single threshold to be used to signals at all frequencies since the system 1/f noise is removed.

When multiple slices are done over time, a spectrogram (or waterfall) plot is created as shown in Figure 7-12.

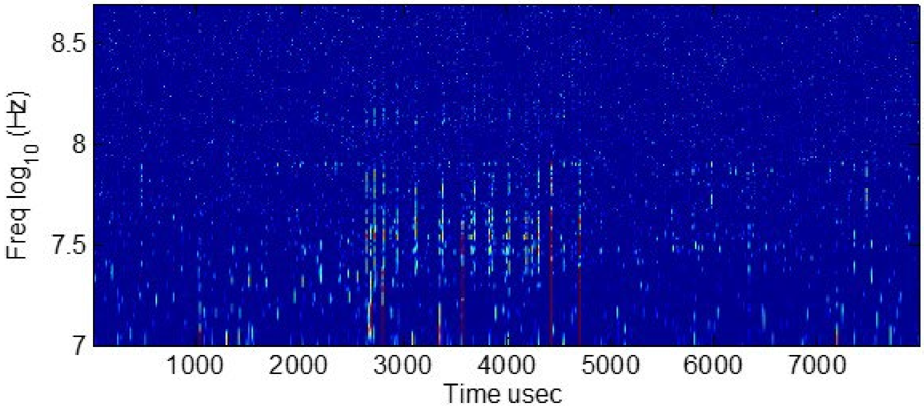

Figure 7-12. Example waterfall, x-axis is the time, y-axis is the $\log_{10}(f)$ and the intensity is the PSD of the time slice.

While spectrograms are often plotted with linear frequency, the logarithmic frequency often helps visualize subtleties not seen in a linear plot. This ‘image’ can be processed as an image or varying number of time slices to detect very faint signals of interest.

7.3 THRESHOLDING METHODS & CONSTANT FALSE ALARM RATE-

For computationally efficient algorithms, minimizing the amount of 'bad' data that gets detected maximizes performance. Thresholds are the key to this. Determining the threshold should be done on the enhanced or filtered signal, ideally without a target of interest. In other words, the threshold should be based on the noise of the system as applied to the processed signal. For thermal imaging systems, this may change over time as the focal plane changes temperature. If possible, a baseline can be taken by putting a lens cap over the sensor and collecting some background frames. If this is not possible, the following methods can provide an approximation to the background.

- For imaging systems, applying the spatial filter described in section 7.2.2 will provide only spatially small signals that can only be noise such as would be in a background image.
- For spectrometers, applying a spectral filter to remove the spectral content or using the noise in spectral regions known not to have signal
- For RF or other time domain signals applying the filter described in section 7.2.2 may help. Alternatively, when there is a trigger, data before the trigger can represent background noise.

For all cases noise will be dependent on exposure or integration time (t_{int}). The noise is then defined as the unbiased estimator of the 'background' signal as:

$$\sigma(t_{\text{int}}) = \left(\frac{1}{N-1}\sum_{i=1}^{i=N}\left(dn(\,t_{\text{int}}, i) - \overline{dn}(t_{\text{int}})\right)^2\right)^{0.5} \tag{7-24}$$

Where dn is the digital number (counts) and i is the pixel or sample location. For images, i is related to the rows and columns of the image. The threshold can be computed based on the minimum, non-zero, dn (dn_{low}) which is often computed using the lower histogram stretch value (see section 7.2.4). The threshold is now:

$$dn_{\text{thresh}}(t_{\text{int}}) = dn_{\text{low}}(t_{\text{int}}) + nDevs \cdot \sigma(t_{\text{int}}) \tag{7-25}$$

Where $nDevs$ is the number of standard deviations to use for this threshold, typically 3-6.

Sometimes a large amount of data may still come through. A typical constant false alarm rate (CFAR) algorithm adjusts the threshold based on noise floor or number of detections. For imaging, this can simply be allowing only a certain number of pixels per frame to be allowed.

7.4 SIMPLE CLUSTERING ALGORITHM

As of this writing, there were about 42 different clustering algorithms. Most of these require a priori knowledge of the number of clusters. For instance, k-means (seemingly the most used) is a nearest neighbor method that aims to cluster the data into k- clusters. This section focusses on a nearest-neighbor algorithm developed 30 years ago but has never been published. Only a cursory examination of the method is contained herein. The MATLAB implementation is available for examination.

This clustering algorithm allows for clusters to be created based on a distance metric. The distance can be pixel distance or any other distance (spectral wavelength, etc.). The pre-clustering algorithm and the clustering of clusters use the same basic algorithm. The input data to this module is an n-rows by three-column matrix where the three columns are:

data = [r, c, dn(r,c)] ,

where dn(r,c) is the digital number of the output at row, r and column, c.

The clustering consists of the following steps:

1. Sort data by rows.
2. For each row, create a subset of data that includes the present row and the adjacent rows, datNow.
3. Sort datNow by columns and find the points that are within the specified distance apart. For subclusters, the distance is one pixel such that each subcluster consists of adjacent pixels.
4. Remove all clusters/subclusters that do not meet size/density requirements.

A shift/add image implementation can make this algorithm extremely efficient. The centroids from the clustering algorithm can be the input to this same algorithm with a larger distance threshold allowing clustering of subclusters.

7.5 SQUARE WAVE EXCITATION ON A TEMPORAL FILTER

This section discusses the received excited population for square wave excitation when subject to a temporal filter. While this is classically done for electronics, Trainham et al. (2015) proposed that the excited return from a fluorescence signal could be treated as a filter. This section provides processing methods related to a fluorescence return from square wave excitation.

Lakowicz (2006, pages 193-194) derives the equations that are the basis for both time and frequency-domain lifetime measurements. Typically, the laser sends either multiple pulses or for frequency modulated fluorescence multiple sine waves to derive the lifetime information of the material being excited. Square wave excitation can possibly minimize the number of frequencies.

For a sine wave, the time dependent intensity of the received fluorescence is the convolution of the excitation signal ($L(t)$, equation 7-26) and the intensity decay of the fluorescence ($I(t)$, equation 7-27).

$$L(t) = a + bsin(\omega t) \tag{7-26}$$

$$I(t) = I_0 e^{t/\tau} \tag{7-27}$$

Where a is the offset, b is the amplitude and ω is the radial frequency (2πf) of the excited signal, t is time, I_0 is the initial intensity and τ is the fluorescence lifetime of the material being excited.

Ignoring loss and noise, the intensity received from the excited population, $N(t)$, is thus:

$$N(t) = I_0 \tau \left\{ a + \frac{b}{\sqrt{1+\omega^2\tau^2}} \cos(\omega t - \operatorname{atan}(\omega\tau))) \right\} \tag{7-28}$$

It is assumed that the excited population return follows the form:

$$N(t) = A + \frac{B}{\sqrt{1+\omega^2\tau^2}} \cos(\omega t - \varphi)) \tag{7-29}$$

Using simple algebra, the familiar modulation, m, and phase, φ, relationships are derived as:

$$m = \frac{B/A}{b/a} = \frac{1}{\sqrt{1+\omega^2\tau^2}} \text{ and } \tan(\varphi) = \omega\tau \qquad 7\text{-}30$$

To extend this to a square wave, each harmonic must be included in the convolution integral. If the square wave excitation is:

$$L(t) = a + b\sum_{n=1}^{\infty} \frac{\sin((2n-1)\omega t)}{2n-1} \qquad 7\text{-}31$$

Where n is the harmonic number. Each harmonic is convolved separately with the intensity decay of the fluorescence signal. This results in the excited population return of:

$$N(t) = I_0\tau\left\{a + b\sum_{n=1}^{\infty} \frac{1}{(2n-1)\cdot\sqrt{1+(2n-1)^2\omega^2\tau^2}} \cos((2n-1)\omega t - \text{atan}\,((2n-1)\omega\tau))\right\} \qquad 7\text{-}32$$

Notice that both the modulation and phase relationship for the fundamental and each harmonic differ based on their frequency. The frequency dependent relationship of this return can possibly be exploited to reduce the number of frequencies that must be swept to get the lifetime of the excited material using a deconvolution technique.

7.6 DETECTION AND CLASSIFICATION

Detection and classification are the last steps in any algorithm chain. Methods may include Bayesian classification, Machine Learning (ML), Deep Learning (DL), artificial intelligence (AI) or others. When a temporal stream of data is available, some form of tracker is required.

7.6.1 Bayesian Inference

Bayesian inference is a statistical method to infer if an object belongs to a class of objects. It includes an update of the transitional probabilities based on data as more evidence is provided. It assumes that the posteriori probability, $p(x_i)$, is known. The Bayesian inference is denoted as:

$$p(x_i \lfloor Z_k) = \frac{p(Z_K \lfloor x_i)}{\sum_i p(Z_K \lfloor x_i) p(x_i)} \qquad 7\text{-}33$$

Where:

$p(x_i \lfloor Z_k)$ is the transitional probability that relates the measured to the target class
x_i is the target class
Z_K is a set of K measurements equal to $\{z_K, z_{K-1}, \dots z_1,\}$

Assuming all measurements are statically independent, we get the form:

$$p(x_i \lfloor Z_k) = \frac{p(z_K \lfloor x_i) p(x_i \lfloor Z_{K-1})}{\sum_j p(Z_k \lfloor x_j) p(x_j \lfloor Z_{K-1})} \qquad 7\text{-}34$$

The key to implementation is the definition of the conditional probabilities. See Chang for more on implementation (Chang, 1996, Chang, 1997).

7.6.2 Machine Learning & Neural Networks Reference Material

Machine Learning (ML) was initially described by Arthur Samuel in 1959. Depending on who you ask, ML includes other artificial intelligence (AI) algorithms or AI includes ML. In any case, these are all considered in the category of trained algorithm include neural networks (NN). These trained algorithms fall into four categories:

- Supervised – a known training set (both true and false object) is provided and the operator. The predictions learned by the algorithm are corrected by the operator until the desired performance is achieved.
- Semi-supervised – Instead of just known true and false data, there is unlabeled data added to the training set.
- Unsupervised – the algorithm looks for patterns in the unlabeled data and organizes the data into groups.
- Reinforcement learning – This includes rules for the ML algorithm to explore such as actions, parameters and end values. This method adapts from past experience.

ML typically requires some form of up front denoising and/or feature extraction, especially for image processing applications. Without this upfront processing, it is nearly impossible to make ML sensor agnostic, meaning any sensor under any lighting condition. Ideally data will be vectorized for classification. Unlike Bayesian classification, the training set provides the initial data and the algorithm 'learns' what is a true and what is a false object.

Broadly speaking, these algorithms can be prone to overfitting, impacting performance as they evolve. A consequence of the classical point estimation and modeling setup is that it delivers models that are generally incapable of addressing uncertainties, thus many do not provide a likelihood ratio needed for target declaration. These also may be more computationally intensive than a physics-based algorithm.

In spite of these shortcomings, these types of algorithms should always be investigated as a possible way to optimize the results of the total algorithm path. These are also possible tracker solutions.

7.6.3 Object Tracking Methods

Trackers are often needed to correlate detections from frame to frame. This section is only a starting point for someone developing a tracker. Tracker types are:

1. Kalman filters or quadratic linear estimation
2. Kernelized correlation filters (KCF), which assign a confidence ratio to each object being tracked
3. Detection-based trackers that predict trajectories
4. Convolutional neural network (CNN)
5. Others such as neural networks (NN), machine learning (ML), and AI that use temporal characteristics are possible

Ideally the output includes a probability such that alerts can be sent based on the concept of operation (ConOp).

A Kalman filter uses quadratic linear estimation to predict the next step in a sequence. Initialization of this filter is critical and often requires boundaries. A good Kalman filter definition is contained in section 3.3.1 of Modern Tracking Systems (Blackman, 1999).

8 References

AFRL. “AFRL/RY - COMPASE - Modeling and Simulation.” 2023. Accessed February 7, 2024. https://www.afrl.af.mil/About-Us/Fact-Sheets/Fact-Sheet-Display/Article/2331811/afrlry-compase-modeling-and-simulation/.

ASTM Docs. “ASTM G173-03(2020), ‘Standard Tables for Reference Solar Spectral Irradiances: Direct Normal and Hemispherical on 37° Tilted Surface.’” https://www.astm.org/g0173-03r20.html.

Beckmann, Petr and André Spizzichino. *The Scattering of Electromagnetic Waves from Rough Surfaces*. New York: MacMillan, 1963. P. 9.

Berk, Alexander, Patrick Conforti, Rosemary Kennett, Timothy Perkins, Frederick Hawes, Jeannette van den Bosch, "MODTRAN6: a major upgrade of the MODTRAN radiative transfer code," Proc. SPIE 9088, Algorithms and Technologies for Multispectral, Hyperspectral, and Ultraspectral Imagery XX, 90880H (13 June 2014); https://doi.org/10.1117/12.2050433

Blackman, Samuel and Robert Popoli. *Design and Analysis of Modern Tracking Systems*. Norwood, MA: Artech House Publishers, 1999.

Bohren, Craig F. and Donald R. Huffman. *Absorption and Scattering of Light by Small Particles*. Hoboken, NJ: John Wiley & Sons, Inc. 1983.

Boyd, Robert. *Radiometry and the Detection of Optical Radiation*. Hoboken, NJ: John Wiley & Sons, Inc. 1983.

Cai, Guowei., Ben M. Chen, and Tong Heng Lee. “Coordinate Systems and Transformations.” In *Unmanned Rotorcraft Systems. Advances in Industrial Control,* 23–34. London: Springer, 2011. Accessed September 16, 2024. https://doi.org/10.1007/978-0-85729-635-1_2.

Chang, Kuo-Chu, Jun Liu, and Jing Zhou. “Bayesian probabilistic inference for target recognition.” *Proc. SPIE 2755, Signal Processing, Sensor Fusion, and Target Recognition V*, 1996. https://doi.org/10.1117/12.243157.

Chang, Kuo-Chu and Robert Fung. “Target identification with Bayesian networks in a multiple hypothesis tracking system.” *Optical Engineering* 36, no. 3 (March 1997): 684–691.

Cody, Mac A. "The fast wavelet transform: Beyond Fourier transforms." *Dr. Dobb's Journal* 17, no..4 (1992).

Colina, L. Bohlin, R, Castelli, F, “Absolute Flux Calibrated Spectrum of Vega,” Instrument Science Report CAL/SCS-008, 1996

Domingues, Margarete, Odim Mendes, Jr., and Aracy Mendes da Costa. “On wavelet techniques in atmospheric sciences.” *Advances in Space Research* 35, no. 5 (February 2005): 831-842, February 2005.

Fawcett, Tom. “Introduction to ROC analysis.” *Pattern Recognition Letters* 27, no. 8 (June 2006): 861–874. https://doi.org/10.1016/j.patrec.2005.10.010.

Ghaderpour, Ebrahim, Spiros Pagiatakis, and Quazi K. Hassan. "A Survey on Change Detection and Time Series Analysis with Applications." *Applied Sciences* 11, no. 13 (2021). https://doi.org/10.3390/app11136141.

Goldhirsh, J. "A parameter review and assessment of attenuation and backscatter properties associated with dust storms over desert regions in the frequency range of 1 to 10 GHz." *IEEE Transactions on Antennas and Propagation* 30, no.6 (November 1982): 1121–1127.

Goldhirsh, J. "Attenuation and backscatter from a derived two-dimensional duststorm model." *IEEE Transactions on Antennas and Propagation* 49, no. 12 (December 2001): 1703–1711.

Gordon, I.E., L. S. Rothman, R. J. Hargreaves, R. Hashemi, E. V. Karlovets, F. M. Skinner, et al., "The HITRAN2020 molecular spectroscopic database", J. Quant. Spectrosc. Radiat. Transfer 277, 107949 (2022). [doi:10.1016/j.jqsrt.2021.107949]

Hasan, H. and C. J. Burrows. "Telescope Imaging Model (TIM)." *Astronomical Society of the Pacific* 107 (1995): 289–298.

Harvey, James E. and R. V. Shack. "Light-Scattering Characteristics of Optical Surfaces." Air Force Systems Command Report SD-TR-80-70, February 1981.

Horiba Technical Note. "Lorentz Dispersion Model." Accessed July 15, 2020. https://www.horiba.com/fileadmin/uploads/Scientific/Downloads/OpticalSchool_CN/TN/ellipsometer/ Lorentz_Dispersion_Model.pdf.

Horiba Technical Note. "Drude Dispersion Model." Accessed July 15, 2020. https://www.horiba.com/fileadmin/uploads/Scientific/Downloads/OpticalSchool_CN/TN/ellipsometer/Drude_Dispersion_Model.pdf.

Hudson, Richard D. *Infrared System Engineering.* New York: John Wiley & Sons, 1969.

Islam, M. R., Z. E. Elshaikh, O. Elshaikh, O. O. Khalifa, A. H. M. Zahirul Alam, S. Khan, and A. W. Naji. "Prediction of signal attenuation due to duststorms using Mie scattering." *IIUM Engineering Journal* 11, no. 1 (2010): 71–87.

Keim, Robert. "Comparing Optical Sensors: Understanding D-star." All about circuits. Updated April 2018. Accessed March 20, 2024. https://www.allaboutcircuits.com/technical-articles/evaluating-and-comparing-photodetectors-understanding-d-star/.

Kolmogorov, A. N., "The local structure of turbulence in incompressible viscous fluid for very large Reynolds numbers," Dokl. Akad. Nauk SSSR 30, 301–305 (1941).

Lakowicz, J. R.. *Principles of Fluorescence Spectroscopy*, 3rd ed. New York: Springer Science+Business Media, 2006.

Magris, M. and A. Iosifidis. "Bayesian learning for neural networks: an algorithmic survey." Artificial Intelligence Review 56 (2023): 11773–11823. https://doi.org/10.1007/s10462-023-10443-1.

Matzler, C., "MATLAB Functions for Mie Scattering and Absorption." University of Bern, Research report No. 2002-08, June 2002.

Matzler, C. "MATLAB Functions for Mie Scattering and Absorption, version 2." Research report No. 2002-11. University of Bern, August 2002.

Meissner, T. and F. Wentz. “The Complex Dielectric Constant of Pure and Sea Water from Microwave Satellite Observations.” *IEEE Transactions on Geoscience and Remote Sensing* 42, no. 9 (Sept 2004).

National Aeronautics and Space Administration Science Mission Directorate. “Introduction to the Electromagnetic Spectrum.” 2010. Accessed July 28, 2022. http://science.nasa.gov/ems/01_intro.

National Instruments. “Understanding FFTs and Windowing.” Accessed September 12, 2024. https://download.ni.com/evaluation/pxi/Understanding%20FFTs%20and%20Windowing.pdf.

Nelson, D. H., D. L. Walters, E. P. MacKerrow, M. J. Schmitt, C. R. Quick, W. M. Porch, and R. R. Petrin. “Wave optics simulation of atmospheric turbulence and reflective speckle effects in CO2 lidar.” *Applied Optics* 39, no. 12 (April 2000).

Newberg, L. “Some Useful Statistical Definitions.”2006. Accessed October 3, 2024. https://www.cs.rpi.edu/~leen/misc-publications/SomeStatDefs.html.

Nicodemus, F. E. “Reflectance Nomenclature and Directional Reflectance and Emissivity.” *Applied Optics* 9, no. 6 (1970): 1474–1475.

Odedina, M. O. and T. J. Afullo. “Determination of rain attenuation from electromagnetic scattering by spherical raindrops: Theory and experiment.”, *Radio Science* 45, no.1 (2010). https://doi.org/10.1029/2009RS004192.

Ohio State Useful Astronomical Data http://www.astronomy.ohio-state.edu/~martini/usefuldata.html, accessed Jan 2025

Olson, D. K. "Converting Earth-centered, Earth-fixed coordinates to geodetic coordinates." *IEEE Transactions on Aerospace and Electronic Systems* 32, no.1 (January 1996): 473–476.

O’Neill, M. “Data Analysis User Manual.” NNSS internal document, 2022.

O’Neill, M. and T. Myers. “High Speed Spectrometer Characterization Procedure.” Internal Mission Support and Test Services document. February 24, 2024.

Parigger, Christian G. “Diatomic Line Strengths for Fitting Selected Molecular Transitions of AlO, C2, CN, OH, N+2 , NO, and TiO, Spectra.” *Foundations 2023* 3, no. 1 (January 2023): 1–15. https://doi.org/10.3390/foundations3010001.

Paschotta, R. "Fresnel Equations." RP Photonics Encyclopedia. Accessed December 11, 2024. https://www.rp-photonics.com/fresnel_equations.html.

Persson, B. N. J. “Contact mechanics for randomly rough surfaces.” *Surface Science Reports* 61 (2006): 201–227.

Phillip, H. R. and E. A. Taft. “Kramers-Kronig Analysis of Reflectance Data for Diamond.” *Physical Review* 136 (1964): A1445–A1448.

Pilat, Mmichael J. and David S. Ensor. "Plume Opacity and Particulate Mass Concentration" *Atmospheric Environment* 4, no.2 (1970): 163–173.

Planck, M. "On the Theory of the Energy Distribution Law of the Normal Spectrum." In *The Old Quantum Theory*, edited by Dirk ter Haar. Oxford: Pergamon Press, 1967. Page 82.

Polyanskiy, Mikhail. Refractive Index Database. Accessed September 2, 2020. https://refractiveindex.info/?shelf=main&book=C&page=Phillip.

Qian, S-E., "Enhancing space-based signal-to-noise ratios without redesigning the satellite." SPIE Newsroom. January 5, 2011. https://spie.org/news/3421-enhancing-space-based-signal-to-noise-ratios-without-redesigning-the-satellite.

Racine, R. "The Telescopic Point-Spread Function." *Astronomical Society of the Pacific* 108 (1996): 699–705.

Rivolta, C. "Airy disk diffraction pattern: comparison of some values of f/No. and obscuration ratio." *Applied Optics* 25 (1986): 2404.

Rogalski, Antoni. "Optical detectors for focal plane arrays." *Opto-electronics Review* 12 (2004).

Sacek, Vladimir. "Telescope Optics." November 2018. http://www.telescope-optics.net/telescope_resolution.htm.

Sandin, C. "The Influence of diffuse scattered light." *Astronomy & Astrophysics* 567 (2014): A97.

Shanthamallu, U. S., A. Spanias, C. Tepedelenlioglu, and M. Stanley. "A brief survey of machine learning methods and their sensor and IoT applications." Presented at the 8th International Conference on Information, Intelligence, Systems & Applications (IISA), Larnaca, Cyprus, 2017.

Smith, W. *Modern Optical Engineering*. New York: McGraw Hill, 1966, pages 140–141

Sharif S. "Attenuation Properties of Dusty Media Using Mie Scattering Solution." *Progress in Electromagnetics Research M* 43 (2015): 9-18.

Shumaker, D. L., J. S. Accetta, and W. D. Rogatto. "Infrared & Electro-Optical Systems Handbook." *Electro-Optical Components Vol. 3*. Ann Arbor, MI: Infrared Information and Analysis Center, 1993

Space Telescope Science Institute (STScI) WFC3 Instrument Handbook, Ch 9, Sky Background, Version 9, 2017 http://www.stsci.edu/hst/wfc3/documents/handbooks/currentIHB/c09-exposuretime08.html

Stover, John. *Optical Scattering: Measurement and Analysis*. Bellingham, WA: SPIE – The International Society for Optical Engineering, 1995.

Tatarskii, V. I., *The Effects of the Turbulent Atmosphere on Wave Propagation,* Israel Program for Scientific Translations, Jerusalem, 1971.

Taylor, B. and C. Kuyatt. "Guidelines for Evaluating and Expressing the Uncertainty of NIST Measurement Results." NIST Technical Note 1297, National Institute of Standards, 1994 Edition.

Trainham, R., Mary O'Neill, and Ian J. McKenna. "An Analog Filter Approach to Frequency Domain Fluorescence Spectroscopy." *Journal of Fluorescence* 25 (2015): 1801–1812.

Usevitch, Bryan E. "A Tutorial on Modern Lossy Wavelet Image Compression: Foundations of JPEG 2000," *IEEE Signal Processing Magazine* (September 2001): 22–35.

Van de Hulst, H. C. *Light Scattering by Small Particles*. New York: Dover, 1981.

Van Dokkum, P., R.G. Abraham, and A. Merritt. "First Results from the Dragonfly telephoto Array: The apparent lack of a stellar halo in the Massive Spiral Galaxy M101." *Astrophysical Journal Letters* 282:L24 (2014).

Welch, P. "The use of fast Fourier transform for the estimation of power spectra: A method based on time averaging over short, modified periodograms." *IEEE Transactions on Audio and Electroacoustics* 15, no. 2 (June 1967): 70–73. https://doi.org/10.1109/TAU.1967.1161901.

Wikner, D. "Millimeter-Wave Propagation Measurement through a Dust Tunnel." ARL report ARL-TR-4399, March 2008.

Wolfe, William L. and George J. Zissis. *The Infrared Handbook*. Michigan: IRIA Center, 1985.

Zeller, John, Harry Efstathiadis, Gourav Bhowmik, Pradeep Haldar, Nibir Dhar, Jay Lewis, J. Priyalal Wijewarnasuriya, Yash Puri, and Ashok Sood. "Development of Ge PIN Photodetectors on 300 mm Si wafers for Near-infrared Sensing." *International Journal of Engineering Research and Technology* 8 (2015): 23–33.

Zhang, X. "Noise-resistant Wavelet-Based Bayesian Fusion of Multispectral and Hyperspectral Images." *IEEE Transactions on Geoscience and Remote Sensing* 47, no.11 (November 2009): 3834–3843.

Zhu, J.. "Conversion of Earth-centered Earth-fixed coordinates to geodetic coordinates." *IEEE Transactions on Aerospace and Electronic Systems* 30 (1994): 957–961.

Zou, H., Guo, L., Xue, H. et al. "Quantifying and understanding the triboelectric series of inorganic non-metallic materials." *Nat Commun* 11, 2093 (2020). https://doi.org/10.1038/s41467-020-15926-

9 Sample Problems

1) What is the peak wavelength for a blackbody of temperature 300K when plotted in Watts/cm^2- µm?

We use Wein's displacement law:

$$\lambda_{\max}(T) = \frac{2897.8}{T} = \frac{2897.8}{300} = 9.66\mu m$$

Note that if we were plotting in photons/sec-cm^2-µm this would be:

$$\lambda_{\max}(T) = \frac{3669.73}{T} = \frac{3669.73}{300} = 12.23\mu m$$

Why the different numerator – remember the energy of a photon via the Einstein-Planck relationship:

$$E = \frac{hc}{\lambda}$$

Where:
E is the energy of a photon in Joules (aka Watt-seconds)
c is the speed of light = 2.99792458 x 10^8 m/sec
λ is the wavelength in meters

2) Compute the diffraction limit (blur size) of an f/2.5 lens with a 50 mm focal length. What is the spatial resolution at a wavelength of 1.0µm and at distance of 1000 meters?

First, we compute the aperture diameter as:

$$\mathrm{D} = \mathrm{f}/f\# = \frac{50\mathrm{mm}}{2.5} = 20\mathrm{mm}$$

We now use the diffraction limit

$$\alpha_r = 2.44 \cdot \lambda/D = 2.44 \cdot 1x10^{-6}/20x10^{-3}$$

$$= 1.22x10^{-4}\, rad \cdot \frac{1x10^3 mrad}{rad} = 0.122\, mrad$$

The spatial resolution is simply:

$$x = \alpha_r \cdot R = 1.22x10^{-4} \cdot 1000 = 0.0122m \cdot \frac{39.37inch}{m} = 4.8"$$

3) You have a 1-meter diameter target with a radiant exitance of 10 W/cm^2. What is the radiant intensity of this source?

$$\mathrm{J} = \frac{\mathrm{M} \cdot \mathrm{A_s}}{\pi} = \frac{10 \cdot \pi \cdot \left(\frac{1m}{2} \cdot \frac{100cm}{m}\right)^2}{\pi} = 2.5\, x10^4 W/sr$$

What is the irradiance at 10km in Watts/cm^2?

$$\mathrm{H} = \frac{J}{R^2} = \frac{2.5\ x10^4}{\left(10km \cdot \frac{10^5 cm}{km}\right)^2} = 2.5x10^{-8} W/cm^2$$

4) You are going to the field. You are looking for objects that are about 8 inches in diameter, d_{min}. You are using a camera with a 3.85 µm pixel, d_{pix}, and a 25 mm lens, f. How far away will you be when the target is one pixel in size?

Answer: Simple trig problem - but keep track of your units!

$$d_{min} = \frac{R \cdot d_{pix}}{f}$$

$$R = \frac{f \cdot d_{min}}{d_{pix}}$$

$$R = \frac{25x10^{-3} m \cdot 8'' \cdot 0.0254\, m/''}{3.85x10^{-6} m}$$

$$R = 1319.5\, m$$

5) Compute the radiance (aka radiant emittance) from a Lambertian extended, graybody source with emissivity 0.8, Temperature 310K integrated from 7.5 to 13.5 µm.

While radiance and irradiance have the same units, radiance is per unit area of source, irradiance is per unit area of entrance aperture (at range). We use Planck's law sample MATLAB code to do this is:

```
%%%%%%%%%%%%%%%%%%%%%%%%%%%%%%%%%%%%%%%%%%%%%%%%%%%%%%%%%%%%%%%%%%%%%
% function M = flux(LamMin,LamMax,T)
% Computes inband flux radiated by blackbody
% M = flux(LamMin,LamMax,T)  where
%   LamMin is the minimum wavelength in um
%   LamMax is the maximum wavelength in um
%   T = temperature in Kelvins
% Returns with M = radiant flux per unit area of source in watts/sq.cm.
% divide by pi to get radiance (W/sq.cm.-sr)
% example M=flux_file('dat.txt', 300);
% M. O'Neill, MSTS, 6 June 2025
%%%%%%%%%%%%%%%%%%%%%%%%%%%%%%%%%%%%%%%%%%%%%%%%%%%%%%%%%%%%%%%%%%%%%
function  M = flux(LamMin,LamMax,T)
samp = 2000;                        % number of samples for numerical integration
dLam = (LamMax-LamMin)/(samp-1);    % wavelength delta
Lam=(LamMin:dLam:LamMax)';          % interpolated wavelength range
%% calculate plancks; constants updated from NIST 5/15/25
% spectral radiant emittance W/cm2-um
q = 3.741768797316894e4./((Lam.^5)*ones(size(T)).*(exp((1.4387752e4)./(Lam*T))-1));
q=dLam.*q;                 % W/cm2-um in-band
M=sum(q,1)';              % add up the total in-band energy
```

Thus $M(300) = 0.8 \cdot \frac{0.0174W}{cm^2} \cdot \frac{1000mW}{W} = 13.95mW/cm^2$

6) You have a microbolometer that has an NEDT of 40 mK when assuming a background temperature of 300K with sensor response from 7.5 to 13.5 µm. Compute the approximate NEI of this detector in W/cm^2.

$$NEI = M(T + \mathrm{NEDT}) - M(T) = M(300.04) - M(300)$$

From the problem 5 we know M(300)= 17.44 mW/cm^2

We now compute M(300.04)=17.452037

Thus NEI=17.452037-17.4409399= 1.1097e-02 mW/cm^2

In MATLAB for W/cm^2 we can type at the command prompt:

```
>> NEI=flux(7.5, 13.5, 300.04)-flux(7.5, 13.5, 300)
```

Which returns:

```
>> NEI =   1.1097e-05
```

7) You are going to the field. The event is expected to start with an object at 1 meter and grow to 15 meters in diameter. You have a camera with 1024x1024, 10µm pixels (d_{pix}, read noise of 36 electrons, a well depth of 15,000 electrons and 12 bits. You have chosen a 400 nm +/- 5 nm filter with 90% transmission for this sensor. The sensor response at 400 nm is 0.1 Amps/Watt.
   a) What is the depth of field required for this system?

Consider that the diameter in all dimensions is 15 meters. Also consider that you will focus as best you can on the 1-meter object before the event. To keep the debris as it comes toward you in focus, you need at least 7.5 meters, but to be safe, set the depth of field to 15 meters as it is difficult to focus in high turbulence (late morning/early afternoon).

   b) What is the total field of regard needed?

This is straightforward - we know that the horizontal FOR must subtend 15 meters. To allow for a little mis-centering, we assume 20 meters.

   c) Using this FOR what is the best spatial resolution we can achieve?

$$d_{min} = \frac{20}{1024} = 1.953\ x\ 10^{-2} m$$

   d) Assuming we are placed at 300 meters and want this best resolution, what is the IFOV of the system? What is the focal length in mm?

Basic trig -we know for small angles:

$$\frac{d_{min}}{R} = \frac{d_{pix}}{f} \overset{\mathrm{def}}{=} \phi_{\mathrm{pix}} = \frac{1.953\ x\ 10^{-2}}{300} = 65.1\ \mu rad$$

The focal length is:

$$f = \frac{d_{pix} \cdot R}{d_{min}} = \frac{10\,x\,10^{-6} \cdot 300 \cdot 10^{3} mm/m}{1.953\,x\,10^{-2}} = 153.6mm$$

We thus pick a 150 mm lens.

e) From b and c specify the telescope f/# and aperture in inches.

Assuming a circle of confusion (or blur circle angular diameter, ϕ) Depth of field is:

$$\delta = \frac{2 \cdot d_{\mathrm{pix}} \cdot R^2}{f^2} \cdot f\# \quad \text{manipulating we get:}$$

$$f\# = \frac{\delta \cdot f^2}{2 \cdot d_{\mathrm{pix}} \cdot R^2} = \frac{15 \cdot 0.150}{2 \cdot 10x10^{-6} \cdot 300^2} = f/1.25$$

We know that $f\# = \mathrm{f/D}$ then:

$$\mathrm{D = f}/f\# = \frac{150\mathrm{mm}}{1.25} = 120 \frac{\mathrm{mm}}{\frac{25.4mm}{inch}} = 4.72\,inches$$

Food for thought: What if you have an f/3.0, 150 mm telescope, can you use it assuming you have enough sensitivity?

Yes – the DoF will be greater than 15 meters but the aperture smaller, so fewer photons

8) The maximum graybody temperature that you must capture without saturating (<90% of well) is 3000K. While the emissivity/particle density product is small, some area will be resolvable, thus assume an emissivity of 0.5 and assume an extended source.
   a) Given the system derived, what exposure time do you need?

We must push photons to the detector. Since we are given responsivity in Amps/Watt (coulombs/W-sec), we use Planck's in Watts and not photons:

$$e_{\mathrm{tar}} = \frac{W(T) \cdot \varepsilon_{\mathrm{tar}} \cdot T_a \cdot T_o \cdot t_{\mathrm{int}} \cdot A_{pix}}{4 \cdot f\#^2} \cdot \mathrm{R} \cdot C$$

Where

e_{tar} number of electrons from the target = 0.9* 15,000 electrons=13,500e$^-$

A_{pix} is pixel area $= 10x10^{-6}$ meters

T_a transmission through the atmosphere, =1.0

T_o transmission through the optics & filter =0.90

ϕ_{pix} Approximate subtense of the pixel in radians = 33.33 µrad

R is responsivity = 0.1 Amps/Watt = 0.1 Coulombs/W-Sec Responsivity in Amps/Watt

$\varepsilon_{\mathrm{tar}}$ emissivity of the target, set to 0.5

$f\#$ is the f-number we derived = 2.5

C=6.24150975 x 10^{18} electrons/coulomb

t_{int} integration (exposure) time

We manipulate the equation to solve for t_{int} :

$$t_{\text{int}} = \frac{4 \cdot f\#^2 \cdot e_{\text{tar}}}{W(T) \cdot \varepsilon_{\text{tar}} \cdot T_a \cdot T_o \cdot A_{pix} \cdot \mathrm{R} \cdot C}$$

We then use Planck's law to compute W(3000) (remember flux.m?), our filter is 400±5 nm so:

M=flux(0.395, 0.405, 3000)=0.2271 W/cm^2=2271 W/m^2

Now we plug everything in:

$$t_{\text{int}} = \frac{4 \cdot 2.5^2 \cdot 13500}{2271 \cdot 0.5 \cdot 1.0 \cdot 0.9 \cdot (10\ \text{x}10^{-6})^2 \cdot 0.1 \cdot 6.24150975\ \text{x}\ 1018} = 5.3\ \mu Sec$$

b) What is the maximum frame rate that you can achieve assuming the readout time is 100nSec?

Answer: $fps = \frac{1}{t_{\text{int}} + t_{\text{read}}} = \frac{1\ x\ 10^6}{5.3+0.1} = 185{,}185\ fps$

Food for thought: If we wanted to use this system for a higher temperature, we can stop down the aperture. For instance, if we want to set the saturation limit to 3500 K, we can set the aperture such that we have an f/6.0 system and would get a 5.5 µSec exposure time.

APPENDIX A: SYMBOLS AND ABBREVIATIONS USED IN THIS BOOK

Symbol	**Meaning**
A_s	area of source
A_p	area of the pixel, = d_{pix}^2.
A_o	area of the entrance aperture
$A_s\Omega_{\text{source}}$	etendue of the source
$A_o\Omega_{\text{pixel}}$	etendue of the system.
d_{pix}	pixel size
α	extinction coefficient
β	extinction modifier
c	Coulomb = 6.24150975 x 10^{18} electrons/Coulomb
c	speed of light = 2.99792458x10^{10} cm/s
c_1	first radiation constant = $2\pi hc^2$ = 3.7415 x 10^4 W-cm^{-2} µm^4
c_2	second radiation constant = ch/k = 1.43879 x 10^4 µm-K
CE	collection efficiency based on the portion of the PSF impinging on a pixel
dn	digital number typically in counts
Δf	Equivalent noise bandwidth
D	Diameter of the entrance aperture
D*	Specific detectivity The inverse of noise equivalent power into 1 Hz bandwidth, $\sqrt{A_p.\Delta f}/\mathrm{NEP}$
δ	depth of field
δ'	depth of focus
e	number of electrons
ε	Permittivity of a material
$\varepsilon(\lambda)$	spectral emissivity
ϵ	ratio of the obscuration diameter to the primary aperture diameter
E	energy of a photon in Joules = Watt-seconds
Flick	Spectral radiance units = W/sr-cm^2-µm
f	focal length (efl) of the system
$f\#$ or f/no	f-number of the optic
$\mathcal{F}[x]$	Fourier transform of function in brackets, in this case, x
G	sensor gain in dn/electron
γ	frequency due to the damping constant
h	Planck's constant = 6.6260693x10^{-34} W-s^2 or the system response to a time signal
$H(\lambda, T)$	spectral irradiance in W/m^2-nm or W/cm^2-µm of aperture area
$H(T)$	irradiance in W/m^2 or W/cm^2 of aperture area
H	Transfer function as the Fourier transform of the system response, h
J	radiant intensity in W/sr-µm
J_1	order 1 Bessel function of the first kind

k	Boltzmann's constant = 1.38054 x 10^{-23} W- sec/K, or imaginary part of the index of refraction
K	Kelvin = °C+273.16
λ	Wavelength in μm, integrated over the filter from λ_1 to λ_2
l	Line spread function (LSF)
$L(\lambda, T)$	spectral radiance in W/sr-cm^2-μm
$L(T)$	radiance in W/sr-cm^2
$M(\lambda, T)$	spectral radiant exitance in W/m^2-nm or W/cm^2-μm of source area
M	surface brightness is mag/arc-sec^2
μ	Permeability of a material
μm	Micro-meter = 10^{-6} meters
MTF	modulation transfer function
OTF	optical transfer function
ω_p	plasma frequency
ω_0	resonance frequency due to the spring constant
n	real part of the index of refraction
nm	Nanometer=10^{-9} meters
NEP	Noise equivalent Power
NEDT	Noise equivalent Delta Temperature
Ω	Solid angle is steradians (sr)
PhTF	phase transfer function
PSF	point spread function
ϕ_{tar}	angular subtense of the target in radians
ϕ_{pix}	angular subtense of the pixel in radians
ϕ^2	Solid angle in steradians (sr)
φ	Power spectral density
$Q(T)$	in-band radiant photon emittance in ph-sec^{-1}cm^{-2}
QEFF	quantum efficiency, fill factor, electrons/photon
$\dot{q}$	Noise equivalent photon rate in ph-sec^{-1}
q	the number of photons on a detector
r_0	coherence radius and $\kappa = 2\pi/\lambda$ where λ is the wavelength
$\rho(\lambda)$	spectral reflectance
R	range or distance between the source and the entrance aperture
$\mathcal{R}(\lambda)$	relative spectral response (RSR) vs wavelength
$\mathfrak{R}(\lambda)$	Sensor responsivity in Amps/Watt (Coulombs/Watt-Sec)
σ	Standard deviation, Stefan-Boltzmann constant, wavenumber, extinction cross section
SNR	signal to noise ratio
SCR	signal to clutter ratio also contrast
χ'	real part of susceptibility
χ''	imaginary part of susceptibility
T	absolute temperature in Kelvin
T_o	the optics transmission
T_a	transmission through the atmosphere
$T_{\mathrm{filt}}(\lambda)$	spectral transmission of the filter
t_{int}	exposure time

$\tau(\lambda)$	Spectral transmission
$\tan(\delta)$	loss tangent
$W(\lambda, T)$	spectral radiant exitance in W/m^2-nm